THE UNIVERSITY
of EDINBURGH

Dissipative Effects in the Early Universe

Thomas P. Metcalf

Doctor of Philosophy
University of Edinburgh
2015

For my parents

and in memory of

Graeme Metcalf

1961-2014

Declaration

I declare that this thesis was composed entirely by myself and that the work is my own, unless explicitly stated otherwise.

Some of the results presented in Chapter 5, Chapter 6 and Chapter 7 are published in:

Mar Bastero-Gil, Arjun Berera, Thomas P. Metcalf and João G. Rosa
Delaying the waterfall transition in warm hybrid inflation
Journal of Cosmology and Astroparticle Physics, arXiv:1312:2961 [hep-ph], 2014

Thomas P. Metcalf
June, 2015

Acknowledgements

First of all I would like to thank my supervisor Arjun Berera for his guidance and encouragement. His advice and enthusiasm has helped me immensely during my time as a student and I have had the opportunity to learn a considerable amount of physics under his supervision.

I would like to express an enormous amount of thanks to João Rosa for his patience and support. He has consistently helped me throughout my PhD and has always been more than generous with his time whenever I needed assistance. The research presented in this thesis would not have been possible without his support. Particular thanks is also due to Mar Bastero-Gil. Her consistently useful advice and encouragement was invaluable during the completion of this thesis.

Part of the research presented in this thesis was done whilst visiting the Gravitation Group at the University of Aveiro. I would like to express my thanks to all the members of the group for their hospitality during my visit.

For giving me the opportunity to do research in physics I would like to express my gratitude to all the staff in the Higgs Centre for Theoretical Physics, with particular thanks to Brian Pendleton, Einan Gardi and Luigi Del Debbio. I would like to thank all my fellow PhD students in the PPT group for an enjoyable four years, with special thanks to the PhD students in my year, Nathan Hartland, Ashley Cooke and Samuel Abreu.

Finally I would like to thank my parents for all the encouragement and enthusiasm they have shown towards my education, and without whom I would never have been able to reach this stage. This thesis is dedicated to them.

Abstract

Inflationary cosmology is the leading candidate for explaining the homogeneity, isotropy and spatial flatness of the universe whilst also providing the mechanism for the seeding of large scale structure. The central theme of inflationary dynamics involves the evolution of a scalar field, called the inflaton, such that its potential drives an accelerated expansion.

Warm inflation is the dynamical realization in which interactions between the inflaton and other fields can lead to dissipation of inflaton energy to other dynamical degrees of freedom. Heavy fields coupled to the inflaton mediate the transfer of inflaton energy to light degrees of freedom which thermalize and heat the universe. This damps the inflaton's motion and allows for the potential formation of a thermal bath during the inflationary period.

Hybrid inflation models are a natural way in which warm inflation can be realized, with dissipation of inflaton energy mediated by the waterfall fields to fields in the light sector. In this thesis I outline the dynamics and observational predictions of supersymmetric hybrid inflation driven by radiative corrections in the warm regime. As in the standard cold inflationary scenario inflation ends when the effective mass squared of the waterfall field becomes negative, with the tachyonic instability driving the system to a global minimum in a process called the waterfall transition. I present the effect of including thermal mass corrections to the waterfall fields, and SUSY mass splittings on the quantum effective potential and the resulting dissipation coefficient. I show that including

dissipative effects can significantly prolong the inflationary period to produce 50-60 e-folds of inflation with an observationally consistent primordial spectrum.

Inflation still requires a microphysical description within a fundamental theory of quantum gravity. This has prompted the search for inflaton candidates within the superabundance of scalar fields present in string theory compactifications, with brane-antibrane inflation in particular emerging as a concrete implementation of SUSY hybrid inflation in a UV complete particle physics model. Inflation proceeds in a brane-antibrane system through the movement of a stack of branes towards a stack of antibranes, with the inflaton field being the interbrane distance. Warm inflation can be implemented in a brane-antibrane system with dissipation of inflaton energy mediated by fields corresponding to strings stretched between the brane and antibrane stacks. It has been shown that this dissipation of inflaton energy in warm inflation can greatly alleviate the η-problem in brane-antibrane scenarios. Whilst these strings mediating dissipation have end points fixed on to both the D3 and $\overline{\text{D3}}$ stacks, the compact nature of the geometry within which the system is constructed allows these strings to have different winding modes. We investigated how strings with increasing winding number can provide an enhancement to the dissipation coefficient, allowing a significant reduction in the number of branes and antibranes in the warm inflation system, whilst also modifying the inflationary dynamics by reducing the speed at which the system evolves. This may go some way to alleviating the η-problem associated with some constructions of brane-antibrane inflation whilst also potentially providing the best way to motivate the large field multiplicities associated with warm inflation models.

Contents

Chapter 1

Introduction

The best developed candidate for explaining the high levels of large scale homogeneity and isotropy in the universe, whilst also providing the mechanism for the seeding of large scale structure, is the theory of cosmic inflation. Initially proposed in [1], and then further developed in [2], the central theme of inflationary dynamics involves the evolution of a scalar field called the inflaton, such that its potential drives an accelerated expansion of the universe some 10^{-34} seconds after the big bang singularity. The fluctuations in the Cosmic Microwave Background (CMB), measured recently to unprecedented accuracy by the Planck Mission [3], gave further validation to the theory of inflation, observing the small variations in the density of the primordial universe that grew via gravitational instability into the observed large scale structure (LSS).

There are, however, two distinct dynamical realizations of inflation, termed warm inflation and cold inflation, with cold inflation seen as the standard picture. In cold inflation the inflaton is taken to be an isolated system, with interactions between the inflaton and other fields only being considered when making radiative corrections to the scalar potential. Any other initial component of energy density is redshifted and the universe is left in a supercooled state, with a phase of "reheating" required once inflation has ended to bring the universe into an era of

radiation dominated expansion.

Warm inflation [4, 5] is the realization that interactions between the inflaton and other fields leads not only to radiative corrections to the scalar potential, but also to dissipation of inflaton energy to other dynamical degrees of freedom. This typically happens because the fields coupled to the inflaton, though heavy due to their coupling to the inflaton, are unstable against decay into light degrees of freedom and thus mediate dissipation of inflaton energy to the light sector. This both damps the inflaton's motion and enables particle production, which can in turn lead to the formation of a thermal radiation bath. The work presented in this thesis focuses on developing particle physics models of inflation in the warm regime.

One of the best motivated particle physics models of inflation is hybrid inflation. Hybrid inflation involves two coupled scalar fields, one that acts as the inflaton and is responsible for driving inflation, and another, called the waterfall field, that is responsible for ending inflation when its effective mass squared becomes negative and the false vacuum can no longer be sustained. Hybrid models [6] are thus a class of particle physics models of inflation that provide a natural framework within which warm inflation can be realized, with the waterfall fields mediating dissipation of inflaton energy to fields in the light sector. In this thesis I present the dynamics and observational predictions of supersymmetric (SUSY) hybrid inflation driven by radiative corrections in the warm regime. We have included several novel effects in the analysis, including the effect of dissipation from both the on-shell and the off-shell modes of the waterfall fields, the effects of SUSY mass splittings in the effective potential, the effect of thermal mass corrections to the waterfall fields due to their coupling with the radiation bath, and the effect of varying the initial value of the inflaton field. For comparison I also include results for supersymmetric hybrid inflation driven by radiative corrections in the standard supercooled regime. It is shown, once all

effects are considered, that including dissipative effects significantly prolongs the inflationary period to produce $50-60$ e-folds of inflation with an observationally consistent primordial spectrum.

Inflationary cosmology is still in need of a microphysical description within a fundamental theory of quantum gravity and this has motivated the extensive search for inflaton candidates within the superabundance of scalar fields that are present in string theory compactifications. One of the most promising avenues of research that has emerged in this endeavor is brane-antibrane inflation. The brane-antibrane inflation setup involves a stack of branes separated from a stack of antibranes within a compact space. The inflaton field corresponds to the interbrane distance and inflation proceeds as the stack of branes moves through the compact space towards the stack of antibranes, with inflation ending when the two stacks collide. In generic constructions this collision has been shown to happen before an adequate amount of inflation has occurred to produce the levels of homogeneity in the universe. This is known as the η-problem. Brane-antibrane inflation can occur in the warm regime with dissipation being mediated by fields that correspond to strings stretched between the brane and antibrane stacks. In warm brane-antibrane inflation it has been shown that dissipative effects can slow the evolution of the system to allow for enough inflation, alleviating the η-problem, provided there are a sufficient number of branes to enable dissipation.

The compactified geometry of the brane-antibrane construction can be modeled as a probe brane stack within a hypercubic lattice of "images" of the antibrane stack. Inflation proceeds as the probe brane travels through the lattice of images towards an antibrane stack, with strings stretched between the probe brane and all the brane images. We show that dissipation mediated by the fields associated with strings stretched to all the brane images significantly enhances the dissipation coefficient, allowing the number of branes required in the system to be drastically reduced. The enhancement to the dissipation coefficient further

modifies the equations of motion of the system, causing it to evolve even slower, further alleviating the η-problem.

1.1 Thesis Outline

In ***Chapter 2: The Standard Big Bang Model of Cosmology*** some of the basics of the standard model of cosmology are reviewed. This involves a review of the Einstein equations and how they provide a framework for the standard model of cosmology. Friedmann-Robertson-Walker cosmology is introduced, as well as the shortcomings of the standard model of cosmology, particularly the unexplained high levels of homogeneity and isotropy.

Inflationary cosmology is introduced in ***Chapter 3: Inflation***, where it is shown how an early period of accelerated expansion can result in a universe that is naturally driven to high levels of homogeneity and isotropy. It is also explained how primordial density fluctuations during inflation seed the formation of large scale structure. Two different dynamical realizations of inflation, cold inflation and warm inflation, are introduced.

The dynamics and observational predictions of warm inflation are reviewed in ***Chapter 4: Fluctuation Dissipation Dynamics in Warm Inflation***. The form of the dissipation coefficient is introduced along with the warm inflation equations of motion and observational predictions.

In ***Chapter 5: Hybrid Inflation*** the hybrid model of inflation is introduced. The original 2-field model is reviewed, followed by the supersymmetric version and then the implementation of hybrid inflation in the warm regime is discussed. The dynamics and observational predictions of hybrid inflation in both the cold and warm regime are analyzed in the large inflaton field value limit.

In ***Chapter 6: Finite Temperature Corrections and the CJT Formalism*** finite temperature corrections, arising from the interactions between

the waterfall fields and the fields in the radiation bath created during warm inflation, are made to the effective potential of the hybrid model. This is done using the CJT formalism to obtain an improved form of the effective potential.

In ***Chapter 7: Dissipative Effects in Warm Hybrid Inflation*** the dynamics and observational predictions of hybrid inflation in the warm regime are investigated with several additional effects. The effects of mass splittings in the effective potential and dissipation coefficient are included and the effect of finite temperature corrections to the effective potential is then studied. Finally the effect of a larger initial inflaton field value is investigated.

In ***Chapter 8: Brane-Antibrane Inflation*** the basics of brane-antibrane inflation are reviewed, along with the η-problem associated with brane-antibrane constructions. The implementation of a warm brane-antibrane system is then introduced.

In ***Chapter 9: Dissipation from Compactification*** the effect of compactified extra dimensions in warm brane-antibrane inflation is investigated. The compactified geometry of the brane-antibrane system results in the presence of strings with increasing winding modes mediating dissipation of inflaton energy. It is shown that the contribution to dissipation from these strings significantly enhances the dissipation coefficient, offering a natural way in which the large field multiplicities in warm inflation can be motivated.

Finally, in ***Chapter 10: Conclusion***, the results presented in this thesis are summarized.

Chapter 2

The Standard Big Bang Model of Cosmology

The most profound observation we have made about our universe is that the galaxies we see in the sky, with the exception of a few of the nearest ones, are moving away from us [7]. Furthermore, the speed at which these galaxies are receding, measured through their redshift, increases the further away the galaxy is [8]. These simple observations bring us to the conclusion that the universe is a dynamical system, expanding as it evolves with clusters of galaxies retreating ever further away from each other as time proceeds. This chapter will be a review of some of the fundamentals of the standard model of modern cosmology and how it provides the framework through which the evolution of the universe can be understood. The standard big bang model of cosmology has been the subject of many reviews and the reader is referred to [9–13].

2.1 Einstein Equations

This dynamical behavior of the universe can be understood within the framework of Einstein's theory of General Relativity, in which matter and geometry are

intrinsically related through the Einstein equations:

$$G_{\mu\nu} + g_{\mu\nu}\Lambda \equiv R_{\mu\nu} - \frac{1}{2}g_{\mu\nu}R + g_{\mu\nu}\Lambda = 8\pi G T_{\mu\nu} \ , \tag{2.1}$$

where G is the Newton's constant of gravitation, $T_{\mu\nu}$ is the energy-momentum tensor and Λ is the cosmological constant. The Einstein tensor $G_{\mu\nu}$ is defined by the Ricci tensor $R_{\mu\nu}$ and Ricci scalar R, given by:

$$R_{\mu\nu} = \Gamma^{\alpha}_{\mu\nu,\alpha} - \Gamma^{\alpha}_{\mu\alpha,\nu} + \Gamma^{\alpha}_{\beta\alpha}\Gamma^{\beta}_{\mu\nu} - \Gamma^{\alpha}_{\beta\nu}\Gamma^{\beta}_{\mu\alpha} \ , \tag{2.2}$$

$$R \equiv g^{\mu\nu}R_{\mu\nu} \ . \tag{2.3}$$

The Ricci tensor $R_{\mu\nu}$, which provides a measure of the curvature of spacetime, is constructed out of various derivatives of the metric tensor $g_{\mu\nu}$ given by the Christoffel symbols:

$$\Gamma^{\mu}_{\alpha\beta} \equiv \frac{g^{\mu\nu}}{2}\left[g_{\alpha\nu,\beta} + g_{\beta\nu,\alpha} - g_{\alpha\beta,\nu}\right] \ , \tag{2.4}$$

with commas denoting partial derivatives. It should be noted that the Einstein equation, governing all gravitational interactions, is essentially an equation relating tensors, in this case 4×4 matrices, and so is actually 16 separate equations.

2.2 The Cosmological Principle and FRW Cosmology

The whole of modern cosmology is embodied on the cosmological principle, which states that no observer can occupy a preferred position in the universe. This implies that the universe is both homogeneous and isotropic. The spacetime of a universe that is both homogeneous and isotropic on large scales can be described

by the Friedmann-Robertson-Walker (FRW) metric:

$$ds^2 = -dt^2 + a^2(t)\left(\frac{dr^2}{1-kr^2} + r^2\left(d\theta^2 + \sin^2\theta d\phi^2\right)\right) \ , \tag{2.5}$$

where (r, θ, ϕ) are the spherical-polar coordinates parameterizing the spatial dimensions, t is time and the scale factor $a(t)$ characterizes the relative size of a hypersurface for varying times. k is the curvature parameter and is:

- $+1$ for hypersurfaces with positive curvature
- 0 for flat hypersurfaces
- -1 for hypersurfaces with negative curvature

The FRW metric expresses distances in comoving coordinates. The universe expands as $a(t)$ increases but stationary observers keep fixed coordinates r, θ and ϕ. The actual physical distance between observers can then be realized by multiplying the scale factor, $R = a(t)r$. The expansion rate of the universe is given by the Hubble parameter:

$$H \equiv \frac{\dot{a}}{a} \ . \tag{2.6}$$

The Hubble parameter H is positive for an expanding universe and has units of inverse time. The characteristic length-scale of the universe is the Hubble length $d \sim H^{-1}$, setting the size of the observable universe, whilst the characteristic time-scale is the Hubble-time $t \sim H^{-1}$, setting the age for the universe. Furthermore the recession velocity, v, of a distant galaxy is related to its distance from us, r_0, via the Hubble law:

$$v = H_0 r_0 \ , \tag{2.7}$$

where H_0 is the present day Hubble parameter, given by:

$$\begin{aligned} H_0 &= 100\ h\ \text{km sec}^{-1}\text{Mpc}^{-1} \\ &= \frac{h}{0.98 \times 10^{10}\ \text{years}} \\ &= 2.133 \times 10^{-33}\ h\ \text{eV}/\hbar\ , \end{aligned} \tag{2.8}$$

where $h = 0.72 \pm 0.08$ and the astronomical length scale of a megaparsec (Mpc) is 3.0856×10^{24} cm [12].

2.3 Friedmann Equations

The FRW model assumes that the matter content of the universe is comprised of a perfect fluid, and is thus described by just two quantities, the energy ρ and the pressure p. The Einstein equations in Eq. (2.1) that describes the gravitational interactions in the universe essentially states that gravity can be interpreted as a deformation of the geometry of the universe, which is expressed through the metric tensor $g_{\mu\nu}$, due to the presence of matter, which is described through the energy-momentum tensor $T_{\mu\nu}$. The energy-momentum tensor of the universe, $T_{\mu\nu}$, can be defined by introducing a set of observers whose worldlines are tangential to the timelike 4-velocity:

$$u^\mu \equiv \frac{dx^\mu}{d\tau}\ , \tag{2.9}$$

with τ being the proper time for the observers, resulting in $g_{\mu\nu}u^\mu u^\nu = -1$. The evolution of the universe is well approximated by homogeneous and isotropic perfect fluids, which have no heat conduction or viscosity and can be described by their energy density ρ and pressure p. Perfect fluids can be thought of as being "isotropic in the rest frame", in which $T^{\mu\nu}$ is diagonal and there is no net flux of momentum in any orthogonal direction. The energy-momentum tensor for a

perfect fluid is given by the expression:

$$T^{\mu}_{\nu} = g^{\mu\alpha}T_{\alpha\nu} = (\rho + p)u^{\mu}u_{\nu} - p\delta^{\mu}_{\nu} \ . \tag{2.10}$$

When the observers are in a frame moving with the fluid the 4-velocity can be set as $u^{\mu} = (1, 0, 0, 0)$, resulting in the stress-energy tensor:

$$T^{\mu}_{\nu} = \begin{pmatrix} \rho & 0 & 0 & 0 \\ 0 & -p & 0 & 0 \\ 0 & 0 & -p & 0 \\ 0 & 0 & 0 & -p \end{pmatrix} \ . \tag{2.11}$$

With the stress-energy tensor in this form the Einstein equations become the two coupled differential equations known as the Friedmann equation:

$$H^2 \equiv \left(\frac{\dot{a}}{a}\right)^2 = \frac{8\pi G}{3}\rho - \frac{k}{a^2} \ , \tag{2.12}$$

and the acceleration, or Raychaudhuri equation:

$$\dot{H} + H^2 = \frac{\ddot{a}}{a} = -\frac{4\pi G}{3}(\rho + 3p) \ , \tag{2.13}$$

where dots represent derivatives with respect to time. In an expanding universe containing ordinary matter we have $\dot{a} > 0$ and $\rho + 3p \geq 0$, which implies $\ddot{a} < 0$. From the simple observation that the universe is expanding, with the scale factor growing in time, we can deduce that at earlier times the scale factor would have been smaller. Furthermore, and assuming general relativity and the Friedmann equations are valid for arbitrarily high energy scales, this indicates the existence of an initial singularity at some finite time in the past at $a(t \equiv 0) = 0$. From the

Friedmann equations we get the continuity equation:

$$\frac{d\rho}{dt} + 3H(\rho + p) = 0 \ , \tag{2.14}$$

which, defining an equation of state parameter $w \equiv p/\rho$, results in:

$$\rho \propto a^{-3(1+w)} \ . \tag{2.15}$$

The evolution of the scale factor with respect to time can be derived by combining this result with the Friedmann equations:

$$a(t) \propto \begin{cases} t^{2/3(1+w)} & w \neq -1 \\ e^{Ht} & w = -1 \end{cases} \tag{2.16}$$

We thus have three distinct ways that a flat universe (with $k = 0$) will evolve depending on the matter and radiation content, with $a(t) \propto t^{2/3}$ universe containing mainly non-relativistic matter ($w = 0$), $a(t) \propto t^{1/2}$ for a universe dominated by radiation ($w = \frac{1}{3}$) and $a(t) \propto e^{Ht}$ for a cosmological constant ($w = -1$). These results are summarized in the Table (2.1). Also, since the

	w	$\rho(a)$	$a(t)$
Matter Dominated	0	a^{-3}	$t^{2/3}$
Radiation Dominated	$\frac{1}{3}$	a^{-4}	$t^{1/2}$
Cosmological Constant	-1	a^{0}	e^{Ht}

Table 2.1: Three possible evolutions for a flat universe ($k = 0$)

universe contains many matter species (baryons, photons, dark matter, neutrinos etc) we refer to the energy density and pressure as the sum of all the different i components, so that:

$$\rho \equiv \sum_i \rho_i \ , \qquad p \equiv \sum_i p_i \ , \qquad w_i \equiv \frac{p_i}{\rho_i} \ . \tag{2.17}$$

We define the present ratio of the energy density relative to the critical energy density $\rho_c \equiv 3H_0^2/8\pi G$ for each matter species 'i':

$$\Omega_i \equiv \frac{\rho_0^i}{\rho_c} \ , \tag{2.18}$$

with 0 denoting the quantity at the present time. If we normalize the scale factor to present time, ($a_0 = a(t_0) \equiv 1$) then the Friedmann equation becomes:

$$\left(\frac{H}{H_0}\right)^2 = \sum_i \Omega_i a^{-3(1+w_i)} + \Omega_k a^{-2} \ , \tag{2.19}$$

where the curvature is parameterized with $\Omega_k \equiv -k/a_0^2 H_0^2$. Evaluated at the present time we derive the expression:

$$\sum_i \Omega_i + \Omega_k = 1 \ , \tag{2.20}$$

whilst evaluating the Raychaudhuri equation at the present time gives:

$$\frac{1}{a_0 H_0^2}\frac{d^2 a_0}{dt^2} = -\frac{1}{2}\sum_i \Omega_i (1 + 3w_i) \ . \tag{2.21}$$

This forms the framework of the Hot Big Bang model of cosmology which describes an expanding universe. This expansion implies that at earlier times the universe was increasingly hot and dense, and the big bang model finds that the very early universe was in fact in an era of radiation domination.

One of the most remarkable successes of the standard hot big bang model of cosmology was the discovery of the cosmic microwave background radiation (CMB). Successive satellite experiments, such as the Cosmic Background Explorer (COBE) [14], the Wilkinson Microwave Anisotropy Probe (WMAP) [15] and the Planck satellite [3] have measured the CMB to increasing accuracy, finding the CMB to have a nearly perfect blackbody spectrum at a temperature

$T_0 = 2.725K$, in agreement with predictions of the hot big bang model. The observed tiny fluctuations in the CMB, at one part in 10^5, are completely consistent with the predictions of the hot big bang model.

Furthermore this idea that the early universe was both smaller and hotter has been tested, with the formation of light elements, such as hydrogen, helium, deuterium and lithium, through big bang nucleosynthesis BBN. Calculations of the abundances of these elements from BBN are in excellent agreement with observations, with 25% of the visible matter content of the universe being helium [11]. Likewise the observed abundance of deuterium, with an abundance ratio to hydrogen at about 1/50,000, is also consistent with the predictions of the hot big bang model.

Thus we conclude that the standard big bang model of modern cosmology provides a robust framework for studying the evolution of the universe. It provides a reliable and tested account of the history of the universe, explaining its expansion and the presence of the cosmic microwave background, whilst also accurately describing the mechanism for the nucleosynthesis of light elements.

2.4 Problems with Big Bang Cosmology

The standard big bang model is not however without its limitations, with features such as the observed levels of large scale homogeneity, isotropy and spatial flatness within the universe left unexplained by the model. That the standard big bang model has these "problems" does not suggest that there is an inconsistency within the big bang model itself, but that the model is potentially incomplete with some underlying dynamical mechanism responsible for these peculiar features.

2.4.1 The Horizon Problem

We define the position and velocities of all particles on a spatial slice (3-surface) of constant time Σ. Then the laws of physics are used to evolve the system dynamically with respect to time.

The spatial distribution of matter is describe by the density $\rho(\mathbf{x})$ and pressure $p(\mathbf{x})$, with coordinates $\mathbf{x}$. Inhomogeneities by their nature are gravitationally unstable and so will grow with time. This implies that the small inhomogeneities we observe in the universe presently must have been even smaller in the past. How can this initial smoothness of the universe be understood? In the standard big bang model the early universe has a large number of causally disconnected regions of space. Yet when we look at these regions today they appear to have very similar physical properties. The question is how did these apparently causally disconnected regions develop to appear so similar? This problem of initial homogeneity is known as the horizon problem, and can be understood through the way that light propagates in an FRW spacetime.

Conformal Time, Geodesics and Horizons

The causal structure of the FRW spacetime is determined by the propagation of light, with photons, being massless, following null geodesics, $ds^2 = 0$. Introducing conformal time with the definition:

$$\tau = \int \frac{dt}{a(t)} \ , \tag{2.22}$$

the FRW metric can be written as:

$$ds^2 = a(\tau)^2 \left[-d\tau^2 + \left(d\chi^2 + \Phi_k(\chi^2) \left(d\theta^2 + \sin^2\theta d\phi^2 \right) \right) \right] \ , \tag{2.23}$$

with:

$$r^2 = \Phi_k(\chi^2) \equiv \begin{cases} \sinh^2\chi & k = -1 \\ \chi^2 & k = 0 \\ \sin^2\chi & k = +1 \end{cases} \tag{2.24}$$

We can simplify this expression for the FRW metric by assuming that, since the universe is isotropic, the radial propagation of light is determined by the two-dimensional line element:

$$ds^2 = a(\tau)^2 \left[-d\tau^2 + d\chi^2\right] \ . \tag{2.25}$$

Considering the FRW metric in this form we can infer that in conformal time the radial null-geodesics of light in the FRW spacetime satisfy $\chi(\tau) = \pm\tau + \text{constant}$, meaning that in the $\tau - \chi$ plane light will travel in straight lines at an angle of 45^o. The maximum distance that a particle can travel from an initial time t_i to a later time t_f is defined as the comoving particle horizon, and is given by:

$$\chi(\tau) = \tau - \tau_i = \int_{t_i}^{t_f} \frac{dt}{a(t)} \ . \tag{2.26}$$

If we take the initial time t_i as being the time of the initial singularity, such that $t_i = 0$, $a(t_i \equiv 0) = 0$ then we can use the scale factor to relate the comoving particle horizon to the physical particle horizon:

$$d_p(t) = a(t)\chi \ . \tag{2.27}$$

This means that the standard big bang model of cosmology has an initial time t_i at some finite point in the past, meaning the particle horizon is finite and thus putting a limit on the regions of the universe that can be causally connected. Information sent at a given moment of time τ will never be received by an observer at some point in the future if that observer is beyond the event horizon. The event

horizon in comoving coordinates is given by:

$$\chi > \chi_{event\ horizon} = \int_{\tau}^{\tau_{max}} d\tau = \tau_{max} - \tau \ , \tag{2.28}$$

where τ_{max} is the maximum value of time (either finite or infinite). From this we get the physical size of the event horizon:

$$d_e(t) = a(t)\chi_{event\ horizon} \ . \tag{2.29}$$

The comoving particle horizon τ is the maximum distance light can travel between $t_i = 0$ and $t_f = t$, and is given by:

$$\tau \equiv \int_0^t \frac{dt'}{a(t')} = \int_0^a \frac{da}{Ha^2} = \int_0^a d\ln a \left(\frac{1}{aH}\right) \ , \tag{2.30}$$

where the comoving Hubble radius, $(aH)^{-1}$, is used to express the comoving hoizon. If the universe is dominated by a fluid with equation of state w then:

$$(aH)^{-1} = H_0^{-1} a^{\frac{1}{2}(1+3w)} \ . \tag{2.31}$$

The behavior of the comoving Hubble radius therefore depends on whether the equation of state w renders $(1 + 3w)$ positive or negative. Significantly, if the universe is radiation dominated (RD) or matter dominated (MD) then:

$$\tau = \int_0^a \frac{da}{Ha^2} \propto \begin{cases} a & RD \\ a^{1/2} & MD \end{cases} \tag{2.32}$$

Thus the growth of the comoving horizon is monotonic with time, implying that comoving scales that are entering the horizon were outside the horizon at the time of decoupling. In contrast to this the homogeneity of the CMB implies a universe that was very homogeneous at the time of last scattering at a scale that

encompasses large causally disconnected regions of space.

	w	$\rho(a)$	$a(t)$	$a(\tau)$	τ_i
Matter Dominated	0	a^{-3}	$t^{2/3}$	τ^2	0
Radiation Dominated	$\frac{1}{3}$	a^{-4}	$t^{1/2}$	τ	0
Cosmological Constant	-1	a^0	e^{Ht}	$-\tau^{-1}$	$-\infty$

Table 2.2: Evolutions for a flat universe ($k = 0$) with conformal time

2.4.2 Flatness Problem

The flatness problem arises from the realization that the energy density of the universe is currently close very close to its critical value ρ_c. To ensure that the universe evolves in time towards higher and higher levels of homogeneity the initial fluid velocities must have precise values. Too high a velocity and the expansion happens too rapidly and the universe becomes nearly empty. Too low a velocity and the universe collapses. Considering this problem in combination with the horizon problem means that the initial fluid velocities need to be fine-tuned across causally-disconnected regions. This fine-tuning of initial velocities is often called the flatness problem.

That the universe is so closely approximated to a flat euclidean space is peculiar, given that the Einstein equations show that spacetime is dynamical, being distorted by the matter content of the universe. Defining $\Omega(a) \equiv \rho(a)/\rho_c(a)$ and $\rho_c(a) \equiv 3H(a)^2/8\pi G$ the Friedmann equation:

$$H^2 = \frac{8\pi G}{3}\rho(a) - \frac{k}{a^2} \ , \tag{2.33}$$

can be rewritten:

$$1 - \Omega(a) = \frac{-k}{(aH)^2} \ . \tag{2.34}$$

$\Omega(a)$ is now time-dependent, and, in the standard big bang cosmology, the Hubble radius $(aH)^{-1}$ grows with time. The result of this is that a growing Hubble radius

implies that $|\Omega-1|$ diverges with time, with critical value $\Omega = 1$ being an unstable fixed point. Thus the present value $|\Omega(a_0) \sim 1|$ requires an extremely fine-tuned initial value in the early universe. Moreover, it has been found that deviations from flatness at the time of big bang nucleosynthesis (BBN), the GUT era and at the Planck scale have to satisfy the conditions [9]:

$$|\Omega(a_{BBN}) - 1| \leq O(10^{-16}) \ , \tag{2.35}$$

$$|\Omega(a_{GUT}) - 1| \leq O(10^{-55}) \ , \tag{2.36}$$

$$|\Omega(a_{Planck}) - 1| \leq O(10^{-61}) \ . \tag{2.37}$$

Differentiating the Friedmann equation and making use of the continuity equation gives:

$$\frac{d\Omega}{d\ln a} = (1+3w)\Omega(\Omega-1) \ . \tag{2.38}$$

From this we can see that $\Omega = 1$ is an unstable fixed point:

$$\frac{d|\Omega-1|}{d\ln a} > 0 \qquad \Leftrightarrow \qquad 1+3w > 0 \ . \tag{2.39}$$

That the standard cosmological model has the horizon and flatness problems does not suggest that there is an inconsistency within the big bang model itself, but that the model is potentially incomplete with some underlying dynamical mechanism responsible for these peculiar features. The homogeneity and flatness of the universe simply cannot be predicted by the standard cosmological model but must be assumed in the initial conditions, representing a shortcoming in the predictive power of the model. The idea of inflation has emerged as the leading candidate to explain the dynamical origin of these initial conditions for the universe.

Chapter 3

Inflation

It has been shown that the increasing comoving Hubble radius $(aH)^{-1}$ results in the horizon and flatness problems of the standard cosmological model. This chapter will show how inflation offers a solution to these problems. Inflation has been the subject of several reviews [9, 13, 16–18] and is recognized as the leading, and best developed, explanation for many of the characteristics of the observable universe, such as its spatial flatness and large scale homogeneity. Originally proposed in [1, 2], the idea of inflation is to invert the behavior of the comoving Hubble radius, such that it is decreasing in the early universe. This corresponds to an accelerated expansion of space, and results in a universe that is naturally driven to high levels of homogeneity and spatial flatness. Relating the pressure and acceleration of the universe to the Hubble radius gives:

$$\frac{d}{dt}\left(\frac{H^{-1}}{a}\right) < 0 \qquad \Rightarrow \qquad \frac{d^2a}{dt^2} > 0 \quad \Rightarrow \quad \rho + 3p < 0 \ . \tag{3.1}$$

Therefore, in order to have an epoch of inflationary expansion to solve the horizon and flatness problems we can assume that we will need a decreasing Hubble

sphere, which requires:

$$\frac{d}{dt}\left(\frac{1}{aH}\right) < 0 \ . \tag{3.2}$$

By considering the expression:

$$\frac{d}{dt}(aH)^{-1} = \frac{-\ddot{a}}{(aH)^2} \ , \tag{3.3}$$

we can infer that a shrinking Hubble radius corresponds to a period of accelerated expansion, with $\frac{d^2a}{dt^2} > 0$. If we introduce the slow-roll parameter $\epsilon \equiv -\dot{H}/H^2$ then we are able to relate $\ddot{a}$ to $\dot{H}$:

$$\frac{\ddot{a}}{a} = H^2\left(1-\epsilon\right) \ . \tag{3.4}$$

Therefore a period of accelerated expansion is possible as long as:

$$\epsilon = -\frac{\dot{H}}{H^2} = -\frac{d\ln H}{dN_e} < 1 \ , \tag{3.5}$$

where we have define the number of e-folds of inflation N_e, with $dN_e = Hdt = d\ln a$. It is typical to express the amount of inflation in terms of the number of e-folds of accelerated expansion, given by the expression:

$$N_e = log\left(\frac{a_e}{a_i}\right) \tag{3.6}$$

where a_i and a_e are the scale factors at the beginning and end of inflation respectively. Finally, the Friedmann equations that describe how the universe evolves in time will allow for an accelerated expansion for a stress-energy:

$$p < -\frac{1}{3}\rho \ . \tag{3.7}$$

From these collective ingredients we can deduce that any period of inflationary expansion will involve a decreasing Hubble sphere, an accelerated expansion and

a negative pressure. The comoving horizon can be defined as an integral of the comoving Hubble radius:

$$\tau = \int_0^a d\ln a' \frac{1}{a'H(a')} \ . \tag{3.8}$$

The difference between the comoving Hubble radius $(aH)^{-1}$ and the comoving horizon τ is that particles separated by distances greater than comoving Hubble radius are causally disconnected in the present, whereas particles separated by the comoving horizon have never been causally connected. If τ is much larger than $(aH)^{-1}$ then particles that are outside the Hubble radius in the present where in causal contact at some point in the past. This is possible if the comoving horizon is able to get most of its contribution in the early universe due to the Hubble radius being larger in the past. A larger Hubble radius at some point in the past is possible if there is a phase of decreasing Hubble radius. This is something that happens during inflation due to the scale factor a grows exponentially whilst H remains approximately constant.

3.1 Homogeneity Problem Solved

If the comoving Hubble radius were decreasing then it allows for large scales that are entering the horizon in the present to have been causally connected inside the horizon at some point in the past. This allows for causal physics to establish the homogeneity of the universe. In conformal time, with $d\tau = dt/a(t)$, the flat FRW spacetime metric is:

$$ds^2 = a^2(\tau)\left[-d\tau^2 + d\mathbf{x}^2\right] \ . \tag{3.9}$$

A null geodesic has $ds^2 = 0$, and so in conformal coordinates we have $d\tau = \pm\sqrt{d\mathbf{x}^2}$. As we have seen the scale factor evolves during matter and radiation

domination as:

$$a(\tau) \propto \begin{cases} \tau^2 & \text{Matter Domination} \\ \tau & \text{Radiation Domination} \end{cases} \tag{3.10}$$

which implies the existence of a singularity at $\tau_i = 0$, with scale factor $a(\tau_i = 0) = 0$. The horizon problem becomes obvious by considering the light cone associated with each spacetime point which defines its causal history. Causally connected points have intersecting lightcones at the point of the initial singularity in conformal time, $\tau_i = 0$. When the universe was approximately $380,000$ years old photons decoupled from electrons and were able to traverse the universe without significant interaction with electrons or any other particles. At this time, called last scatting τ_{CMB}, the universe would have had many causally disconnected regions out of thermal equilibrium. The scale factor during inflation is given by:

$$a(\tau) = -\frac{1}{H\tau} \ . \tag{3.11}$$

In an inflationary period H is approximately constant, which means that at some point in the infinite past with $\tau_i \to -\infty$ the scale factor a is 0. Likewise when $\tau = 0$ the scale factor a becomes infinite, implying inflation continuing into the infinite future. When inflation ends this expression for the scale factor breaks down. Thus the initial singularity has been pushed back to an infinite conformal time $\tau \ll 0$ and the $\tau = 0$ now represents the end of the inflationary phase. Points that appear causally disconnected are actually in causal contact because the light cones can extend back in conformal time through $\tau = 0$ to $\tau = -\infty$.

3.2 Flatness Problem Solved

Inflation also provides a solution to the Flatness problem. We have the Friedmann equation for a flat universe:

$$|1 - \Omega(a)| = \frac{1}{(aH)^2} \ . \tag{3.12}$$

If the comoving Hubble radius $(aH)^{-1}$ is decreasing then the solution $\Omega = 1$ is an attractor and the universe becomes driven towards flatness.

3.3 Kinematics of Inflation

We have seen that a shrinking Hubble parameter can result in an inflationary period that offers a solution to the horizon and flatness problems. This leads to questions about what the physical mechanism responsible for an accelerated expansion in the early universe could be. Particle physics models of inflation have been the subject of several reviews, notably in [9, 19, 20]. A universe dominated by a cosmological constant would expand at an exponential rate indefinitely and so is ruled out. We therefore conclude that, in order for the universe to experience a period of radiation dominated expansion once inflation has ended, the vacuum energy density responsible for driving inflation must be a dynamical quantity that evolves in time. We can model this dynamical evolution with a scalar field with action:

$$S = \int d^4x \sqrt{-g}\mathcal{L} \ , \tag{3.13}$$

where g is the determinant of the metric $Det(g_{\mu\nu})$ and the Lagrangian of the field is:

$$\mathcal{L} = \frac{1}{2} g^{\mu\nu} \partial_\mu \phi \partial_\nu \phi - V(\phi) \ . \tag{3.14}$$

Assuming a homogeneous scalar field, $\phi(t, \mathbf{x}) = \phi(t)$, and using the FRW metric we can assume the energy-momentum tensor takes the form of a perfect fluid, with:

$$\rho_\phi = \frac{1}{2}\dot{\phi}^2 + V(\phi) \ , \tag{3.15}$$

$$p_\phi = \frac{1}{2}\dot{\phi}^2 - V(\phi) \ , \tag{3.16}$$

so that the equation of state is ,

$$w_\phi = \frac{p_\phi}{\rho_\phi} = \frac{\frac{1}{2}\dot{\phi}^2 - V(\phi)}{\frac{1}{2}\dot{\phi}^2 + V(\phi)} \ . \tag{3.17}$$

It can be seen from Eq. (3.16) that a negative pressure can be generated with a scalar field when the potential $V(\phi)$ dominates over the kinetic term $\frac{1}{2}\dot{\phi}^2$. We therefore typically require the inflaton field to be "slowly-rolling".

3.4 Inflation: Two Dynamical Realizations

The search for a realistic particle physics construction responsible for driving slow-roll inflation has led to two distinct dynamical realizations of inflation. In the original picture, termed cold inflation, the inflaton field is treated as an isolated system, with the interactions between the inflaton and other fields only being considered when making radiative corrections to the scalar potential. The other dynamical realization is warm inflation, as originally proposed in [4, 5]. In warm inflation the interactions between the inflaton field and other fields leads to dissipation of inflaton energy, allowing particle production to occur concurrently with inflationary expansion. There are by now many models of warm inflation [21–74]. In this section we will introduce some of the key equations involved in understanding the dynamics of inflation, with a more detailed derivation of some of these equations presented in Appendix A.

3.4.1 Cold Inflation

In cold inflation the equation of motion for the inflaton field is given by:

$$\ddot{\phi} + 3H\dot{\phi} + V_{,\phi} = 0 \ , \tag{3.18}$$

with:

$$H^2 = \frac{1}{3m_p^2}\left(\frac{1}{2}\dot{\phi}^2 + V(\phi)\right) \ , \tag{3.19}$$

where we have recall the expression $m_p = 1/\sqrt{8\pi G}$ for the reduced Planck mass. If the universe is dominated by a homogeneous scalar field then the acceleration equation becomes:

$$\frac{\ddot{a}}{a} = -\frac{4\pi G}{3}(\rho_\phi + 3p_\phi) = H^2(1-\epsilon) \ , \tag{3.20}$$

where we have used the slow-roll parameter $\epsilon \equiv \frac{3}{2}(w_\phi + 1) = \frac{1}{2}\dot{\phi}^2/H^2$. We can relate this to the evolution of the Hubble parameter with the expression:

$$\epsilon = -\frac{\dot{H}}{H^2} = -\frac{d\ln H}{dN_e} \ . \tag{3.21}$$

A period of accelerated expansion will be maintained for as long as $\epsilon < 1$. This can be realized with the de Sitter condition $p_\phi \to -\rho_\phi$, in which $\epsilon \to 0$ and the kinetic energy remains subdominant to the potential $\dot{\phi}^2 \ll V(\phi)$. In order to have a sufficiently long period of accelerated expansion we require the second derivative of the inflaton field ϕ to remain small, such that:

$$|\ddot{\phi}| \ll |3H\dot{\phi}|, |V_{,\phi}| \ . \tag{3.22}$$

This requires a second slow-roll parameter:

$$\eta = -\frac{\ddot{\phi}}{H\dot{\phi}} = \epsilon - \frac{1}{2\epsilon}\frac{d\epsilon}{dN_e} < 1 \ . \tag{3.23}$$

It is shown in Appendix A that the slow-roll parameters can be expressed in terms of the shape of the shape of the potential, leading us to the slow-roll conditions:

$$\epsilon_\phi = \frac{1}{2} m_p^2 \left(\frac{V_{,\phi}}{V} \right)^2 < 1 \ , \tag{3.24}$$

$$\eta_\phi = m_p^2 \frac{V_{,\phi\phi}}{V} < 1 \ , \tag{3.25}$$

where $V_{,\phi}$ and $V_{,\phi\phi}$ are the first and second derivative of the potential with respect to the inflaton field ϕ respectively. Under these assumptions the background evolution is:

$$H^2 \approx \frac{1}{3m_p^2} V(\phi) \approx \text{constant} \ , \tag{3.26}$$

$$\dot{\phi} \approx -\frac{V_{,\phi}}{3H} \ , \tag{3.27}$$

and spacetime becomes approximately de Sitter with the scale factor $a(t) \sim e^{Ht}$. Note that the slow roll parameters that depend on the potential can be related to the Hubble slow-roll parameters $\epsilon = \epsilon_\phi$ and $\eta = \eta_\phi - \epsilon_\phi$, with inflation ending once slow-roll is violated $\epsilon = \epsilon_\phi \equiv 1$. We can calculate the number of e-folds of inflation using:

$$\begin{aligned} N(\phi) &\equiv \ln \frac{a_{end}}{a} \\ &= \int_t^{t_{end}} H dt = \int_\phi^{\phi_{end}} \frac{H}{\dot{\phi}} d\phi \approx \int_{\phi_{end}}^{\phi} \frac{V}{V_{,\phi}} d\phi \ . \end{aligned} \tag{3.28}$$

In terms of the slow-roll parameters this result can be written as:

$$N(\phi) = \int_{\phi_{end}}^{\phi} \frac{d\phi}{\sqrt{2\epsilon}} \approx \int_{\phi_{end}}^{\phi} \frac{d\phi}{\sqrt{2\epsilon_\phi}} \ . \tag{3.29}$$

In order to have enough inflation to solve the horizon and flatness problems a period of $50 - 60$ e-folds is required. Thus:

$$e^{N_e} \equiv \frac{a_{end}}{a_{start}} \approx 50 - 60 \ . \tag{3.30}$$

As has been noted, in cold inflation the inflaton is treated as an isolated system and so any other initial component of energy density is rapidly redshifted away during the expansion and the universe is left in a supercooled state. To bring the universe into a radiation-dominated era of expansion a separate phase called reheating is required once the inflationary period is over [75]. This can be achieved if, at the end of inflation, the inflaton oscillates coherently around the minimum of the potential, with the inflaton acting as pressureless matter:

$$\frac{d\bar{\rho}_\phi}{dt} + 3H\bar{\rho}_\phi = 0 \ . \tag{3.31}$$

In order for the inflaton to decay it must be coupled to other degrees of freedom, and this decay of the inflaton field alters the equation of motion for the inflaton energy density with the inclusion of a dissipation coefficient, Υ:

$$\frac{d\bar{\rho}_\phi}{dt} + (3H + \Upsilon)\bar{\rho}_\phi = 0 \ . \tag{3.32}$$

This allows for particle production to occur once inflation has ended and the standard Hot Big Bang evolution proceeds. The dissipation coefficient Υ coincides with the standard decay width of the field Γ_ϕ when the field is oscillating about the minimum. This is typically negligible during inflation since:

$$\Gamma_\phi < m_\phi \ll H \ . \tag{3.33}$$

3.4.2 Warm Inflation

Warm inflation is the realization that the interactions between the inflaton and other fields can lead to dissipation of inflaton energy to other dynamical degrees of freedom [29,76]. This means that particle production can occur concurrently with an inflationary expansion as long as the scalar potential remains the dominant component of energy density in the universe, with the ambient temperature greater than the Hubble scale. Radiation can naturally come to dominate the energy density of the universe through this particle production without the need for the separate reheating phase of cold inflation.

The simplest warm inflation scenario is the case where particles that are produced thermalize faster than the Hubble expansion, resulting in a quasi-adiabatic and near-equilibrium evolution with the leading effect being a modification to the inflaton field's equation of motion with the inclusion of a dissipation coefficient Υ that behaves as a friction term. Assuming that the produced particles are light compared to the ambient temperature (i.e. relativistic) then the inflaton's energy is dissipated into a nearly-thermal radiation bath. Under these assumptions the evolution equations for the inflaton field and the radiation energy density are:

$$\ddot{\phi} + 3H\dot{\phi} + \Upsilon\dot{\phi} + V_{,\phi} = 0 \ , \tag{3.34}$$

$$\dot{\rho}_R + 4H\rho_R = \Upsilon\dot{\phi}^2 \ , \tag{3.35}$$

where $V_{,\phi}$ is the first derivative of the scalar potential with respect to the inflaton field ϕ and the radiation energy density is given by $\rho_R = (\pi^2/30)g_*T^4$ for g_* light degrees of freedom. Defining the dissipative ratio $Q = \Upsilon/3H$ and assuming the system is in the slow-roll regime, with $\ddot{\phi} \ll 1$, these equations become:

$$3H(1+Q)\dot{\phi} \simeq -V_{,\phi} \ , \tag{3.36}$$

$$4H\rho_R \simeq \Upsilon\dot{\phi}^2 \ . \tag{3.37}$$

Slow-roll inflation is sustained in the warm regime for as long as the conditions $\eta, \epsilon < (1+Q)$ are satisfied, which, in the case of the strongly dissipative regime, with $Q \geq 1$, can be maintained without the need for any fine-tuning of the scalar potential. The subdominance of the radiation energy density to the potential can be expressed with the relation:

$$\frac{\rho_R}{\rho_\phi} \simeq \frac{\epsilon}{2}\frac{Q}{(1+Q)^2} \leq 1 \ . \tag{3.38}$$

Once the system enters the strong dissipative regime Q becomes large and the radiation energy density may increase relative to the scalar potential, allowing radiation to provide a significant fraction of the total energy density of the universe when slow-roll inflation ends with $\epsilon \sim 1+Q$. Typically if inflation ends in the strong dissipative regime, with $Q \gg 1$, then radiation will come to dominate the energy density of the universe soon after the slow-roll regime has ended [21].

3.5 Inflation Observables

A requirement of any successful physical theory is that it is consistent with observations. Cosmology is itself an observational discipline, as opposed to particle physics which primarily uses collider experiments to probe physics at higher energy scales. We have seen how an inflationary expansion in the early universe results in a universe that is naturally driven to the high levels of homogeneity and spatial flatness we observe today. In addition to this the shrinking Hubble radius also has the effect of enabling the quantum generation of cosmological fluctuations that seed the formation of large scale structure, with inhomogeneities in the inflaton field ϕ generating density perturbations that are

gravitationally unstable. Inflationary perturbations have been the subject of many reviews, particularly [77, 78].

Inflaton fluctuations arise because the inflaton is a quantum field. Heisenberg's uncertainty principle prevents the determination of the value of a field and its associated momentum with absolute certainty and so we can expect the inflaton field to have small quantum fluctuations around its homogeneous value:

$$\phi(\mathbf{x}, t) = \bar{\phi}(t) + \delta\phi(\mathbf{x}, t) \ , \tag{3.39}$$

where $\bar{\phi}(t)$ satisfies the classical equations of motion that we have analyzed in the previous sections and $\delta\phi \ll \bar{\phi}(\mathbf{x}, t)$. During an inflationary expansion the Hubble parameter H stays approximately constant, whilst the scale factor $a(t)$ increases by one e-folding in a time interval of order H^{-1}. Meanwhile, microphysical processes cannot operate on length scales greater than $\mathcal{O}(H^{-1})$. Investigating the length scales of perturbations we can consider the ratio of the physical wavenumber to the Hubble constant, given by k/aH.

In order to be causally connected, every scale in the universe must have $k/aH < 1$ prior to inflation. During the inflationary expansion the Hubble radius decreases and eventually reaches a point called horizon crossing, with $k/aH \simeq 1$. Once $k/aH > 1$ microphysical processes cannot operate and the perturbations become frozen, evolving classically and behaving as a cosmological perturbation. These classical density perturbations cause gravitational instabilities that enable the formation of large scale structure when they re-enter the horizon later on when we end up with $k/aH > 1$ again. The inflaton field fluctuations are given by:

$$\delta\ddot{\phi} + 2aH\delta\dot{\phi} + k^2\delta\phi = 0 \ , \tag{3.40}$$

with the amplitude of inflaton field fluctuations as a function of comoving scale

k given by the expression:

$$\mathcal{P}_\phi(k) = \frac{H^2}{2k^3} \propto k^{-3} \ . \tag{3.41}$$

As inflation proceeds quantum fluctuations of the inflaton field make the underlying spacetime slightly inhomogeneous. During inflation the energy density of the universe is dominated by the inflaton field so any perturbations in the inflaton field will lead to perturbations in the energy-momentum tensor and consequently in the metric of the expanding spacetime. These perturbations become stretched and amplified to macroscopic sizes with their amplitude freezing as they are stretched beyond the horizon. Perturbations of the metric, which is a tensor with 10 independent components, require a more complicated analysis than fluctuations of a single scalar field like the inflaton. The conventional approach to studying perturbations of the metric is to decompose the perturbations in terms of scalar, vector and tensor perturbations:

$$\begin{aligned} ds^2 &= g_{\mu\nu} dx^\mu dx^\nu \\ &= -(1+2\Phi)dt^2 + 2aB_i dx^i dt + a^2 \left[(1-2\Psi)d_{ij} + E_{ij}\right] dx^i dx^j \ , \end{aligned} \tag{3.42}$$

where Φ and Ψ are scalar potentials, B_i is a vector quantity and E_{ij} is a tensor quantity. Vector perturbations are not in fact generated and decay away during inflation so can be neglected, leaving only the scalar and tensor perturbations.

The generation of scalar perturbations can be understood within the context of considering different areas of the universe that have slightly different values for the inflaton field. These areas will follow the same slow-roll evolution but inflation will end at slightly different times, resulting in different regions experiencing slightly different amounts of expansion. Consequently when inflation ends there is a distribution of the energy density proportional to fluctuations in the scale

factor, causing curvature and hence density perturbations to be generated. The gauge invariant comoving curvature perturbation generated during inflation is given by:

$$\Re = \Psi - \frac{H}{\rho + p}\delta q \simeq \Psi + \frac{H}{\dot{\phi}}\delta\phi \ , \tag{3.43}$$

where δq is the scalar part of the 3-momentum density $T_i^0 = \partial_i(\delta q)$. The power spectrum for the comoving curvature perturbation is given by:

$$\mathcal{P}_\Re(k) = \left(\frac{H}{\dot{\phi}}\right)^2 \mathcal{P}_\phi \ , \tag{3.44}$$

and it is common to express this power spectrum as the resulting dimensionless power spectrum:

$$\Delta^2_\Re \equiv \frac{k}{2\pi^2}\mathcal{P}_\Re(k) = \left(\frac{H}{\dot{\phi}}\right)^2 \left(\frac{H}{2\pi}\right)^2 \ . \tag{3.45}$$

Using the slow-roll equations it can be shown that the dimensionless power spectrum can be written as:

$$\Delta^2_\Re \equiv \frac{1}{24\pi^2}\frac{V}{m_p^4}\frac{1}{\epsilon_\phi} \ . \tag{3.46}$$

An important observational measurement for particle physics models of inflation is the departure of the primordial density fluctuations from scale invariance. Deviations from scale invariance are characterized by the scalar spectral index, defined as:

$$n_s - 1 = \frac{d\ln\Delta^2_\Re}{d\ln k} \ . \tag{3.47}$$

In the slow-roll approximation this yields:

$$n_s - 1 \simeq -m_p^2\frac{V'(\phi)}{V(\phi)}\frac{1}{\Delta^2_\Re}\frac{d\Delta^2_R}{d\phi} \ , \tag{3.48}$$

$$n_s - 1 \simeq 2\eta_\phi - 6\epsilon_\phi \ . \tag{3.49}$$

Another observable of inflation is the tensor-to-scalar ratio r. Tensor perturbations of the metric are generated during inflation and result in primordial gravitational waves, just as scalar perturbations are linked to curvature perturbations. The spectrum of tensor perturbations is given by:

$$\Delta_t^2 = \frac{2H^2}{\pi^2 m_p^2} \ . \tag{3.50}$$

Defining the tensor index as $n_t = -2\epsilon_\phi$, the tensor-to-scalar ratio is given by:

$$r = 8|n_t| \ . \tag{3.51}$$

These results provide the observational predictions for slow-roll inflation in the standard supercooled regime. In warm inflation the observational predictions are modified by fluctuation-dissipation dynamics, which will be presented in the following chapter.

3.5.1 Planck Constraints

These primordial density perturbations are the seeds that will grow to become the large-scale structure of the universe as well as the perturbations in the temperature of the Cosmic Microwave Background (CMB). The recent measurements of the anisotropy of the CMB by the Planck mission support the theory of inflation, with observations pointing to models of inflation based on a slowly rolling scalar field that generates a primordial spectrum of density perturbations that is essentially adiabatic, gaussian and almost completely scale-invariant. The Planck mission has considerably narrowed down the parameter space for viable models of inflation. The most recent measurement by the Planck satellite is [3]:

$$\Delta_{\mathcal{R}}^2 = 2.2 \times 10^{-9} \ , \tag{3.52}$$

and Planck has measured the spectral index to be:

$$n_s = 0.9603 \pm 0.0073 \ . \tag{3.53}$$

To date the tensor mode has not been detected but progress has been made excluding possible regions of the parameter space to further constrain models of inflation. The regions of parameter space allowed for models of inflation is most commonly summarized by the n_s vs. r exclusion plot, shown in Fig. (3.1).

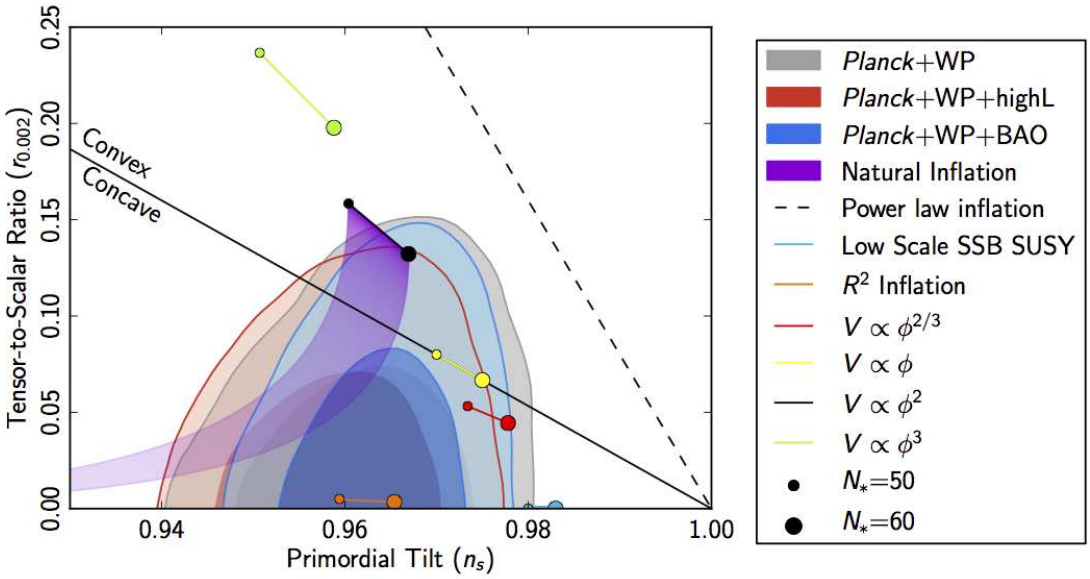

Figure 3.1: The n_s vs. r exclusion plot produced by the Planck mission measurements of the perturbations in the temperature of the Cosmic Microwave Background (CMB) [3]. The plot shows the marginalized joint 68% and 95% CL regions for n_s and r from Planck in combination with other data sets compared to theoretical predictions of inflationary models.

Chapter 4

Fluctuation Dissipation Dynamics in Warm Inflation

As we have seen in the previous chapter the interactions between the inflaton and other fields can lead to dissipative effects during the inflationary phase [79, 80] and this has motivated the construction of a robust particle physics mechanism that can enable dissipation. In this Chapter I will review the current literature regarding how dissipation of inflaton energy can be implemented in a particle physics model of inflation as well as reviewing the dynamics and observational predictions of warm inflation.

Direct dissipation of inflaton energy to light degrees of freedom is unrealistic due to the large thermal corrections to the inflaton mass that would be induced and the fact that fields coupled to the inflaton typically acquire large masses unless the couplings are suitably suppressed. Dissipation of inflaton energy to light degrees of freedom can however occur if the fields coupled to the inflaton are themselves unstable against decay into light fields. This forms the basis of what has come to be known as the two-stage decay mechanism for the inflaton [43, 52, 61, 66, 70]. The fields coupled to the inflaton acquire large masses from the inflaton vacuum expectation value (vev). These fields are then unstable against

decay into light degrees of freedom, and so mediate the transfer of inflaton energy to the light sector enabling the production of radiation. The large masses of these mediator fields means that they are effectively in a zero-temperature state, suppressing thermal corrections to the inflaton potential despite the formation of a thermal bath.

The construction of viable particle physics models of inflation often involves studying theories beyond the Standard Model of Particle Physics, with one of the most viable extensions of the Standard Model being Supersymmetry. In supersymmetric theories radiative corrections are naturally suppressed resulting in very flat scalar potentials that provide a natural framework within which particle physics models of inflation can be constructed.

4.1 Supersymmetry and Warm Inflation Model Building

Supersymmetry (SUSY) is a symmetry that relates two different classes of elementary particles, bosons (which have an integer spin) with fermions (which have half-integer spin). Under supersymmtery each of the elementary particles are paired with another particle that has spin differing by a half-integer, with supersymmetric transformations turning a bosonic state into a fermionic one, and vice versa. For each Standard Model boson there exists an accompanying fermion, and likewise a boson for each Standard Model fermion. These as of yet undiscovered particles are called the superpartners. There are, for example, "squarks" which are the superpartners of the quarks, "sleptons" which are the superpartners of the leptons and "gauginos" which are the superpartners of the gauge fields. Many extensions of the Standard Model of Particle Physics involve supersymmetry and supersymmetry itself has been the subject of many reviews, in particular [81, 82].

When supersymmetry is unbroken each of the superpartners has the same mass as the particle it is paired with. An example would be the "selectron" (the superpartner of the electron) having the same mass as the electron. The superpartners of the elementary particles of the Standard Model have never been observed, and so if supersymmetry exists then it must be broken, with the masses of the superpartners above the energies probed by collider experiments so far.

Supersymmetric theories are capable of having more than one type of supersymmetry transformation. Theories known as extended supersymmetric theories have more than one type of supersymmetry transformation with the number of supersymmetries in a theory, $\mathcal{N}$, typically being a power of 2 (i.e. $\mathcal{N} = 1, 2, 4, 8$). In the most common $\mathcal{N} = 1$ version there are "chiral" supermultiplets that contain a complex scalar field (spin 0) and a chiral fermion field (spin 1/2), and "gauge" supermultiplets that contain a gauge field (spin 1) and a gaugino field (spin 1/2). The fields of these supermultiplets are contained within a single entity called a superfield. The interactions between the bosonic and fermionic components are codified in the superpotential W, which is a function of superfields, and the kinetic terms are encoded in the Kähler potential K. We can consider a simple superpotential of the form:

$$W = g\Phi X^2 \ , \tag{4.1}$$

where Φ and X are superfields. The Lagrangian density describing interactions between the scalar components of the Φ and X superfields can be derived from the superpotential through the expression:

$$\mathcal{L}_{scalar} = \left| \frac{\partial W}{\partial \Phi_i} \right|^2_{\Phi_i = \phi_i} \ . \tag{4.2}$$

The Lagrangian density describing the interactions of the fermionic components

of the superfields can be derived from the superpotential using the expression:

$$\mathcal{L}_{fermion} = \frac{1}{2}\frac{\partial^2 W}{\partial\Phi_i \partial\Phi_j}\bar{\psi}_i P_L \psi_j \Big|_{\Phi_i=\phi_i} + \text{h.c.} \ , \tag{4.3}$$

where $P_L = (1-\gamma_5)/2$ is the left-handed chiral projector.

The relation between fermions and bosons provided by supersymmetry has important consequences for inflation model building, with the effective scalar potential receiving radiative corrections from both the bosonic and fermionic components of the superfields in the theory. When the supersymmetry is unbroken these contributions from both fermionic and bosonic components are equal but opposite, completely canceling each other. Once supersymmetry is broken this cancellation is imperfect, resulting in the radiative corrections being suppressed. It has been shown in [48] that in warm inflation supersymmetry suppresses radiative corrections, despite the finite temperature of the radiation bath, due to this imperfect cancellation between the fermionic and bosonic contributions to the radiative corrections. In a supersymmetric theory the two-stage decay chain for the inflaton can be realized with a superpotential of the form [52, 61, 66, 70]:

$$W = f(\Phi) + \frac{g}{2}\Phi X^2 + \frac{h}{2} X Y^2 \ , \tag{4.4}$$

where the inflaton field is the scalar component of the Φ chiral multiplet, with $\phi = \sqrt{2}\Phi$, the term $f(\Phi)$ contains any interactions in the inflaton sector and the scalar potential is $V(\phi) = |f'(\phi)|^2 > 0$. The bosonic and fermionic components of the X fields gain a mass $m_X \simeq (g/\sqrt{2})\phi$, which is typically large, particularly for large inflaton values. In the case of the Y bosons and fermions they remain massless and the last Yukawa term in the superpotential allows for the decays $\chi \to yy$, $\chi \to \psi_y\psi_y$ and $\psi_\chi \to y\psi_y$ where χ and ψ_χ are the bosonic and fermionic components of the X superfield, and likewise y and ψ_y are the bosonic and fermionic components of the Y superfield. We derive the Lagrangian density describing the interactions

between the inflaton vev and the scalar components of the superfields X and Y in the warm inflation superpotential to be:

$$\begin{aligned}\mathcal{L}_{scalar} &= V(\phi) + \frac{g^2}{2}\phi^2|\chi|^2 + \frac{g}{2}\sqrt{V(\phi)}(\chi^2 + \chi^{\dagger 2}) + \frac{g^2}{4}|\chi|^4 + \\ &+ \frac{h}{2}g\phi\left(\chi y^{\dagger 2} + \chi^{\dagger} y^2\right) + \frac{h^2}{4}|y|^4 + h^2|\chi|^2|y|^2 \ . \end{aligned} \tag{4.5}$$

Similarly the interactions between the scalar inflaton and the fermionic components ψ_χ and ψ_y are:

$$\mathcal{L}_{fermion} = \frac{g}{2}\phi\bar{\psi}_\chi P_L\psi_\chi + h\chi\bar{\psi}_y P_L\psi_y + \frac{h}{2}y\bar{\psi}_y P_L\psi_\chi + \text{h.c.} \ . \tag{4.6}$$

4.2 Dissipation Coefficient

Dissipation in quantum field theory has been studied in [37, 83]. The dissipation coefficient that appears in the inflaton's equation of motion in Eq. (3.34) has been computed using standard techniques of thermal field theory [52, 66, 70]. The interaction between the inflaton and the X fields leads to a modification to the inflaton's effective action at the quantum level, with the leading one-loop effect being the creation and annihilation of X-pairs coupled to the background condensate. For a static background this only leads to radiative corrections to the scalar potential [36]. For a dynamical background, like in inflation, this induces time non-local corrections to the full effective action with the creation and annihilation of X-pairs occurring at different times with different values of the background field. In the slow-roll regime the inflaton field changes by $\Delta\phi \simeq \dot{\phi}\Delta t$, resulting in the dissipation coefficient $\Upsilon\dot{\phi}$ being included in the inflaton's equation of motion. Because the inflaton field is a dynamical quantity that is evolving in time there is an asymmetry between the processes of creation and annihilation, the result of which is a net particle production that sources the radiation bath.

The dissipation coefficient itself receives contributions from both the on-shell

and off-shell modes of both the bosonic χ and fermionic ψ_χ X fields, with the leading contribution in the regime where $m_X \gtrsim T$ coming from the off-shell scalar χ mode that decays into y scalars. Thus we have a decay chain for the inflaton

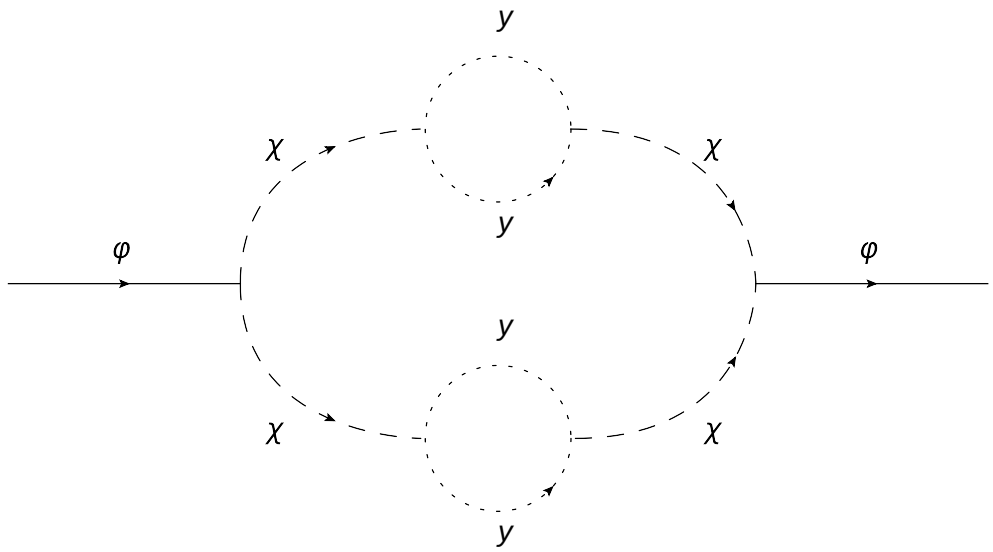

Figure 4.1: The interaction of the inflaton field ϕ with heavy fields χ that mediate dissipation of inflaton energy to light fields y. As inflation proceeds the interactions the inflaton field emits quantum fluctuations that propagate in space and time and are then reabsorbed at some later point. Because ϕ is an evolving quantity during inflation the value of ϕ changes between emission and absorption times. The result of this is that there is an asymmetry between creation and annihilation processes that produces a net particle production.

in which the fields in the X sector are unstable against decay into fields in the light Y supermultiplets, in particular with $\chi \to yy, \psi_y\psi_y$ and $\psi_\chi \to y\psi_y$. The interaction that enables this decay is shown in Fig. (4.1). The result of this is that the Y sector becomes the ultimate destination for the inflaton energy [60]. Assuming these fields thermalize via decay and scattering processes then this decay of the inflaton field sources the formation of a radiation bath. The leading bosonic contribution to the dissipation coefficient has been calculated in the low temperature regime, where $m_{\chi_{R,I}}, m_{\psi_\chi} > T$, in [66, 70], where it is shown that the fermionic contribution is subdominant. Generalizing the results in [66, 70] for

generic scalar masses gives an expression for the dissipation coefficient:

$$\begin{aligned}\Upsilon &= \Upsilon_{LM} + \Upsilon_P \\ &= \sum_{i=\chi_{R,I}} \Bigg[0.64 h^2 g^8 N_X N_Y \frac{T^3 \phi^6}{m_i^8} \\ &\quad + \frac{16}{\sqrt{2\pi}} \frac{g^2 N_X}{h^2 N_Y} \left(\frac{2g^2\phi^2}{2g^2\phi^2 + m_i^2} \right) \sqrt{T m_i} e^{-m_i/T} \Bigg] \ , \end{aligned} \tag{4.7}$$

where there are N_x fields coupled to the inflaton that have N_y decay channels. The first term in this expression, Υ_{LM}, gives the contribution mediated by the off-shell "low-momentum" modes of the mediator fields. The second term, Υ_P, gives the contribution mediated by the on-shell "pole" modes of the mediator fields. Assuming we are in the low-temperature regime, with the mass of the mediator fields being significantly large than the ambient temperature $m_\chi > T$, the dominant contribution to the dissipation coefficient comes from the low-momentum contribution Υ_{LM}. The low-momentum contribution has a dominant decay channel $\chi_{R,I} \to yy$, whilst the pole contribution has an equal contribution from both scalar and fermionic decay channels. The total decay width is given by the expression [70]:

$$\Gamma_{\chi_i} = \Gamma(\chi_i \to yy) + \Gamma(\chi_i \to \psi_y \psi_y) = \frac{h^2 N_Y}{16\pi} \left(\frac{2g^2\phi^2}{m_i} + m_i \right) \ . \tag{4.8}$$

As we can see from the expression the pole contribution is exponentially suppressed in the low temperature regime with $m_{\chi_R}/T > 1$. At the large inflaton field values that result in a large mass for the mediator field the expression for the dissipation coefficient can thus be approximated as [66, 70]:

$$\Upsilon_{LM} = C_\phi \frac{T^3}{\phi^2} \ , \qquad C_\phi = 0.08 h^2 N_X N_Y \ . \tag{4.9}$$

Details of the calculation of the dissipation coefficient can be found in [66, 70],

where the assumption has been made that a flat space computation is valid. This assumption is valid as long as the condition:

$$T > H \ , \tag{4.10}$$

is maintained. Furthermore, to ensure an adiabatic evolution of the field and expansion compared to the relevant microphysical processes and that near-thermal equilibrium configurations can be maintained during inflation we require [61]:

$$\Gamma_\chi > H, \dot{\phi}/\phi \ . \tag{4.11}$$

The dissipation coefficient is a dynamical quantity, depending on both the ambient temperature T and the value of the inflaton field ϕ, and thus evolves throughout inflation. This allows one to consider scenarios where dissipation is weak (i.e. $Q \ll 1$) at the epoch when the largest currently observable scales left the horizon, but gradually increases during the inflationary phase, entering a strong dissipative regime ($Q \gg 1$) before the end of inflation. The warm inflation requirement that the ambient temperature be greater than the Hawking temperature can, by making use of the slow-roll equations, be expressed by the condition [84]:

$$\frac{T}{H} = \frac{C_\phi}{4C_R}\left(\frac{d\log\phi}{dN_e}\right)^2 \simeq \frac{15}{8\pi^2}\left(\frac{\Delta\phi}{\phi}\right)^2 N_e^{-2}\frac{N_X}{g_*} > 1 \ . \tag{4.12}$$

In order to maintain the condition $T > H$ whilst achieving 50-60 e-folds of inflation we typically require $N_X = 10^4 - 10^6$ fields [61, 71]. This large field multiplicity is altogether not so unrealistic in scenarios where the inflaton is taken as a singlet field under the Standard Model gauge group or its extensions. In this scenario the inflaton is potentially able to interact with an abundance of additional fields typically proposed in extensions of the standard model. Furthermore in brane-antibrane systems large field multiplicities $N_X = N_c^2$ can

be found for only a moderately large multiplicity of N_c branes [68], and this will be further discussed in later chapters.

4.3 Warm Inflation Equations of Motion

The warm inflationary dynamics have been reviewed in [54,59,61]. Having set the functional form of the dissipation coefficient $\Upsilon(\phi, T)$ we can derive the equations of motion and observable predictions of warm inflation. Referring the reader to the derivation in Appendix A, the slow-roll relation between radiation energy density, the dissipative ratio Q and the evolution of the inflaton field, $4\rho_R = 3Q\dot{\phi}^2$ can all be combined to obtain an expression for the relation between Q and ϕ [61]:

$$Q^{1/3}(1+Q)^2 = 2\epsilon_\phi \left(\frac{C_\phi}{3}\right)^{\frac{1}{3}} \left(\frac{C_\phi}{4C_R}\right) \left(\frac{H}{\phi}\right)^{\frac{8}{3}} \left(\frac{m_p}{H}\right)^2 , \tag{4.13}$$

with $C_R = \rho_R/T^4 = \pi^2 g_*/30$ for g_* light degrees of freedom. This expression allows us to derive expressions for the equations of motion of the inflaton field ϕ, the dissipative ratio Q and the ratio between the ambient temperature and the Hubble parameter T/H with respect to the number of e-folds of inflation:

$$\frac{d\phi/m_p}{dN_e} = -\frac{\phi}{m_p}\frac{\sigma_\phi}{1+Q} , \tag{4.14}$$

$$\frac{dQ}{dN_e} = \frac{Q}{1+7Q}(10\epsilon_\phi - 6\eta_\phi + 8\sigma_\phi) , \tag{4.15}$$

$$\frac{d\ln T/H}{dN_e} = \frac{2}{1+7Q}\left(\frac{2+4Q}{1+Q}\epsilon_\phi - \eta_\phi + \frac{1-Q}{1+Q}\sigma_\phi\right) , \tag{4.16}$$

where the slow-roll parameters are (as defined before) $\epsilon_\phi = (m_p^2/2)(V_{,\phi}/V)^2$ and $\eta_\phi = m_p^2 V_{,\phi\phi}/V$, and we have introduced another slow-roll parameter $\sigma_\phi = m_p^2 V_{,\phi}/\phi V$. A more detailed explanation of the derivation of these equations of motion is given in Appendix B.

4.4 Warm Inflation Observables

In warm inflation, the spectrum of density perturbations is modified by fluctuation-dissipation effects [4, 5, 26, 76, 84–87], with perturbations in the field and the radiation fluid coupled through the temperature dependence of the dissipation coefficient. Inflaton perturbations are sourced by a gaussian white noise term ξ_k [5, 26, 64]:

$$\delta\ddot{\phi}_k + 3H(1+Q)\delta\dot{\phi}_k + \frac{k^2}{a^2}\delta\phi_k \simeq \sqrt{2\Upsilon T}a^{-3/2}\xi_k \ . \tag{4.17}$$

In this expression ξ_k is stochastic source term that models thermal fluctuations of the inflaton field and can be approximated by a localized gaussian distribution with correlation function [88]:

$$\langle \xi(t,x)\xi(t',x')\rangle = \delta(t-t')\delta^{(3)}(x-x') \tag{4.18}$$

In addition to this the fields in the heavy X sector are able to decay into inflaton particle states through the decay chain:

$$\chi \to yy\phi \ . \tag{4.19}$$

This enables a non-trivial distribution of inflaton particles during inflation so long as interactions between the the inflaton and light degrees of freedom in the thermal bath occurs sufficiently fast [89]. If the inflaton has a phase-space distribution n_* when observable CMB scales leave the horizon then the dimensionless power spectrum becomes [5, 26, 85, 89–91]:

$$\Delta^2_{\mathcal{R}} = \left(\frac{H_*}{\dot{\phi}_*}\right)^2 \left(\frac{H_*}{2\pi}\right)^2 \left(1 + 2n_* + \frac{2\sqrt{3}\pi Q_*}{\sqrt{3+4\pi Q_*}}\frac{T_*}{H_*}\right) \ , \tag{4.20}$$

where $_*$ indicates a quantity evaluated at the epoch when the largest currently observable scales left the horizon and $n_* = n_{BE}(a_* H_*, T_*)$ for the equilibrium Bose-Einstein distribution $n_{BE}(k,T) = (e^{k/aT} - 1)^{-1}$. In the limit that $n_*, Q_*, T_* \to 0$ then the standard cold inflation expression for the dimensionless power spectrum is recovered. Taking the limit $Q_* \ll 1$ the power spectrum becomes:

$$\Delta^2_{\Re} \simeq \left(\frac{H_*}{\dot{\phi}_*}\right)^2 \left(\frac{H_*}{2\pi}\right)^2 \left[1 + 2n_* + 2\pi Q_* \frac{T_*}{H_*}\right] \ , \tag{4.21}$$

where once again n_* gives the effect of non-trivial inflaton occupation numbers and the last term in the brackets gives the leading effect of fluctuation-dissipation dynamics. Due to their weak coupling to matter the spectrum of primordial gravity waves is not significantly altered by fluctuation-dissipation dynamics and the tensor spectrum remains in the form [84]:

$$\Delta^2_t = \frac{2H^2_*}{\pi^2 m^2_p} \ . \tag{4.22}$$

The effect of this is that the tensor to scalar ratio is reduced, with its relation to the tensor index $n_t = -2\epsilon_*$ modified from the standard cold inflation version, $r = 8|n_t|$, to:

$$r \simeq \frac{8|n_t|}{1 + 2n_* + 2Q_* T_*/H_*} \tag{4.23}$$

In our analysis of dissipative effects in inflation we will look at the simplest case, with inflaton particles not produced sufficiently fast resulting in any initial non-trivial occupation numbers being quickly redshifted away by the inflationary expansion even though the thermal bath of light particles remains in near equilibrium. Therefore in our analysis we can neglect the effect of $n_* = 0$ on the spectrum. Assuming that $Q_* \ll 1$ then the power spectrum $\Delta^2_{\Re}$ is given by the expression [89]:

$$\Delta^2_{\Re} = \frac{1}{24\pi} \frac{V(\phi_*)}{\epsilon_*} \left(1 + 2\pi Q_* T_*/H_*\right) \ . \tag{4.24}$$

The spectral index is derived from the power spectrum with:

$$n_s - 1 \simeq \frac{d\ln\Delta^2_{\mathcal{R}}}{d\ln k} \simeq -m_p^2\frac{V_{,\phi}}{V}\frac{1}{\Delta^2_{\mathcal{R}}}\frac{d\Delta^2_{\mathcal{R}}}{d\phi} \simeq 2\eta_* - 6\epsilon_* + \frac{2\kappa_*}{1+\kappa_*}(7\epsilon_* - 4\eta_* + 5\sigma_*)\ , \tag{4.25}$$

where $\kappa = 2\pi QT/H$. Again assuming $n_* = 0$ and $Q_* \ll 1$, the tensor to scalar ratio becomes:

$$r \approxeq \frac{16\epsilon_*}{1 + 2\pi Q_* T_*/H_*}\ . \tag{4.26}$$

Chapter 5

Hybrid inflation

The success of the inflationary paradigm in explaining the homogeneity and isotropy of the universe whilst also providing the mechanism for the seeding of large scale structure has motivated the search for a well defined particle physics description of inflation. The embedding of inflationary physics within a quantum field theory framework that describes high energy physics processes can have particular significance for the specific details about how the universe enters into the standard hot big bang evolution once inflation has ended, as well as the characteristics of the small density perturbations that end up seeding the observed large scale structure in the universe along with the temperature anisotropies in the cosmic microwave background radiation. Furthermore, precision measurements of the temperature anisotropies may allow one to differentiate between different particle physics models of inflation.

One of the best motivated particle physics models of inflation is hybrid inflation [6] due to the ease at which hybrid models can be embedded in various high energy physics frameworks like supersymmetry, supergravity, grand unified theories and extra dimensional theories. Combining the features of a slowly evolving scalar field typical of inflationary scenarios with an ending of inflation due to spontaneous symmetry breaking, hybrid inflation involves the scalar

inflaton field being coupled to one or more scalar fields with a Higgs-like potential, known as the waterfall field(s). Whilst the scalar inflaton field is responsible for driving slow-roll inflation, the waterfall field(s) acquires its mass from the vacuum expectation value of the inflaton and is responsible for ending inflation. Initially the inflaton is displaced from its minimum at some large field value. The waterfall fields become heavy and are kept at the metastable minimum with a non-zero vacuum energy. As inflation proceeds the inflaton rolls down the nearly flat potential until it reaches a critical value $\phi = \phi_c$. At this point the mass squared of the waterfall field becomes negative and the tachyonic instability in the waterfall field drives the system to global minimum, ending inflation in a process called the waterfall transition. Hybrid models have been extensively discussed in the literature [92–104]. Our motivation will be the implementation of hybrid inflation in the warm regime and we will investigate the dynamics and observational predictions of hybrid inflation.

In this Chapter I will introduce the original 2-field model of hybrid inflation, originally proposed in [6], and then the supersymmetric version. I will then discuss how hybrid inflation provides a natural framework in which warm inflation can be realized. Finally I will study the warm hybrid inflation dynamics at large field values, which has previously been done in [61], and present the numerical results that I produced. The results presented in this Chapter are also presented in [73].

5.1 Original 2-field Model

The original hybrid model, proposed by Linde [6] in the early 1990s as a way to end inflation with spontaneous symmetry breaking and a phase transition, simply involved two coupled scalar fields, with one acting as the scalar inflaton ϕ and one acting as the waterfall field χ. The interaction between the scalar inflaton

field and the waterfall field can be described with the hybrid potential:

$$V(\phi,\chi) = \frac{1}{2}m^2\phi^2 + \frac{\lambda}{4}(\chi^2 - M^2)^2 + \frac{g}{2}\phi^2\chi^2 \ , \tag{5.1}$$

where λ and g are coupling constants and M is a mass parameter that sets the

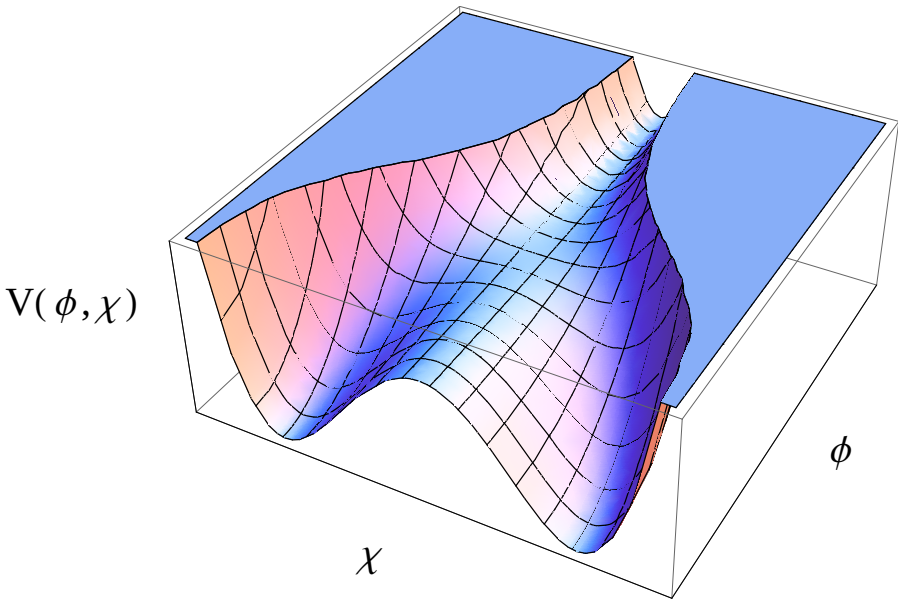

Figure 5.1: The inflaton rolls down the nearly flat potential until it reaches a critical value, triggering the waterfall transition and the end of inflation.

scale of inflation. This hybrid potential is shown in Fig. (5.1). One can include other terms in this potential and go beyond this lagrangian to study a more general inflaton potential, but we will focus on potential shown. In this setup inflation proceeds in the false vacuum along the valley $\langle\chi\rangle = 0$ until the scalar inflaton field ϕ reaches a critical value given by:

$$\phi^2 = \phi_c^2 = \frac{\lambda M^2}{g} \ . \tag{5.2}$$

At this point the waterfall field χ develops a tachyonic instability and the false vacuum can no longer be sustained, with the system driven to the global minimum in a process called the waterfall, or hybrid, transition, with $\langle\phi\rangle = 0$

and $\langle\chi\rangle = \pm M/\lambda^{1/2}$. The universe can then enter into a radiation dominated era of expansion through the standard reheating process, with the inflaton and waterfall fields oscillating coherently around the minimum of the potential.

5.2 Supersymmetric Hybrid Model

Realistic implementations of hybrid inflation must have a flat enough potential in the $\langle\chi\rangle = 0$ valley to enable the inflaton field to slowly-roll for approximately $50 - 60$ e-folds of inflation after the epoch when the largest currently observable scales left the horizon. As we have seen the coupling between the inflaton field and the waterfall fields in hybrid inflation determines the mass of the waterfall field and hence the stability of the metastable inflationary minimum of the potential. Another consequence of this coupling between the two fields is the generation of quantum corrections to the inflaton effective action, with the most widely studied effect being the generation of radiative corrections to the scalar potential. In supersymmetric models of hybrid inflation the finite vev of the inflaton field spontaneously breaks supersymmetry, with supersymmetry only restored at the minimum of the potential. This broken supersymmetry results in an imperfect cancellation between fermionic and bosonic contributions to the radiative corrections to the scalar potential, resulting in a scalar potential flat enough once radiative corrections are included to allow for a sufficiently long period of slow-roll inflation. This has motivated the construction of a supersymmetric hybrid inflation model. Hybrid inflation can naturally be implemented within a supersymmetric model with a superpotential of the form [95–104] shown below:

$$W = g\Phi(X^2 - M^2), \tag{5.3}$$

where we have chiral superfields Φ, corresponding to the inflaton sector, and X, corresponding the waterfall sector, with g as a coupling. If we take the classical

scalar inflaton vacuum expectation value to be $\phi = \sqrt{2}\langle\Phi\rangle$, the scalar components in the waterfall sector to be χ and a single species within each sector, we obtain the interactions:

$$\mathcal{L}_{scalar} = 2g^2\phi^2|\chi|^2 + g^2|\chi^2 - M^2|^2 + \text{h.c.} \ . \tag{5.4}$$

Likewise, if we consider a single species in each sector, the interactions involving the fermionic components of the Φ and X superfields are given by:

$$\mathcal{L}_{fermion} = \sqrt{2}g\phi\bar{\psi}_\chi P_L\psi_\chi + \text{h.c.} \ . \tag{5.5}$$

From the interactions in Eqs. (5.4) and (5.5) we can easily deduce that the fields within the waterfall sector acquire the masses:

$$\begin{aligned} m^2_{\chi_R} &= 2g^2(\phi^2 - M^2) \ , \\ m^2_{\chi_I} &= 2g^2(\phi^2 + M^2) \ , \\ m^2_{\psi_\chi} &= 2g^2\phi^2 \ , \end{aligned} \tag{5.6}$$

where we have a complex scalar field $\chi = (\chi_R + i\chi_I)/\sqrt{2}$ that keeps the supertrace $\text{Str}M_X^2 = m^2_{\chi_R} + m^2_{\chi_I} - 2m^2_{\psi_\chi} = 0$. It can be seen that for inflaton field values below a critical value $\phi < \phi_c = M$ the ground state of the system is the minimum at $\chi = M$ and $\phi = 0$. For large field values above this critical value, $\phi > \phi_c = M$, the scalar potential for the waterfall fields has a non-SUSY minimum at the origin with a potential energy $V_0 = g^2M^4$. During inflation the inflaton field is initially displaced at some point above the critical value $\phi > \phi_c$. As inflation proceeds the inflaton rolls down the scalar potential until it reaches the critical value ϕ_c. At this point the tachyonic instability in the waterfall field drives the system to a global SUSY minimum ending inflation with the waterfall transition.

This supersymmetric hybrid potential has a local minimum at large values

of the inflaton field ϕ, and at tree level the potential is given by the constant V_0, providing a flat direction for inflation. The coupling between the inflaton and the waterfall fields however leads to the generation of radiative corrections, which have the effect of lifting the scalar potential. The bosonic and fermionic components of the X superfield will therefore contribute to the inflaton effective potential via the standard Coleman-Weinberg contribution at order 1-loop [105]. The full inflaton potential is given by the sum of the constant tree level term and the Coleman-Weinberg potential, given as:

$$V(\phi) = V_0 + \frac{N_X}{64\pi^2} \sum_{i=\chi_{R,I},\psi_\chi} m_i^4 \left[\log\left(\frac{m_i^2}{\mu^2}\right) - \frac{3}{2} \right] \ , \tag{5.7}$$

where the renormalization scale is given by μ.

5.3 Implementation of Warm Inflation in SUSY Hybrid

Hybrid models of inflation are a natural scenario in which warm inflation can be realized, and have been previously studied in [49,61] (see also [39]). We have seen how the coupling between the inflaton and the waterfall fields determines the mass of the waterfall fields and the stability of the inflationary minimum. Furthermore we have seen how the interactions between the inflaton and waterfall fields leads to radiative corrections to the scalar potential, tilting the potential in the $\langle\chi\rangle = 0$ valley enabling inflation to proceed with the inflaton field ϕ rolling towards the critical value.

In addition to these effects the coupling between the inflaton and the waterfall fields leads to non-local corrections to the quantum effective action of the inflaton field, which may lead to dissipative effects. Warm inflation can therefore be implemented within a hybrid model, with dissipation of inflaton energy to other

dynamical degrees of freedom, which may be the waterfall fields themselves or other fields coupled to waterfall sector. Assuming these degrees of freedom thermalize faster than the expansion rate this allows for the formation of a radiation bath that counteracts the diluting effect of the Hubble expansion results in an ambient temperature greater than the Hubble scale, $T/H > 1$, typical of warm inflation.

The perturbation spectra and dynamics of hybrid inflation in the warm regime have been analyzed previously with the approximate forms of the effective potential and dissipation coefficient at large inflaton field values in [61]. In order to implement hybrid inflation in the warm regime we take the inflaton to be a singlet field so as to prevent large radiative corrections destroying the flatness of the scalar potential. The waterfall fields may however be charged under the Standard Model or GUT gauge groups, and are thus able to interact with ordinary matter and gauge particles. This makes hybrid inflation a natural framework within which warm inflation can be implemented, with the inflaton being coupled to waterfall fields that are unstable against decay into light fields and are thus capable of mediating dissipation of inflaton energy to the light sector.

In hybrid inflation we have seen that inflation starts with the inflaton field ϕ displaced at some sufficiently large value such that $\phi \gg \phi_c = M$. At these large field values the waterfall fields can acquire masses that are large compared to the ambient temperature, so that any contribution to the inflaton effective potential is Boltzmann-suppressed and the flatness of the potential is maintained. This allows warm inflation to be naturally implemented within the hybrid model, with the waterfall fields dissipating the inflaton energy into light degrees of freedom

Warm hybrid inflation can be implemented with the standard SUSY-hybrid superpotential plus a Yukawa interaction term [52, 61, 66, 70]:

$$W = g\Phi(X^2 - M^2) + hXY^2 \ , \tag{5.8}$$

where we have chiral superfields Φ, X and Y corresponding to the inflaton, waterfall and the light sectors and the last term allows the waterfall field to mediate dissipation of inflaton energy to the light sector Y. Once again M is a constant mass parameter setting the scale of inflation and g and h are real couplings (see [69] for imaginary couplings). We will consider N_X species of waterfall supermultiplets and N_Y light species with interactions given in terms of the coupling constants g and h. With the inclusion of the Yukawa interaction the scalar interactions become similar to those in Eq. (5.4):

$$\begin{aligned}\mathcal{L}_s &= 2g^2\phi^2|\chi|^2 + g^2|\chi^2 - M^2|^2 + \sqrt{2}hg\phi\left(\chi y^{\dagger 2} + \chi^\dagger y^2\right) \\ &\quad + h^2|y|^4 + 4h^2|\chi|^2|y|^2 \ . \end{aligned} \tag{5.9}$$

These interactions are once again written for single species in the X and Y sectors, but in general we will be considering N_X species of waterfall supermultiplets and N_Y light species. Likewise the interactions of the fermionic components are similar to those in Eq. (5.5):

$$\mathcal{L}_{fermion} = \sqrt{2}g\phi\bar{\psi}_\chi P_L\psi_\chi + 2h\chi\bar{\psi}_y P_L\psi_y + hy\bar{\psi}_y P_L\psi_\chi + \text{h.c.} \ . \tag{5.10}$$

The fields in the waterfall sector will acquire the same masses as in the standard supercooled scenario, given in Eqs. (5.6), and the inflaton effective potential at 1-loop is once again given by Eqs. (5.7).

5.4 SUSY Hybrid Dynamics at Large Field Values

Typically we are interested in starting our analysis of the inflationary system with a large value for the inflaton field ϕ, and so making the assumption that $\phi \gg M$

allows us to simplify the potential in Eqs. (5.7) to be:

$$V(\phi) = V_0 \left[1 + \gamma \log\left(\frac{\phi}{\mu}\right)\right] \ , \tag{5.11}$$

with $\gamma = g^2 N_X/(4\pi^2)$ controlling the size of radiative corrections.

5.4.1 Cold SUSY Hybrid

The dynamics of SUSY hybrid inflation in the standard supercooled regime, with $T \ll H$, was first analyzed in [92]. Assuming that the dominant effect of the coupling between the inflaton and the waterfall fields is radiative corrections then the effective potential in the large field limit takes the form Eqs. (5.11). In the standard supercooled scenario dissipative effects are negligible, and assuming that the radiative corrections to the scalar potential are small in comparison to the constant tree level term, $V_0 = g^2 M^4$, then we can approximate our slow-roll parameters to be:

$$\epsilon_\phi \simeq \frac{\gamma^2}{2}\left(\frac{M_P}{\phi}\right)^2 \ , \qquad \eta_\phi \simeq -\gamma\left(\frac{M_P}{\phi}\right)^2 \ . \tag{5.12}$$

It can be approximated that inflation will end when the inflaton field reaches a value $\phi_e \simeq \gamma/\sqrt{2}$. The number of e-folds of inflation since the epoch when the largest currently observable scales left the horizon, with $\phi = \phi_* \gg \phi_e$, can be calculated with:

$$N_e \simeq -M_P^{-2}\int_{\phi_*}^{\phi_e} \frac{V}{V_\phi} d\phi \simeq \frac{1}{2\gamma}\frac{\phi_*^2}{M_P^2} \ . \tag{5.13}$$

The amplitude of the spectrum of density perturbations can be found by approximating the potential as the constant term V_0 and the spectral index and

tensor-to-scalar ratio, assuming γ is small, are given by:

$$n_s - 1 = 2\eta_{\phi_*} - 6\epsilon_{\phi_*} \simeq -\frac{1}{N_e} \ , \qquad r = 16\epsilon_{\phi_*} \simeq 4\gamma(1 - n_s) \ . \tag{5.14}$$

When calculating the spectral index for $N_e > 50$ e-folds of inflation we find $n_s > 0.98$, which is excluded by the observations of the Planck satellite at 95% C.L [3].

5.4.2 Warm SUSY Hybrid

Studying SUSY hybrid inflation in the warm regime at large field values allows some simplifications to be made. Significantly the masses of the waterfall fields are significantly greater than the ambient temperature. Generically the leading contribution to dissipation comes from the low-momentum off-shell modes of the waterfall fields for large values of the inflaton field ϕ with $m_\chi/T > 1$. We can therefore approximate the dissipation coefficient in the large field limit with the low-momentum contribution taking the form in Eq. (4.9). Using this large field form of the dissipation coefficient in the slow-roll equations of motion for warm inflation we can derive the following relations that express both the field and the temperature as a function of the dissipative ratio Q [61]:

$$\begin{aligned} \frac{T}{H} &= \left(\frac{3}{2C_R}\right)^{1/4} \frac{Q^{1/4}}{(1+Q)^{1/2}} \left(\frac{V(\phi)}{3M_P^4}\right)^{-1/4} \epsilon_\phi^{1/4} \ , \\ Q^{1/3}(1+Q)^2 &= 2\epsilon_\phi \left(\frac{C_\phi}{3}\right)^{1/3} \left(\frac{C_\phi}{4C_R}\right) \left(\frac{H}{M_P}\right)^{2/3} \left(\frac{\phi}{M_P}\right)^{-8/3} \ , \end{aligned} \tag{5.15}$$

which leads to the expression:

$$\frac{Q'}{Q} \simeq C_Q \frac{Q^{1/7}(1+Q)^{6/7}}{1+7Q} \ , \tag{5.16}$$

where Q' is the derivative of the dissipative ratio with respect to the number of e-folds, Q_* is the dissipative ratio at the epoch when the largest currently observable scales left the horizon, the prime denotes a derivative with respect to the number of e-folds and $C_Q = 14\gamma(M_P/\phi_*)^2 Q_*^{-1/7}(1+Q_*)^{-6/7}$. This expression shows that the dissipative ratio Q grows during the inflationary period, and so a regime where dissipation is initially weak, with $Q_* \ll 1$, can evolve into a strongly dissipative one, with $Q \gg 1$. Assuming dissipation was weak when the largest currently observable scales left the horizon the number of e-folds of inflation is given by the expression:

$$N_e \simeq \frac{1}{2\gamma}\frac{\phi_*^2}{M_P^2}\left[1 + (\log Q_e - b)Q_*^{1/7}\right] \ , \tag{5.17}$$

with the parameter $b = 1 + \gamma_E + \psi(0, 6/7) \simeq 0.74$. We can see that dissipative effects enhance the number of e-folds of inflation for $Q \gg 1$ by comparing this expression with one for the standard supercooled evolution in Eq. (5.13). The inflationary period ends close to the hybrid transition when the radiative corrections to the scalar potential become significant and the slow-roll conditions are violated. This will occur as the inflaton field ϕ approaches its critical value $\phi_e = \phi_c = M$, at which point the dissipative ratio can be approximated to be $Q_e \simeq (\phi_*/M)^2 Q_*^{1/7}$. This value is typically large if dissipation was not too weak when the largest currently observable scales left the horizon. In warm inflation the scalar spectrum takes the approximate form in Eq. (4.24). In the large field limit the expressions for the spectral index and the tensor-to-scalar ratio are given by:

$$\begin{aligned} n_s - 1 &\simeq 2\eta_{\phi_*} - 6\epsilon_{\phi_*} + \frac{\kappa_*}{1+\kappa_*}\left(14\epsilon_{\phi_*} - 8\eta_{\phi_*} + 10\sigma_{\phi_*}\right) \\ &\simeq -2\gamma\left(\frac{M_P}{\phi_*}\right)^2\left(\frac{1-8\kappa_*}{1+\kappa_*}\right) \ , \end{aligned} \tag{5.18}$$

$$r \simeq \frac{16\epsilon_{\phi_*}}{1+\kappa_*} \simeq \frac{4\gamma(1-n_s)}{1-8\kappa_*} \ , \tag{5.19}$$

where once again we have used the slow-roll parameter $\sigma_\phi = M_P^2 V_\phi/(V\phi)$ and $\kappa_* = 2\pi Q_* T_*/H_*$. The spectrum of density perturbations can be similar in the warm and cold regimes providing $\kappa_* \ll 1$, however with a larger number of e-folds in warm inflation due to dissipative effects. Conversely, if $\kappa_* > 1/8$ then the spectrum becomes blue-tilted, which is disfavored by the observations of the Planck satellite and we will restrict ourselves to scenarios where dissipation was weak when the largest currently observable scales left the horizon with $\kappa_* \ll 1$.

Fig (5.2-5.7) show the evolution of various quantities using the warm inflation slow-roll equations of motion in the large field approximation, with dissipation coefficient $\Upsilon = C_\phi T^3/\phi^2$ and the potential given in Eq. (5.11). The initial conditions have been chosen so as to obtain a spectral index and tensor-to-scalar ratio in agreement with the observations of the Planck satellite, with $n_s \simeq 0.962$, $r \simeq 0.019$. The evolution is compared with the cold inflation evolution for the same initial conditions.

It can be seen in Fig (5.6) that the condition $m_{\chi_R}/T > 1$ becomes violated after approximately 50 e-folds of inflation, invalidating the analysis after this point. Once the mass of the real scalar component of the waterfall field becomes less than the ambient temperature the system will no longer be in the low temperature regime and thermal corrections will start to destroy the flatness of the potential. This analysis has however only included dissipation mediated by the off-shell modes of the waterfall field. As the masses of the waterfall fields becomes smaller dissipation mediated through the on-shell modes will become more significant, and the effect of this will be investigated in Chapter 7.

The evolution shows dissipative effects significantly delaying the onset of the waterfall transition in comparison to the standard cold inflation evolution. The ratio between the ambient temperature and the Hubble parameter, T/H, increases during the inflationary period, with the dissipative ratio Q also increasing as the system enters into the strong dissipative regime approximately

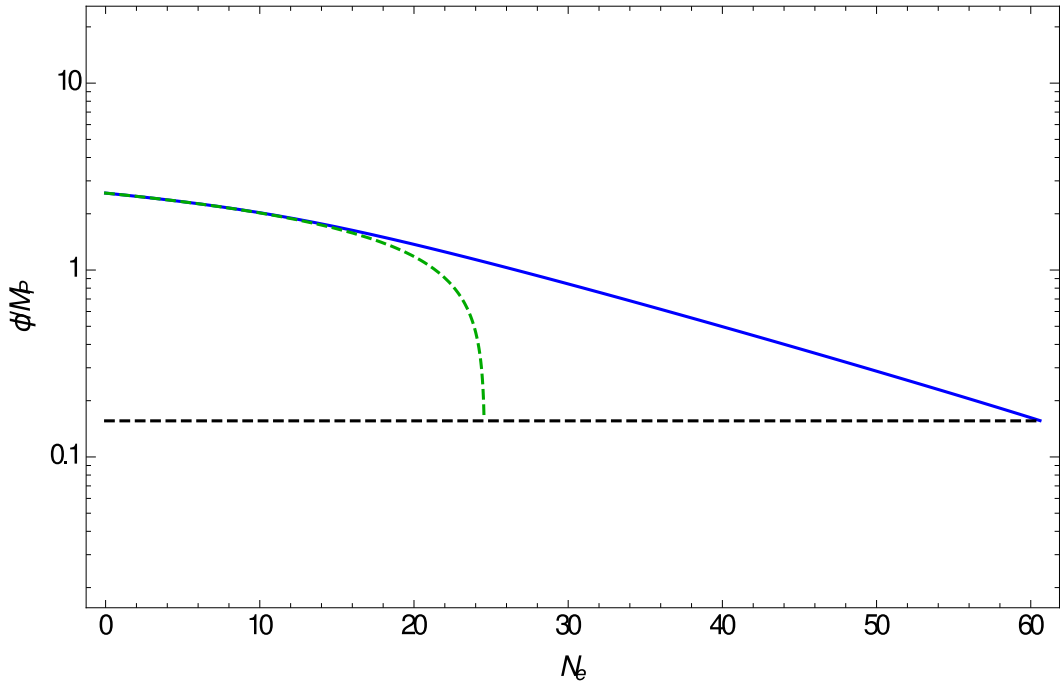

Figure 5.2: Numerical evolution of the inflaton field value ϕ in both the warm regime with $\Upsilon = C_\phi T^3/\phi^2$ (blue), and the cold regime (dashed green) and we have included the the value of the mass scale M (black dashed line). For this example, $g = 10^{-3}$, $h = 0.34$, $N_X = 5 \times 10^6$, $N_Y = 50$ and $M = 0.16 M_P$, choosing $Q_* \simeq 10^{-3}$. For this choice of parameters, the spectral index is $n_s \simeq 0.962$ and the tensor-to-scalar ratio $r = 0.019$, with the amplitude of the power spectrum normalized to the observational value $\Delta^2_{\mathcal{R}} \approx 2.2 \times 10^{-9}$.

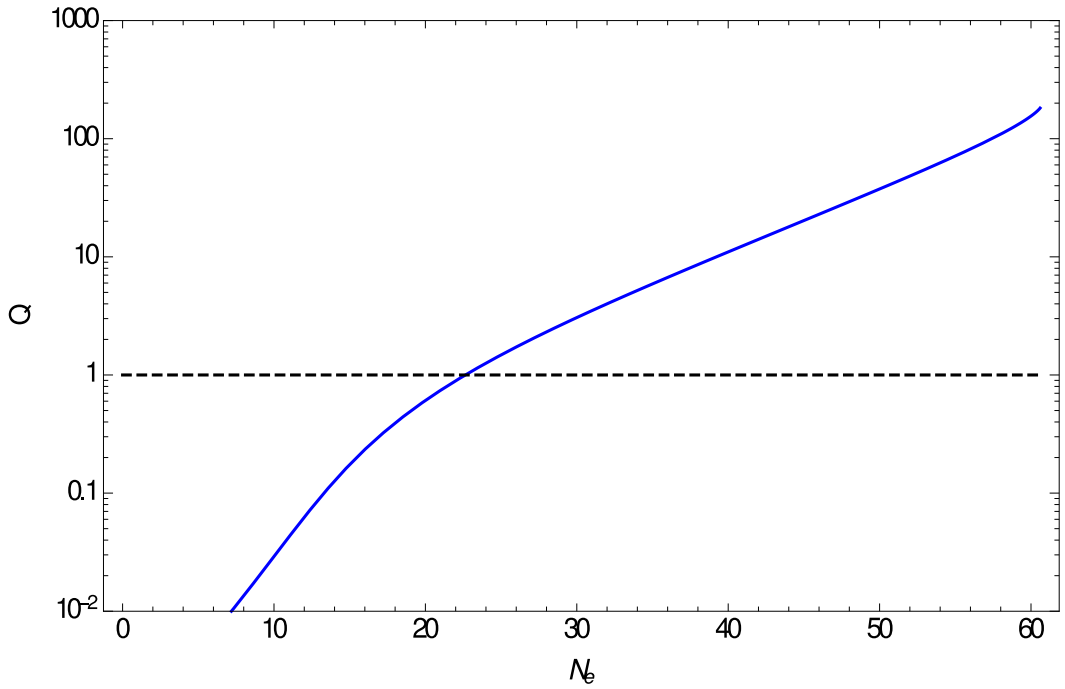

Figure 5.3: Numerical evolution of the dissipative ratio Q using the slow-roll equations for $\Upsilon = C_\phi T^3/\phi^2$. For this example, $g = 10^{-3}$, $h = 0.34$, $N_X = 5 \times 10^6$, $N_Y = 50$ and $M = 0.16 M_P$, choosing $Q_* \simeq 10^{-3}$. For this choice of parameters, the spectral index is $n_s \simeq 0.962$ and the tensor-to-scalar ratio $r = 0.019$, with the amplitude of the power spectrum normalized to the observational value $\Delta^2_{\mathcal{R}} \approx 2.2 \times 10^{-9}$.

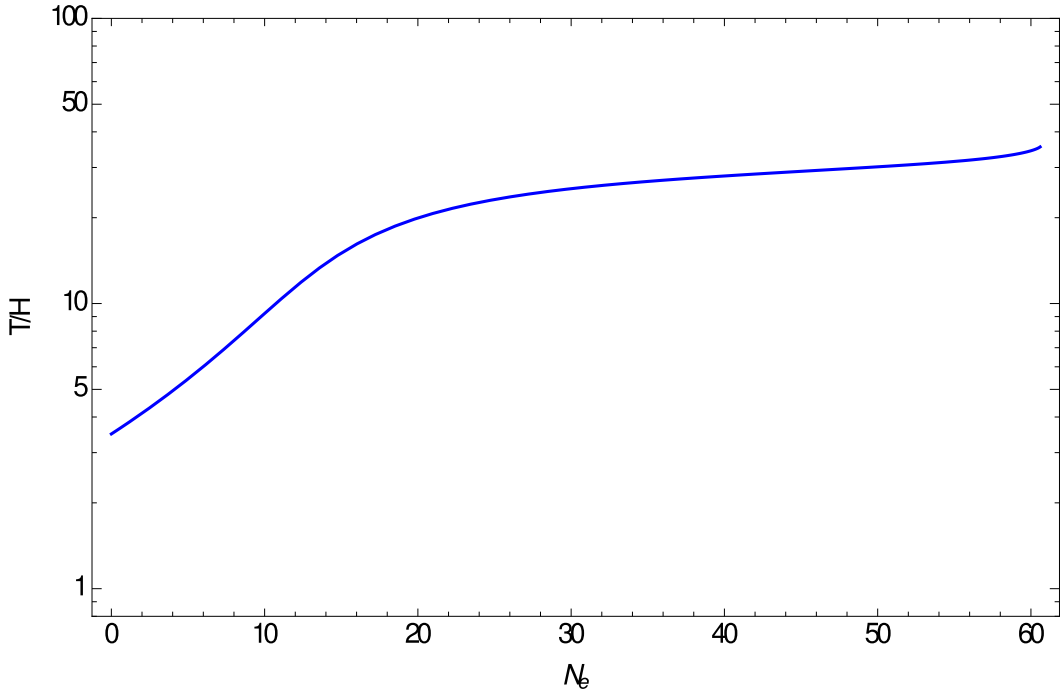

Figure 5.4: Numerical evolution for T/H using the slow-roll equations for $\Upsilon = C_\phi T^3/\phi^2$. For this example, $g = 10^{-3}$, $h = 0.34$, $N_X = 5 \times 10^6$, $N_Y = 50$ and $M = 0.16 M_P$, choosing $Q_* \simeq 10^{-3}$. For this choice of parameters, the spectral index is $n_s \simeq 0.962$ and the tensor-to-scalar ratio $r = 0.019$, with the amplitude of the power spectrum normalized to the observational value $\Delta^2_{\mathcal{R}} \approx 2.2 \times 10^{-9}$.

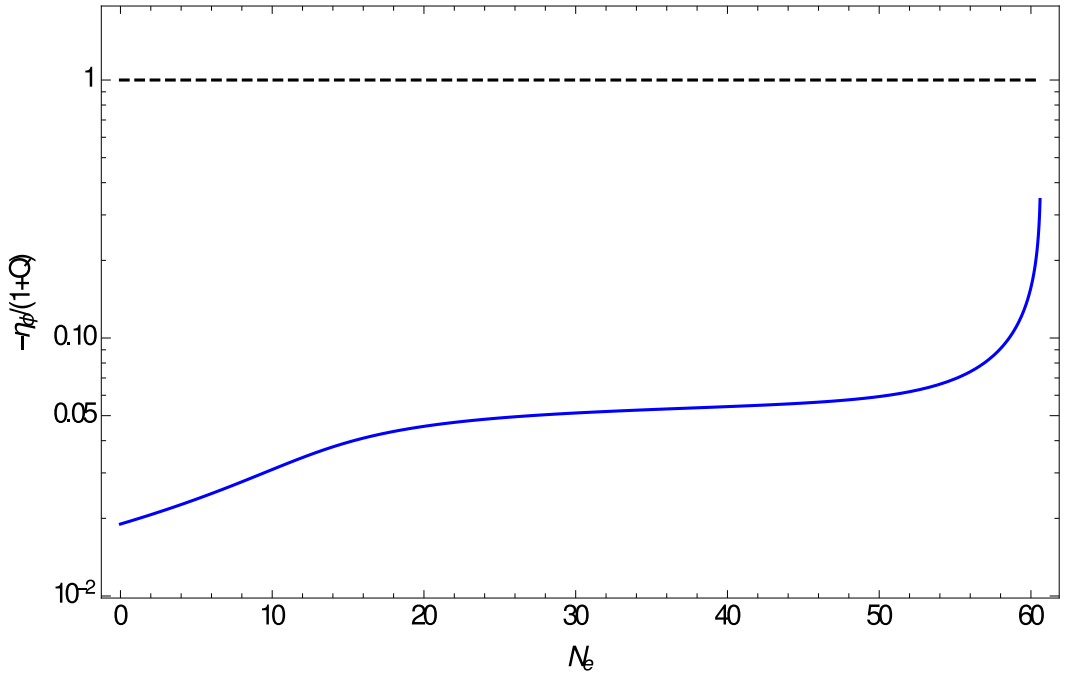

Figure 5.5: Numerical evolution for $-\eta_\phi/(1+Q)$ using the slow-roll equations for $\Upsilon = C_\phi T^3/\phi^2$. For this example, $g = 10^{-3}$, $h = 0.34$, $N_X = 5\times 10^6$, $N_Y = 50$ and $M = 0.16 M_P$, choosing $Q_* \simeq 10^{-3}$. For this choice of parameters, the spectral index is $n_s \simeq 0.962$ and the tensor-to-scalar ratio $r = 0.019$, with the amplitude of the power spectrum normalized to the observational value $\Delta^2_{\mathcal{R}} \approx 2.2\times 10^{-9}$.

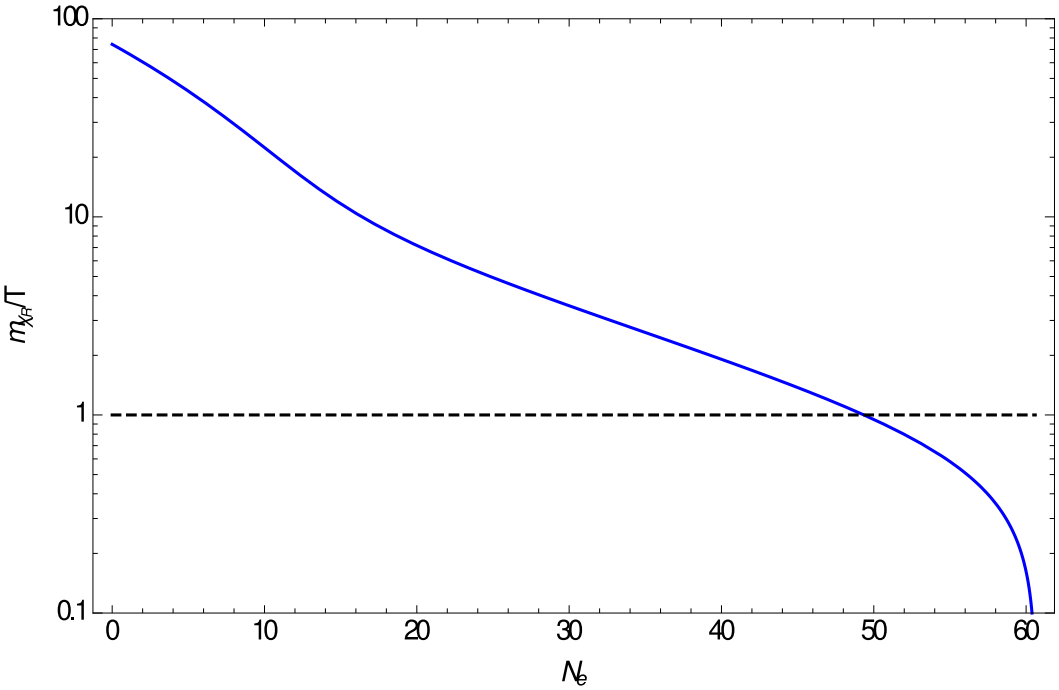

Figure 5.6: Numerical evolution for m_{χ_R}/T using the slow-roll equations for $\Upsilon = C_\phi T^3/\phi^2$. For this example, $g = 10^{-3}$, $h = 0.34$, $N_X = 5 \times 10^6$, $N_Y = 50$ and $M = 0.16 M_P$, choosing $Q_* \simeq 10^{-3}$. For this choice of parameters, the spectral index is $n_s \simeq 0.962$ and the tensor-to-scalar ratio $r = 0.019$, with the amplitude of the power spectrum normalized to the observational value $\Delta^2_{\mathcal{R}} \approx 2.2 \times 10^{-9}$.

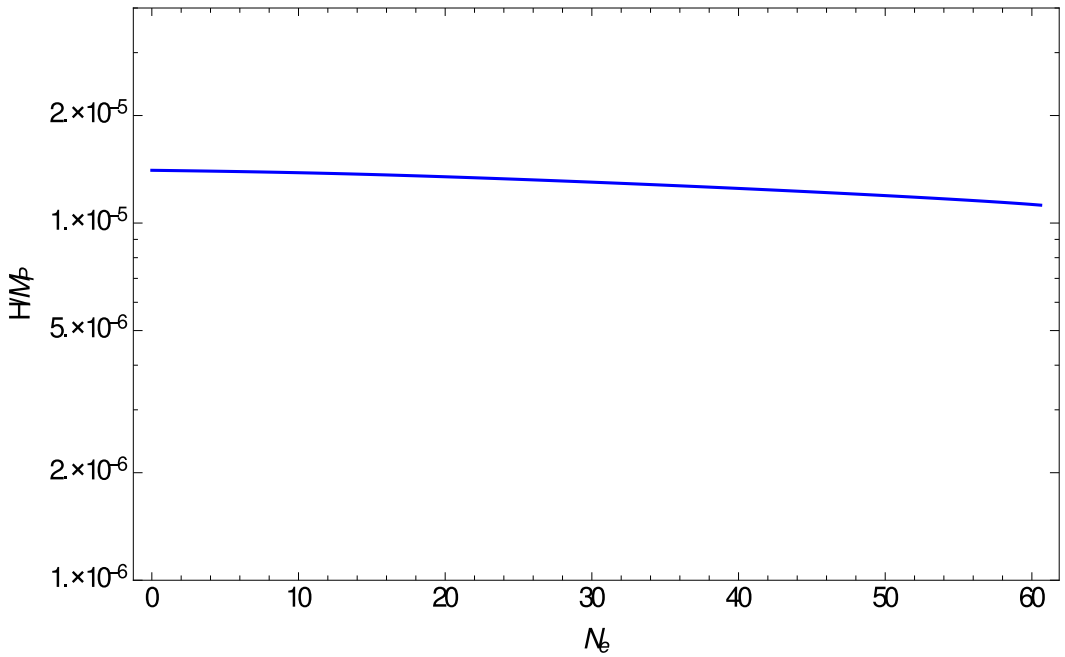

Figure 5.7: Numerical evolution of the Hubble parameter H using the slow-roll equations for $\Upsilon = C_\phi T^3/\phi^2$. For this example, $g = 10^{-3}$, $h = 0.34$, $N_X = 5 \times 10^6$, $N_Y = 50$ and $M = 0.16 M_P$, choosing $Q_* \simeq 10^{-3}$. For this choice of parameters, the spectral index is $n_s \simeq 0.962$ and the tensor-to-scalar ratio $r = 0.019$, with the amplitude of the power spectrum normalized to the observational value $\Delta^2_{\mathcal{R}} \approx 2.2 \times 10^{-9}$.

20 e-folds of inflation into the numerical evolution. The relative abundance of radiation with respect to the potential also increases during inflation, rising towards the end as the system approaches the waterfall transition.

Chapter 6

Finite Temperature Corrections and the CJT Formalism

Models of warm inflation have the inflaton field decaying by a two stage mechanism, whereby the fields coupled to the inflaton mediate the transfer of inflaton energy to the light sector. This is known as the two-stage mechanism and typically proceeds with the inflaton decaying into a heavy particle which then decays into a light one. As we have seen the interactions for this decay chain can be realized with the warm inflation superpotential:

$$W = g\Phi(X^2 - M^2) + hXY^2 \ , \tag{6.1}$$

where the X sector contains a heavy χ boson, and the last term allows the χ field to decay to light degrees of freedom in the Y sector, with the dissipation associated with the decay chain $\phi \to \chi \to y$. The fact that the light fields act as the ultimate destination for the inflaton energy means that we have to consider whether excitations in the light sector enhance the loop corrections to the scalar potential driving inflation, and so we must understand how thermal field theory affects the inflationary dynamics.

In this Chapter I will introduce the Thermal Field Theory we have used to study Finite Temperature corrections to the waterfall field masses in warm hybrid inflation. I will then discuss negative entropy problems that we encountered with our original evaluation of the effective potential. Following this I will introduce some of the details of the CJT formalism and explain how its implementation removes regions of negative entropy from the parameter space when we are studying thermal corrections in the warm hybrid model.

6.1 Finite Temperature Corrections

In hybrid inflation in the warm regime the dissipation of inflaton energy, mediated by the waterfall fields to fields in the light sector, sources the formation of a thermal bath with a slowly varying temperature. The interaction between the waterfall fields and the light degrees of freedom contained within the thermal bath will induce thermal corrections to the masses of the waterfall fields. Thermal corrections to the X, Y and inflaton sectors are generically given by the expression [106]:

$$\Delta V_i^{(T)} = \frac{T^4}{2\pi^2}\mathrm{Str}\int_0^\infty dx x^2 \log\left(1 \mp e^{-\sqrt{x^2+m_i^2/T^2}}\right) \ . \tag{6.2}$$

The overall leading contribution from relativistic fields is of the form $-(\pi^2/90)g_* T^4$, where we have $g_* = g_b + (7/8)g_f$ bosonic and fermionic relativistic degrees of freedom [107]. In the case of non-relativistic fields, such as the waterfall fields with their mass being significantly larger than the ambient temperature, this contribution to the effective potential is Boltzmann-suppressed and the leading contribution is given by the zero-temperature Coleman-Weinberg potential. The decay mechanism for the inflaton therefore involves different sectors that contribute as either relativistic fields, as in the case of the light degrees of freedom that act as the ultimate destination of inflaton energy, or as non-relativistic fields,

with the waterfall fields that mediate dissipation of inflaton energy to the light sector effectively in a zero-temperature state with $m_\chi/T \gg 1$.

Thermal corrections in the warm hybrid construction have been analyzed in [48]. As mentioned, we are interested in implementing warm inflation in a hybrid construction where the fields in the X sector are heavier than the ambient temperature, resulting in any thermal corrections to the inflaton mass being Boltzmann-suppressed. Likewise, since the waterfall fields are effectively in a zero-temperature state the leading contribution to the effective potential is the Coleman-Weinberg Potential in Eq. (5.7).

The Yukawa interactions between the fields in the X and Y sector, which are massless at tree level, lead to thermal corrections to the two-point correlation functions of the waterfall fields, resulting in thermal mass corrections to the field propagators. The result of this is that the zero-temperature Coleman-Weinberg contribution to the effective potential coming from the interaction between the inflaton and waterfall sectors should include full thermal masses, even though the waterfall fields are themselves are effectively in a zero-temperature state. These thermal mass corrections, which are equal for all bosonic and fermionic degrees of freedom due to the underlying supersymmetry, are given by [48]:

$$\begin{aligned} m_{\chi_R}^2 &= 2g^2(\phi^2 - M^2) + \alpha^2 T^2 \ , \\ m_{\chi_I}^2 &= 2g^2(\phi^2 + M^2) + \alpha^2 T^2 \ , \\ m_{\psi_\chi}^2 &= 2g^2\phi^2 + \alpha^2 T^2 \ . \end{aligned} \tag{6.3}$$

The thermal mass correction is parameterized by $\alpha^2 = h^2 N_Y/2$ [70]. The self interactions between the fields in the Y sector will also induce thermal mass corrections to the light fields, but it has been shown in [70] that $m_{y,\psi_y}^2 \sim \mathcal{O}(h^2)$, and so realistically we can ignore these corrections for $h \ll 1$. We can also therefore assume that the fields in the Y sector are relativistic and that dissipative

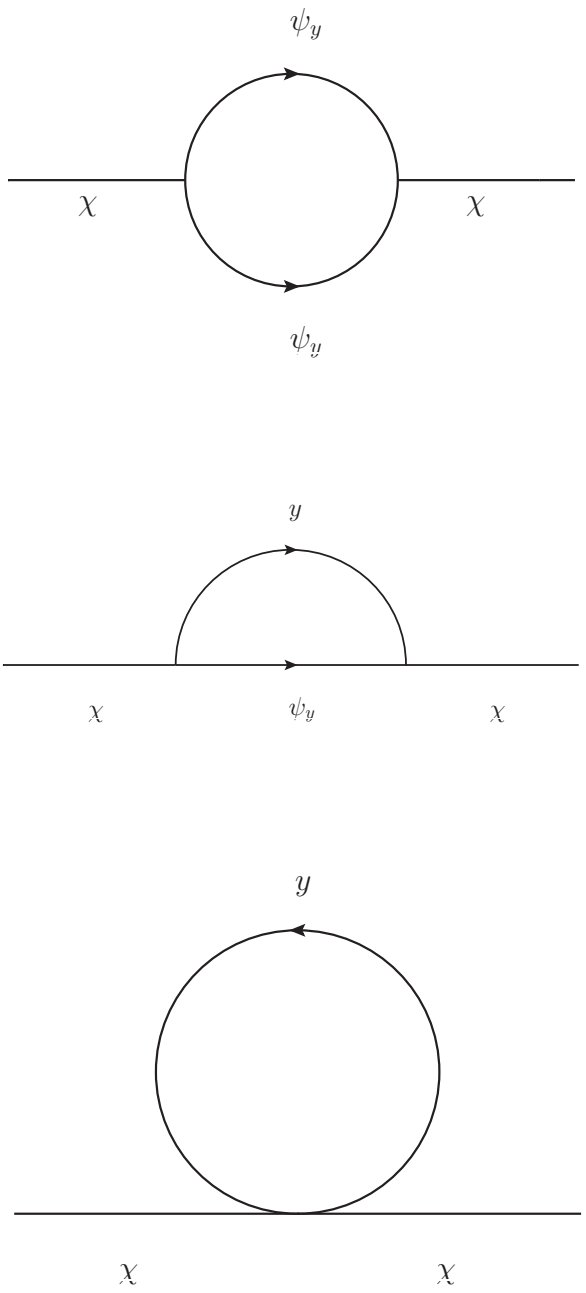

Figure 6.1: These Feynman diagrams contribute towards the self-energy of the χ and ψ_χ fields.

effects source a radiation bath with $g_* = (15/4)N_Y$ light degrees of freedom.

Whilst both dependent on the number of fields in the light sector N_Y, we will

be taking α and g_* to be independent parameters in our analysis. This is because both fields in the X and Y sectors may be charged under the standard model gauge group, or a particular extension, and so it is conceivable that gauge fields may also contribute towards the thermal mass corrections to the waterfall sector. The inflaton field and its superpartners will behave as either a relativistic or non-relativistic species, and so will give a sub-dominant contribution to the effective potential for large field multiplicities in the waterfall sector. Summing over the thermally corrected masses of the waterfall fields in the 1-loop Coleman-Weinberg approximation the effective potential at finite temperature becomes:

$$\begin{aligned} V(\phi,T) &= V_0\left\{1+\frac{\gamma}{16}\left[\xi^2\left(\log\left(\frac{\xi}{\bar{\mu}^2}\right)-\frac{3}{2}\right)+(\xi+4)^2\left(\log\left(\frac{\xi+4}{\bar{\mu}^2}\right)-\frac{3}{2}\right)\right.\right. \\ &- \left.\left.2(\xi+2)^2\left(\log\left(\frac{\xi+2}{\bar{\mu}^2}\right)-\frac{3}{2}\right)\right]\right\}-\frac{\pi^2}{90}g_*T^4\ , \end{aligned} \tag{6.4}$$

where we have introduced the parameter:

$$\xi(\phi,T)=\frac{m^2_{\chi_R}(\phi,T)}{g^2M^2}=\frac{2g^2(\phi^2-M^2)+\alpha^2T^2}{g^2M^2}\ , \tag{6.5}$$

so as to normalize the mass squared of the waterfall fields and we have introduced the dimensionless renormalization scale $\bar{\mu}=\mu/gM$. The significance of including these thermal mass corrections to the waterfall fields is that the waterfall transition will happen when $\xi(\phi,T)<0$, and thus the critical value ϕ_c becomes a dynamical quantity that will evolve throughout the inflationary phase.

6.2 Negative Entropy

This procedure of summing over the thermally corrected masses of the waterfall fields in the Coleman-Weinberg potential does however lead to a double counting of the 'figure of eight' diagram in scalar theories with quartic self interactions [108,109]. We have seen that the coupling between the fields in the waterfall sector

and the relativistic fields in the radiation bath induce thermal corrections to the masses of the waterfall fields. This implies that, whilst the X sector fields are in a zero-temperature state with Boltzmann-suppressed occupation numbers, they may still contribute towards the entropy of the system through the temperature dependence of their masses, with the contribution defined:

$$s_X = -\sum_i \frac{\partial V}{\partial m_i^2}\frac{\partial m_i^2}{\partial T} \ , \tag{6.6}$$

where the index i represents the summation over all components of the N_X waterfall supermultiplets, T is the ambient temperature and V is the effective potential. If we use the effective potential of the form in Eq. (6.4) then the contribution to the entropy coming from the Coleman-Weinberg potential is given by:

$$s_X = -\frac{\gamma}{4}\alpha^2 M^2 T F(\xi) \ , \tag{6.7}$$

where we have introduced the function:

$$F(\xi) = \xi\log(\xi) + (\xi+4)\log(\xi+4) - 2(\xi+2)\log(\xi+2) \ . \tag{6.8}$$

Whilst in general the Coleman-Weinberg potential will be dependent on the renormalization scale, the fact that the system is supersymmetric, and specifically the supertrace condition $\mathrm{Str}\mathcal{M}_X^2 = 0$ in the X sector, means that this result is independent of renormalization scale. We can also see that during the inflationary period we will have $\xi > 0$, and so the function $F(\xi)$ is positive-definite, ranging over the values $0 < F(\xi) < 4\log(2)$. This implies that during the inflationary period $s_X < 0$, with the waterfall fields effectively counteracting the standard entropy contribution to from the relativistic degrees of freedom and reducing the entropy of the system. Furthermore, since the contribution to the entropy from

waterfall sector is linearly dependent on the temperature T, we may find regions of parameter space at low temperature T where s_X overcomes the contribution from the radiation bath that is $\propto T^3$, yielding total entropy $s < 0$. In the large field limit we have:

$$s \simeq \frac{2\pi^2}{45} g_* T^3 \left(1 - \frac{3}{4}\frac{\gamma V_0}{\rho_R}\frac{\alpha^2 T^2}{m_X^2}\right) . \tag{6.9}$$

From this expression it can be seen that if $\gamma V_0 \ll \rho_R \ll V_0$ then the total entropy density of the system can be negative.

6.3 CJT Formalism

The negative entropy result obtained in Sec. (6.2) is physically unacceptable, suggesting that the effective potential obtained by directly substituting thermal masses into the Coleman-Weinberg approximation is poorly defined. Specifically the procedure potentially over-counts certain loop diagrams in the corresponding resummation procedure and this has motivated the implementation of the Cornwall-Jackiw-Tomboulis (CJT) formalism for composite operators [110] to obtain an improved version of the effective potential. The CJT formalism has been used in a number of finite temperature systems [111–114], and provides a non-perturbative framework through which a consistent expansion of the effective potential in terms of the full propagators can be acquired.

6.3.1 Scalar Effective Potential in the CJT formalism

The basic features of the CJT formalism can be demonstrated if we consider a real scalar field φ, that has a bare mass m and a quartic self-interaction $(\lambda/4!)\varphi^4$, coupled to a thermal bath at temperature T. Within the CJT Formalism the

field has an effective potential given by:

$$V = V^{(0)} - \frac{i}{2}\int_p \log G^{-1} - \frac{1}{2}\int_p \Pi G + \Phi[G] \ . \tag{6.10}$$

The tree-level contribution to the potential is given by V^0. The momentum-space integrals have been written in short-hand and include the sum over the Matsubara frequencies in the imaginary-time formalism, given by:

$$\int_p f(p) = iT\sum_n \int \frac{d^3p}{(2\pi)^3} f(i\omega_n, \mathbf{p}) \ . \tag{6.11}$$

The full scalar propagator is given by G, and it is a combination of both the *bare* propagator, $G_0(p) = i/(p^2 - m^2)$, and the corresponding self-energy Π, such that:

$$G(p) = \frac{i}{p^2 - m^2 - \Pi} \ . \tag{6.12}$$

The double counting in the effective potential of Eqs. (6.4) caused by the substituting the bare propagators with the full propagators is corrected by the last term in Eq. (6.10), $\Phi[G]$, which corresponds to a sum of 2-particle irreducible diagrams. A consistent expansion of the effective potential can be achieved in the CJT formalism by imposing the stationarity of the effective potential itself with regards to variations of the full propagator G at fixed values of the bare propagator G_0:

$$\frac{\delta V}{\delta G} = 0 \ . \tag{6.13}$$

The self-energy, and therefore the full propagator G of the field, can be defined through the gap equation:

$$\frac{\delta \Phi}{\delta G} = \frac{1}{2}\Pi \ . \tag{6.14}$$

This can be interpreted as the fact that the diagrams that contribute to the self-energy are obtained by cutting an internal line of the corresponding 2-particle-irreducible diagrams included in Φ [113], and in the example of a scalar field with quartic self-interactions the leading contributions to Φ arise at 2-loop order. These correspond to the "double-bubble" diagram of order λ, and the "sunset", or "cowboy hat", diagram of order λ^2, shown in Fig. (6.2).

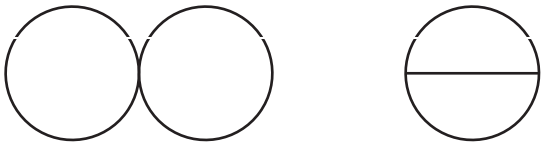

Figure 6.2: 2-loop diagrams contributing to the function $\Phi[G]$, including the "double-bubble" diagram (left) and the "sunset" diagram (right).

It is sufficient to assume that the leading contribution comes from the "double-bubble" diagram, allowing us to simplify our analysis by neglecting the "sunset" diagram [115, 116]. Furthermore, in the case of the hybrid inflation construction, the characteristics of the interactions of the real and imaginary components of the waterfall field suggest that the double-bubble diagram and sunset diagrams are of order $\mathcal{O}(g^2)$ and $\mathcal{O}(g^4 N_X)$ respectively, and thus the sunset diagram is subleading under the assumption that $g^2 N_X \lesssim 1$ if $g \ll 1$. It is also worth noting that hybrid inflation proceeds with the inflaton field slowly-rolling down the valley with $\langle \chi \rangle = 0$, and so up until the waterfall transition there is no tri-linear vertex involving only the χ fields and so the associated sunset diagram disappears. Thus the effective potential for a scalar field φ can be approximated as:

$$\begin{aligned} V(\varphi) &= \frac{\lambda}{4!}\varphi^4 + \frac{1}{2}\int_E \log(p^2 + \Omega^2) - \\ &- \frac{1}{2}P_T(\Omega)\left(\Omega^2 - m^2 - \frac{\lambda}{2}\varphi^2 - \alpha^2 T^2 - \frac{\lambda}{4}P_T(\Omega)\right) , \end{aligned} \tag{6.15}$$

where we have α parameterizing the thermal mass correction due to the

interactions with the thermal bath and Ω is the effective mass of the scalar field φ. We recover the standard Coleman-Weinberg potential and the finite temperature term in the Eqs. (5.7) and (6.2) from the second term after regularization. Following the procedure in [112], we have defined the single φ-bubble:

$$P_T(\Omega) \;=\; \int_p \frac{i}{p^2-\Omega^2}\bigg|_{\overline{DR}} = \frac{\Omega^2}{16\pi^2}\left(\log\frac{\Omega^2}{\mu^2}-1\right)+\int\frac{d^3p}{(2\pi)^3}\frac{n_B(E)}{E}\;. \quad (6.16)$$

We have seen how the stationarity condition renders the CJT effective potential invariant with regards to variations of the full scalar propagator, which in this case corresponds to the variation of the physical scalar mass Ω for a constant bare mass. Therefore:

$$\frac{\partial V}{\partial\Omega^2} = -\frac{1}{2}\frac{\partial P_T}{\partial\Omega^2}\left(M^2-m^2-\frac{\lambda}{2}\varphi^2-\alpha^2T^2-\frac{\lambda}{2}P_T(\Omega^2)\right)=0\;, \quad (6.17)$$

with:

$$P_T(\Omega) = \frac{\partial}{\partial\Omega^2}\frac{1}{2}\int_E \log(p^2+\Omega^2)\;. \quad (6.18)$$

From this we can define the gap equation for the physical mass of the scalar field:

$$\Omega^2 = m^2+\frac{\lambda}{2}\varphi^2+\alpha^2T^2+\frac{\lambda}{2}P_T(\Omega^2)\;. \quad (6.19)$$

Implementing the CJT formalism to improve the effective potential will eliminate the negative contribution to the total entropy density coming from the thermal mass corrections to the waterfall fields in the 1-loop Coleman-Weinberg approximation. We can obtain similar gap equations in the case of the $\chi_{R,I}$ scalars with $\lambda \leftrightarrow g^2$, such that:

$$s_X = \sum_i \frac{\partial V}{\partial\Omega_i}\frac{\partial\Omega_i}{\partial T} = 0\;, \quad (6.20)$$

due to $\partial V/\partial\Omega_i = 0$. A similar procedure can be followed to eliminate the contribution to the total entropy density coming for the fermionic components of the waterfall sector, and this is described in the next subsection. The result of this is that the X sector fields will only contribute to the total entropy density of the universe through the temperature dependence of their Bose-Einstein or Fermi-Dirac distributions, resulting in a positive contribution to the entropy. Under the assumption that the fields in the X sector are heavy and therefore non-relativistic then this contribution is Boltzmann-suppressed and the leading contribution to the total entropy density comes from the light degrees of freedom in Y sector, resulting in a total entropy:

$$s = (2\pi^2/45)g_* T^3 \ , \tag{6.21}$$

where we once again have g_* light degrees of freedom. In the slow-roll approximation we can also recover the equilibrium relationship between the entropy density s and the pressure p, the radiation energy density ρ and the temperature T:

$$s = (p + \rho)/T \ , \tag{6.22}$$

where the total pressure and radiation energy density are given by:

$$\begin{aligned} p &= \frac{1}{2}\dot{\phi}^2 - V(\phi, T) \ , \\ \rho &= \frac{1}{2}\dot{\phi}^2 + V(\phi, T) + Ts \ . \end{aligned} \tag{6.23}$$

Whilst substituting the thermal mass corrections to the waterfall fields into the Coleman-Weinberg potential results in an unphysical result with regards to the entropy density it is still a good approximation for the effective potential itself. If our generic scalar field φ has the characteristics similar to the that of the waterfall fields in the hybrid construction (i.e. in a non-relativistic state and with vacuum

expectation value $\langle\varphi\rangle = 0$) then the gap equation becomes:

$$\Omega^2\left[1 - \frac{\lambda}{32\pi^2}\left(\log\frac{\Omega^2}{\mu^2} - 1\right)\right] = m^2 + \alpha^2 T^2 \ , \tag{6.24}$$

such that the corrections are small for $\lambda \ll 1$ assuming we have a consistent perturbative computation of the Φ function with no large logarithms. With this gap equation the effective potential becomes:

$$V = \frac{\lambda}{4!}\varphi^4 + \frac{\Omega^4}{64\pi^2}\left[\log\frac{\Omega^2}{\mu^2} - \frac{3}{2} - \frac{\lambda}{32\pi^2}\left(\log\frac{\Omega^2}{\mu^2} - 1\right)^2\right] \ , \tag{6.25}$$

resulting in the corrections to the Coleman-Weinberg contribution being suppressed for small enough logarithms and $\lambda \ll 1$. This shows that the effective potential can be well approximated by the substitution of thermal mass corrections into the Coleman-Weinberg potential, but that higher-order corrections such as the "double-bubble" diagram must be taken into account within the CJT formalism when calculating the total entropy density of the universe.

6.3.2 Fermionic Effective Potential in the CJT formalism

Computing the fermionic component of the effective potential in the CJT Formalism can be done in much the same way as the scalar component, albeit in a slightly more complicated way due to the momentum dependence of the fermionic self-energy. To demonstrate this we will consider a generic fermion field ψ with Yukawa coupling $\lambda_f\varphi\bar{\psi}\psi$ to a light scalar field φ in a thermal bath. The bare and dressed propagators for the fermion field are:

$$S_{\psi 0} = \frac{i}{\not{p} - m_f} \ , \qquad S_\psi = \frac{i}{\not{p} - m_f + \Sigma} \ , \tag{6.26}$$

where m_f is the tree-level mass and Σ is the fermionic self-energy. Using the definition of the scalar propagator G_φ in Eq. (6.12) the fermionic effective potential can be written as:

$$V^{(F)} = i\int_p \mathrm{Tr}\ln S_\psi^{-1} - \int_p \mathrm{Tr}\Sigma S_\psi + \Phi^{(F)}(G_\varphi, S_\psi)\,. \tag{6.27}$$

The standard Coleman-Weinberg contribution finite temperature correction is given by the first term and the $\Phi^{(F)}(G_\varphi, S_\psi)$ contribution corresponds to the "fermionic sunset" diagram (the 2-loop vacuum diagram with two fermion and one scalar propagator) up to leading order. The gap equation is obtained by once again enforcing the stationarity of the potential with respect to the physical fermion propagator, $\delta V^{(F)}/\delta S_\psi = 0$:

$$\frac{\delta\Phi^{(F)}}{\delta S_\psi} = \Sigma = i\int_p S_\psi G_\varphi\ . \tag{6.28}$$

In order to solve the gap equation to obtain the improved effective potential one must consider the fact that the fermion self-energy Σ depends on the external momentum:

$$\Sigma(p) = \Sigma_s(p) - \gamma^0\Sigma_0(p) + \gamma\cdot\mathbf{p}\ \Sigma_v(p)\,, \tag{6.29}$$

and so the effective fermion mass is momentum dependent:

$$M_\psi(p) = m_f - \Sigma_s(p)\ . \tag{6.30}$$

It has been shown in [117] that in the Hartree-Fock approximation in studies of nuclear matter that the Σ_v term is found to be negligible and so we can neglect it. We thus define the effective fermion mass as the pole of the full propagator

when $\mathbf{p} \to 0$:

$$(p_0 - \Sigma_0(p_0))^2 = M_\psi^2 \,, \tag{6.31}$$

such that Σ_s and Σ_0 are calculated taking $\mathbf{p} = 0$ and with $|p_0 - \Sigma_0| = M_\psi$. The fermionic effective potential becomes:

$$V^{(F)} \;=\; -\int_E \mathrm{Tr}\ln S_\psi^{-1} - \frac{i}{2}\int_E \mathrm{Tr}\Sigma S_\psi + \frac{i}{2}\int_E \mathrm{Tr}\Sigma^\varphi S_\psi \;. \tag{6.32}$$

The first term in this expression can be written:

$$\begin{aligned} -\int_E \mathrm{Tr}\ln S_\psi^{-1} \;=\; & -\frac{1}{32\pi^2}\Omega_\psi^4\left(\ln\frac{\Omega_\psi^2}{\mu^2} - \frac{3}{2}\right) \\ & -\frac{T^4}{2\pi^2}\int_0^\infty dx x^2\left[\ln(1+e^{-\beta(E_F+\Sigma_0)})\right. \\ & \left.+\ln(1+e^{-\beta(E_F-\Sigma_0)})\right] \;, \end{aligned} \tag{6.33}$$

where $E_F = \sqrt{\mathbf{p}^2 + M_\psi^2}$ and $\Omega_\psi^2 = M_\psi^2 + 2(M_\psi + \Sigma_0)\Sigma_0$. The first term corresponds to the vacuum contribution whilst the second corresponds to the finite temperature contribution. The effective chemical potential Σ_0 and the effective mass of the fermion field M_ψ then obey the following gap equations:

$$\begin{aligned} M_\psi \;=\; & m_f + \lambda_f\frac{M_\psi}{16\pi^2}\left(\ln\frac{M_\psi^2}{\mu^2} - 1\right) \;, \\ & +\frac{\lambda_f T}{2\pi^2}\int dx\frac{x}{2\beta E_F}\left[n_B(x) + \frac{x}{2\beta(E_F - M_\psi)}\left(\tilde{n}_+(E_F) + \tilde{n}_-(E_F)\right)\right] \\ \Sigma_0 \;=\; & \frac{\lambda_f T^2/6}{p_0} - \frac{\lambda_f T}{2\pi^2}\int dx\frac{M_\psi + E_F}{4M_\psi}\left(\tilde{n}_+(E_F) - \tilde{n}_-(E_F)\right) \;, \end{aligned} \tag{6.34}$$

in which $\tilde{n}_\pm(E_F) = \left[e^{\beta(E_F \mp \Sigma_0)} + 1\right]^{-1}$ is the Fermi-Dirac distribution with an effective chemical potential $\pm\Sigma_0$. The remaining terms in the fermionic

contribution to the effective potential give:

$$\begin{aligned} -\frac{1}{2}\int_p \mathrm{Tr}\Sigma S_\psi &= -4M_\psi(\Sigma_s I_F^+ + 2\Sigma_0 I_F^-) \ , \\ -\frac{1}{2}\int_p \mathrm{Tr}\Sigma^\varphi S_\psi &= 4\frac{\lambda_f T^2/6}{p_0} M_\psi I_F^- \ , \end{aligned} \tag{6.35}$$

where the integrals are defined:

$$I_F^+ = \frac{T^2}{2\pi^2}\int dx x^2 \frac{\tilde{n}_+ + \tilde{n}_-}{2\beta E_F} \ , \tag{6.36}$$

$$I_F^- = \frac{T^2}{2\pi^2}\int dx x^2 \frac{\tilde{n}_+ - \tilde{n}_-}{2\beta M_\psi} \ . \tag{6.37}$$

Just as in the scalar case, the leading term in the effective potential for non-relativistic fermions, $M_\psi \gg T$, is the Coleman-Weinberg term. Furthermore, since $p_0 \simeq M_\psi$ in this limit, we have $\Omega_\psi^2 = M_\psi^2 + \lambda_f T^2/3$. In relation to the hybrid inflation setup this means that the leading contribution from the ψ_χ fermion comes from the Coleman-Weinberg approximation for the 1-loop effective potential in Eq. (6.4) with thermal mass corrections to the waterfall fields substituted into the expression. Once again the CJT formalism introduces additional terms that are not sub-leading for the computation of the entropy density and eliminate the unphysical contribution coming from the temperature dependence of the effective fermion mass.

6.4 Summary

From this analysis we draw the conclusion that the effective potential obtained by substituting the thermal mass corrections to the waterfall fields in Eq. (6.3) into the Coleman-Weinberg potential in Eq. (6.4) is a good approximation for the effective potential and a subsequent analysis of the dynamics of SUSY hybrid inflation, assuming that $g \ll 1$ but allowing for $g^2 N_X \lesssim 1$. We can

neglect the contribution to the entropy density of the system coming from the thermally corrected waterfall masses in the Coleman-Weinberg approximation and the total entropy density of the universe is calculated from the temperature of the relativistic degrees of freedom in the radiation bath. The result of this is that whilst the dissipation coefficient and effective potential will be modified, the equations of motion for the inflaton field and the radiation energy density will remain unaffected after the inclusion of thermal corrections in the effective potential.

Chapter 7

Dissipative Effects in Warm Hybrid Inflation

Having successfully defined the effective potential we are able to perform a detailed investigation into the dynamics and observational predictions of hybrid inflation in the warm regime. In this chapter we will analyze the effect of:

- Including the full form of the dissipation coefficient Υ, defined in Eq. (4.7), including contributions for dissipation mediated by both the on-shell and the off-shell modes of the scalar $\chi_{R,I}$ waterfall fields.
- The SUSY mass splittings for the real and imaginary scalar and fermionic fields in the X sector in the effective potential.
- The inclusion of thermal mass corrections to the scalar and fermionic components of the waterfall sector in the effective potential as defined in Eq. (6.4).

This will involve extending the analysis beyond the large field approximation used in Chapter 5 and will enable the investigation into the dynamics towards the end of inflation as the system approaches the waterfall transition. I will present the

numerical results that I obtained from this investigation, some of which are also presented in [73].

7.1 Waterfall Transition

7.1.1 Full Dissipation Coefficient and SUSY Mass Splittings

As has already been discussed, the coupling been the inflaton and waterfall field leads to non-local terms in the inflaton's quantum effective action. In the adiabatic approximation this leads to the inclusion of a friction term, given by the dissipation coefficient Υ, in the inflaton's equation of motion. In addition to this it is also apparent that fields in the waterfall sector are unstable against decay into light degrees of freedom in the Y sector, allowing inflaton energy to be transferred to the Y sector through the decay chains:

$$\phi \to \chi \to yy, \psi_y \psi_y \ , \tag{7.1}$$

$$\phi \to \psi_\chi \to y \psi_y \ . \tag{7.2}$$

Fields in the Y sector may thermalize via decay, inverse decay and scattering processes allowing the decay of the inflaton to source the formation of a radiation bath concurrent with the inflationary expansion. The leading contributions to the dissipation coefficient were calculated in the low temperature regime, with the mass of the mediator fields $m_{\chi_{R,I}}, m_{\psi_\chi} > T > H$, in [66,70] with the contribution from the scalar components being dominant. At large field values the mass splitting in the fields in waterfall sector were neglected, but as the inflaton field approaches its critical value ϕ_c this is approximation is no longer valid and we must take account of the SUSY mass splittings. Thus, we investigate SUSY hybrid inflation in the warm regime with dissipation coefficient in Eq. (4.7) and

we assume that the low-momentum and pole contributions to the dissipation coefficient dominate in differing scenarios. On-shell production leads to a resonant enhancement of the dissipation coefficient, but assuming that the waterfall fields are in a non-relativistic regime the occupation numbers are suppressed. In the low temperature regime we are interested in, with $m_i/T \gg 1$, the low-momentum contribution to the dissipation coefficient dominates since it is unaffected by the Boltzmann-suppression. On-shell particle production will however dominate for $m_i/T \gtrsim 1$, and so as the inflaton approaches the waterfall transition we would expect this to become the dominant contribution, particularly for dissipation mediated by the on-shell mode of the real scalar component of the waterfall field χ_R. Using:

$$dN_e = Hdt \ , \tag{7.3}$$

we can write the full equation of motion for the inflaton field with respect to the number of e-folds as:

$$\phi'' + \frac{1}{2}\left[\frac{V_{,\phi}\phi' + \rho_R'}{V + \rho_R} + \frac{\phi'\phi''}{3M_P^2 - \phi'^2/2}\right]\phi' + 3(1+Q)\phi' + \frac{V_{,\phi}}{H^2} = 0 \ , \tag{7.4}$$

and likewise we can write the equation of motion for the radiation energy density:

$$\rho_R' + 4\rho_R = 3QH^2\phi'^2 \ , \tag{7.5}$$

where once again we have the dissipative ratio defined as $Q = \Upsilon/3H$. We can also express the radiation energy density as a function of the temperature of the radiation bath for a near-equilibrium state via $\rho_R = (\pi^2/30)g_*T^4$. We have seen in Chapter 5 how the hybrid inflation system evolves numerically with respect to the number of e-folds from initial conditions under the approximation of the large field limit. In Fig. (7.1-7.6) we have a comparison, including the effect of SUSY mass splittings in the effective potential and dissipation mediated by both

the on-shell and off-shell modes of the waterfall fields with same initial conditions that give $n_s = 0.962$ and $r = 0.019$ and we have no other relativistic fields other than the Y fields with $g_* = (15/4)N_Y$ and $\alpha^2 = h^2 N_Y/2$.

We have shown the dynamical evolution of the inflaton field ϕ, the temperature T and the related quantities in three different cases:

- Dissipation is mediated by the off-shell "low-momentum" modes of the waterfall fields, with the dissipation coefficient given by $\Upsilon = \Upsilon_{LM}$.
- Dissipation is mediated by both the off-shell and the on-shell modes of the waterfall fields, with the dissipation coefficient given by $\Upsilon = \Upsilon_{LM} + \Upsilon_P$.
- The field evolution in the supercooled standard regime in which dissipative are neglected and $T \ll H$. As is shown, the supercooled regime yields approximately 25 e-folds of inflation before the waterfall transition occurs.

When we study dissipative effects mediated by the off-shell "low-momentum" modes of the waterfall field, corresponding to the first part of Eq. (4.7), we see that the system evolves for well over 60 e-folds of inflation without the waterfall transition. This is caused by the SUSY mass splittings in the scalar $\chi_{R,I}$ fields enhancing the dissipation coefficient.

When we considered dissipation mediated by both the on-shell and off-shell modes of the waterfall fields, corresponding to using the full dissipation coefficient in the equations of motion, the most obvious effect is that the extra dissipation further damps the inflaton's motion, causing the system to evolve even slower and prolonging the evolution in the strong dissipative regime with $Q \gg 1$. The SUSY mass splittings also enhance (reduce) the on-shell dissipation coefficient corresponding to the real (imaginary) component of the complex χ fields. Furthermore the effect of this is even more pronounced than for the off-shell modes since the dissipation coefficient is exponentially dependent on the mass of the waterfall field.

We see that the consistency conditions for $T > H$, $\Gamma_{\chi_{R,I}} > H$ and $m_{\chi_{I,R}} > T$ are satisfied for a substantial number of e-folds, as are the slow-roll conditions $|\epsilon_\phi, \eta_\phi| < (1 + Q)$. Only as the waterfall transition is approached does the mass of the real scalar component of the waterfall field m_{χ_R} fall below the value of the ambient temperature, and so our assumption that the contribution to the entropy density coming from the waterfall fields is Boltzmann-suppressed is accurate. Note that since $\Gamma_{\chi_I} > \Gamma_{\chi_R}$ we only show the most restrictive condition.

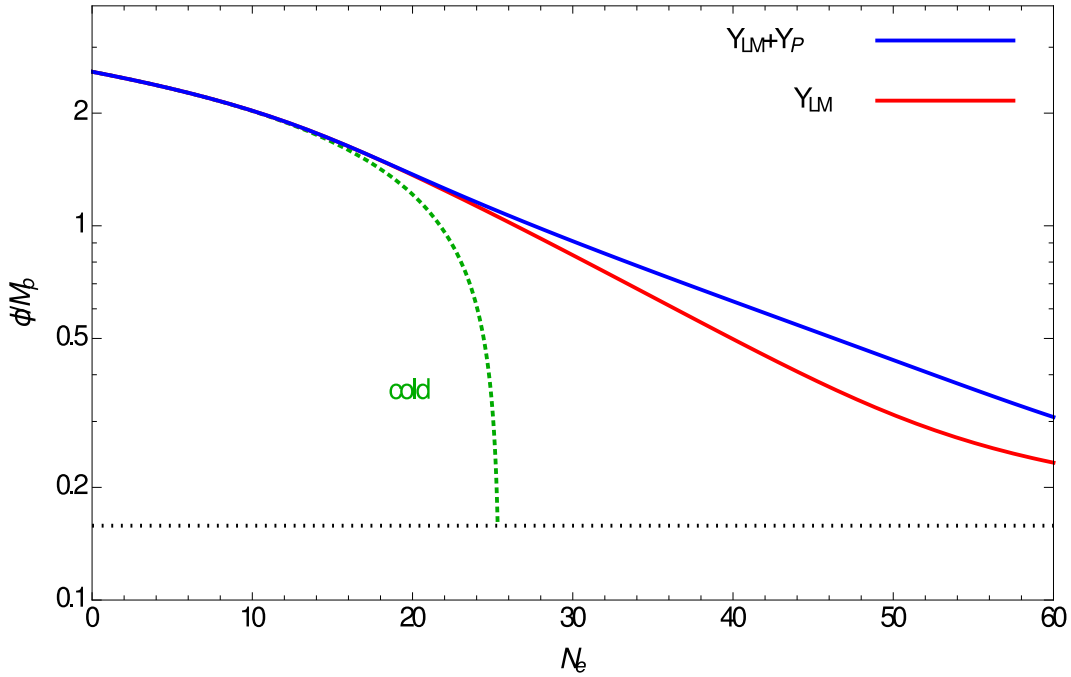

Figure 7.1: Numerical evolution of the inflaton field value ϕ using the full form of the field and radiation equations, considering only the low-momentum contribution to the dissipation coefficient (red curve) and the full dissipation coefficient including on-shell modes (blue curve). The evolution in the standard supercooled regime is shown in green. These results are obtained for $g = 10^{-3}$, $h = 0.34$, $N_X = 5 \times 10^6$, $N_Y = 50$ and $M = 0.16 M_P$, choosing $Q_* \simeq 10^{-3}$ ($\phi_* = 2.58 M_P$). For this choice of parameters, the spectral index is $n_s \simeq 0.962$ and the tensor-to-scalar ratio is $r = 0.019$, with the amplitude of the power spectrum normalized to the observational value $\Delta^2_{\mathcal{R}} \approx 2.2 \times 10^{-9}$.

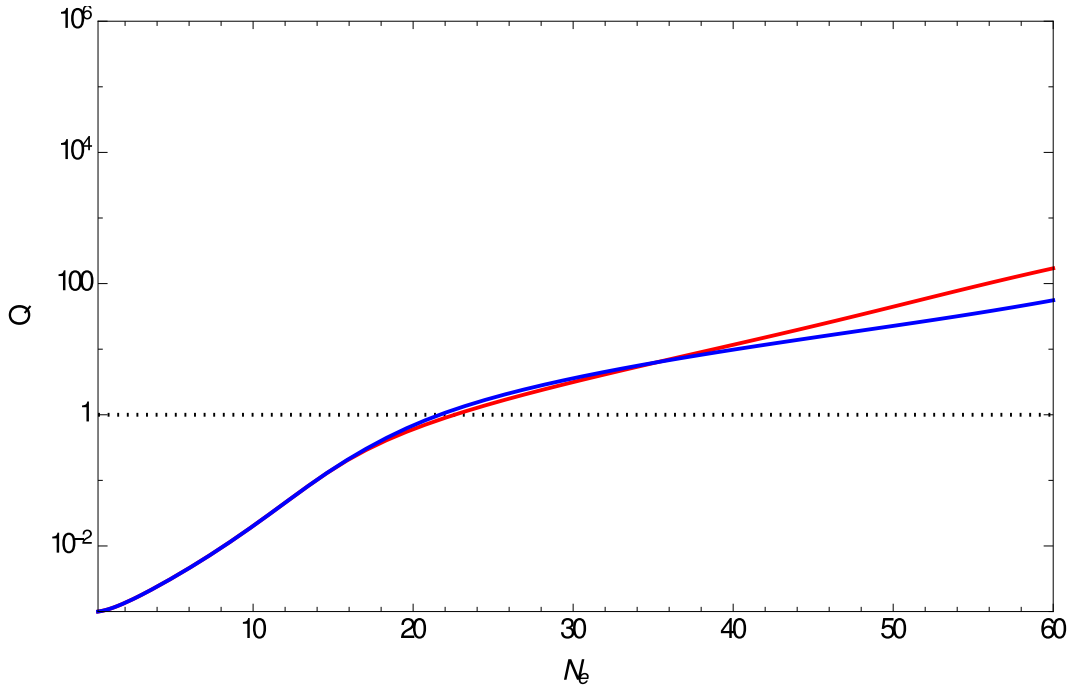

Figure 7.2: The numerical evolution of the dissipative ratio Q using the full form of the field and radiation equations, considering only the low-momentum contribution to the dissipation coefficient (red curve) and the full dissipation coefficient including on-shell modes (blue curve). These results are obtained for $g = 10^{-3}$, $h = 0.34$, $N_X = 5 \times 10^6$, $N_Y = 50$ and $M = 0.16 M_P$, choosing $Q_* \simeq 10^{-3}$ ($\phi_* = 2.58 M_P$). For this choice of parameters, the spectral index is $n_s \simeq 0.962$ and the tensor-to-scalar ratio is $r = 0.019$, with the amplitude of the power spectrum normalized to the observational value $\Delta^2_{\mathcal{R}} \approx 2.2 \times 10^{-9}$.

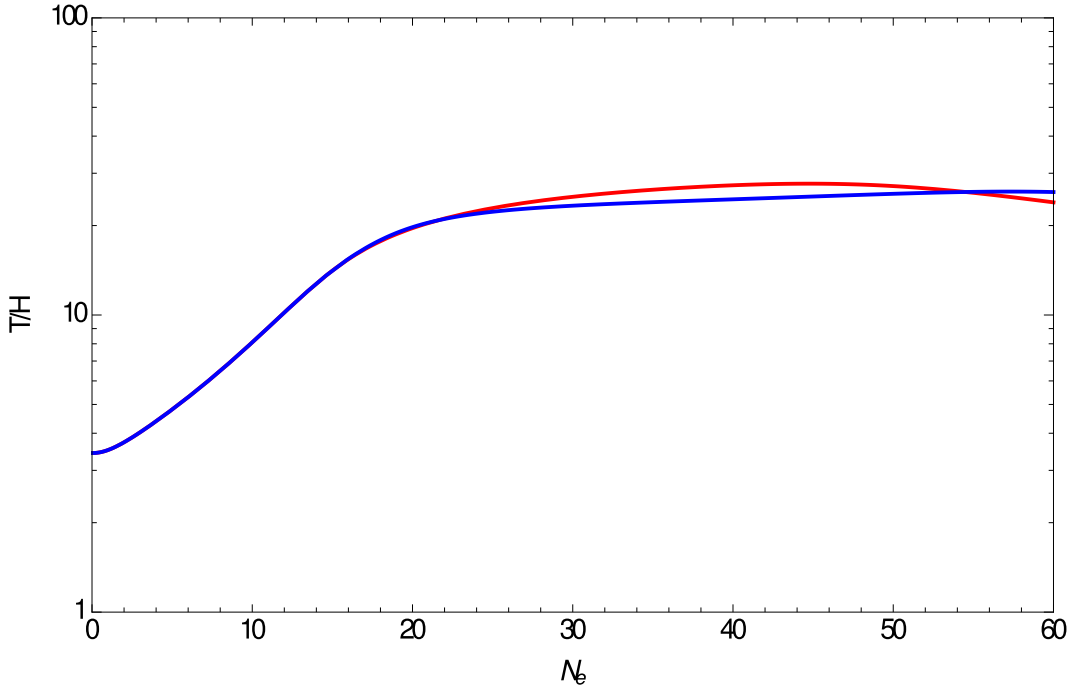

Figure 7.3: The numerical evolution of T/H using the full form of the field and radiation equations, considering only the low-momentum contribution to the dissipation coefficient (red curve) and the full dissipation coefficient including on-shell modes (blue curve). These results are obtained for $g = 10^{-3}$, $h = 0.34$, $N_X = 5 \times 10^6$, $N_Y = 50$ and $M = 0.16 M_P$, choosing $Q_* \simeq 10^{-3}$ ($\phi_* = 2.58 M_P$). For this choice of parameters, the spectral index is $n_s \simeq 0.962$ and the tensor-to-scalar ratio is $r = 0.019$, with the amplitude of the power spectrum normalized to the observational value $\Delta^2_{\mathcal{R}} \approx 2.2 \times 10^{-9}$.

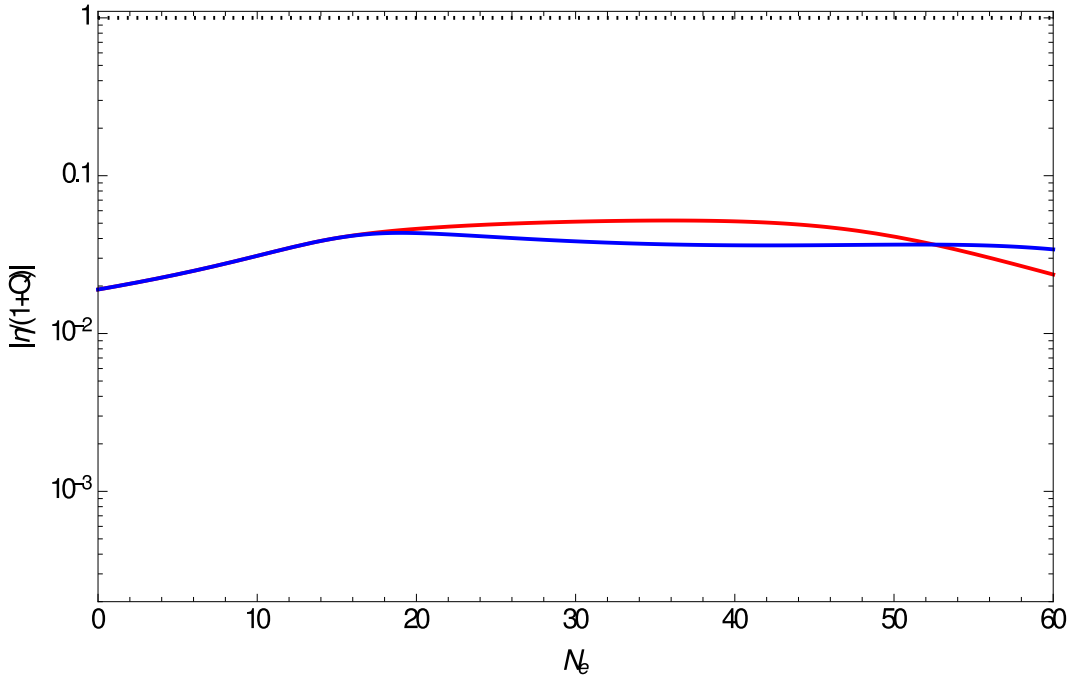

Figure 7.4: The numerical evolution of $|\eta/(1+Q)|$ using the full form of the field and radiation equations, considering only the low-momentum contribution to the dissipation coefficient (red curve) and the full dissipation coefficient including on-shell modes (blue curve). These results are obtained for $g = 10^{-3}$, $h = 0.34$, $N_X = 5 \times 10^6$, $N_Y = 50$ and $M = 0.16 M_P$, choosing $Q_* \simeq 10^{-3}$ ($\phi_* = 2.58 M_P$). For this choice of parameters, the spectral index is $n_s \simeq 0.962$ and the tensor-to-scalar ratio is $r = 0.019$, with the amplitude of the power spectrum normalized to the observational value $\Delta^2_{\mathcal{R}} \approx 2.2 \times 10^{-9}$.

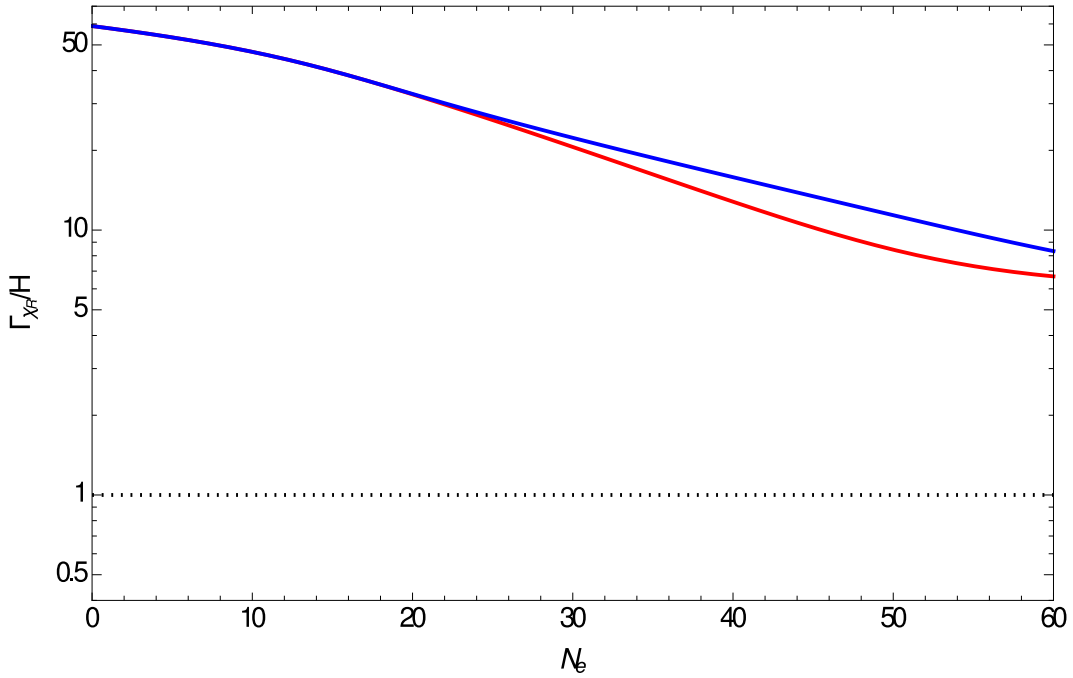

Figure 7.5: The numerical evolution of Γ_{χ_R}/H using the full form of the field and radiation equations, considering only the low-momentum contribution to the dissipation coefficient (red curve) and the full dissipation coefficient including on-shell modes (blue curve). These results are obtained for $g = 10^{-3}$, $h = 0.34$, $N_X = 5 \times 10^6$, $N_Y = 50$ and $M = 0.16 M_P$, choosing $Q_* \simeq 10^{-3}$ ($\phi_* = 2.58 M_P$). For this choice of parameters, the spectral index is $n_s \simeq 0.962$ and the tensor-to-scalar ratio is $r = 0.019$, with the amplitude of the power spectrum normalized to the observational value $\Delta^2_{\mathcal{R}} \approx 2.2 \times 10^{-9}$.

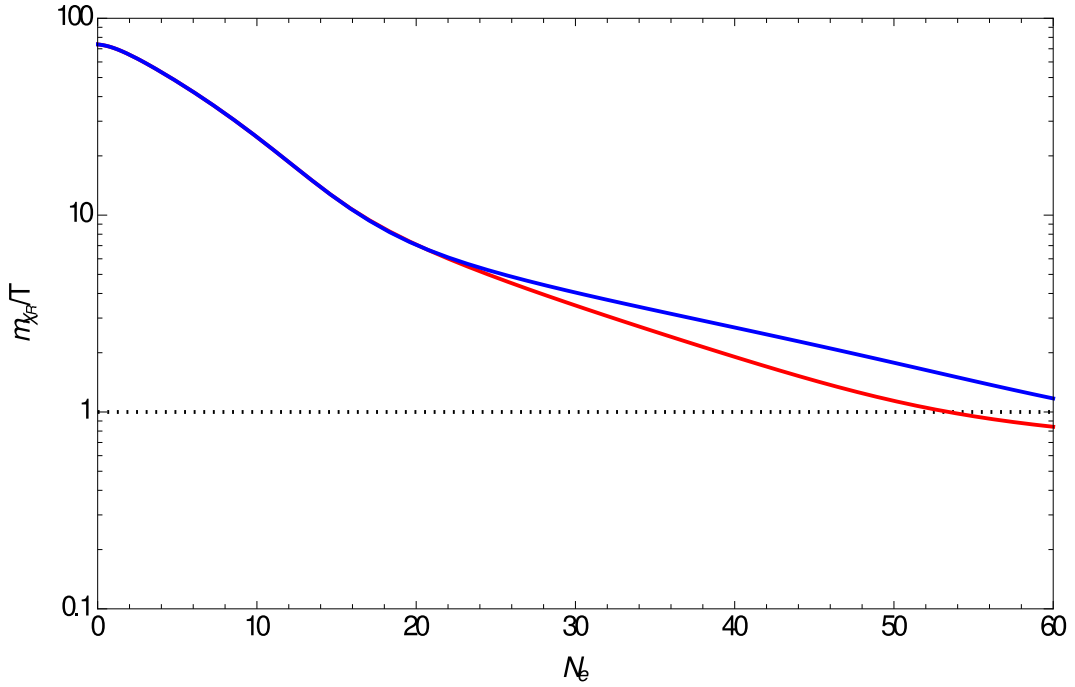

Figure 7.6: The numerical evolution of $m_{\chi R}/T$ using the full form of the field and radiation equations, considering only the low-momentum contribution to the dissipation coefficient (red curve) and the full dissipation coefficient including on-shell modes (blue curve). These results are obtained for $g = 10^{-3}$, $h = 0.34$, $N_X = 5 \times 10^6$, $N_Y = 50$ and $M = 0.16 M_P$, choosing $Q_* \simeq 10^{-3}$ ($\phi_* = 2.58 M_P$). For this choice of parameters, the spectral index is $n_s \simeq 0.962$ and the tensor-to-scalar ratio is $r = 0.019$, with the amplitude of the power spectrum normalized to the observational value $\Delta^2_{\mathcal{R}} \approx 2.2 \times 10^{-9}$.

7.1.2 Thermal Mass Corrections

It was shown in the previous Chapter that the effective potential could be well approximated by substituting thermal mass corrections to the waterfall fields into the Coleman-Weinberg potential and that, despite the implicit temperature dependence of the potential through the thermal masses, the waterfall sector would make no contribution to the entropy density of the system beyond the Boltzmann-suppressed standard contribution from relativistic degrees of freedom, as was demonstrated when implementing the CJT formalism. In addition to this, because the CJT formalism requires that the derivative of the effective potential with respect to the ambient temperature should vanish, we can conclude that the thermal corrections in the effective potential will alter the inflaton's equation of motion.

We now study the dynamical evolution of the system with thermal mass corrections included in Fig. (7.7-7.12), with solid lines showing the evolution with thermal corrections, and the dashed lines showing the previous evolution without them, for both the case where we have considered dissipation mediated by the virtual "low-momentum" modes only and with the full dissipation coefficient.

When thermal corrections are included it is apparent that the waterfall transition, with $m_{\chi_R} \to 0$, happens for values of the inflaton field ϕ below the zero-temperature critical value $\phi_c = M$ since the thermal corrections increase the waterfall field masses. Therefore the waterfall transition will be delayed until a lower value of the inflaton field is reached. There is however another effect of including thermal corrections to the masses of the waterfall fields. Increasing the mass of the waterfall fields by including thermal corrections has the effect of suppressing dissipation, with the effect particularly pronounced as the inflaton field approaches the waterfall transition. Crucially the mass of the waterfall fields are no longer solely dependent on the vacuum expectation value of the inflaton, but also on the ambient temperature. Previously as the inflaton value decreased

the waterfall field masses would also decrease accordingly due to the dependence on the inflaton field, with the effect being an increase in dissipation slowing the evolution of the system. With thermal corrections included the waterfall field masses also gain a dependence on the ambient temperature T, allowing the inflaton field to tend towards 0 faster than the waterfall field masses. Thus as the inflaton field approaches the hybrid transition there is no increase in dissipation, the inflaton field starts to approach the critical value ϕ_c faster, causing dissipation to decrease, lowering the temperature and thus causing the waterfall field masses to rapidly decrease.

This effect can be seen analytically, with the decrease in dissipation caused by the larger effective masses of both the real and imaginary X scalars, by considering the next-to-leading corrections to the low-momentum dissipation coefficient in the large field limit $\phi \gg M, \alpha T/\sqrt{2}g$:

$$\Upsilon_{LM} = C_\phi \frac{T^3}{\phi^2}\left[1 + 10\left(\frac{M}{\phi}\right)^4 - 4\alpha^2\left(\frac{T}{m_X}\right)^2 + \dots\right] , \tag{7.6}$$

where we have made the large field approximation that the leading scalar mass is $m_X = \sqrt{2}g\phi$. This shows that whilst the SUSY mass splittings enhance the dissipation coefficient, the thermal mass corrections to the X sector fields decrease it. Since the SUSY mass splittings are $\mathcal{O}(M/\phi)^4$, whilst the thermal corrections are $\mathcal{O}(T/\phi)^2$, the effect of thermal corrections becomes increasingly significant towards the hybrid transition.

The result of this is that including thermal corrections to the waterfall fields tends to reduce the number of e-folds of inflation. When we consider the full form of the dissipation coefficient the effect is even more pronounced, with thermal corrections decreasing the effect of the dissipation coefficients associated with both the real and imaginary components of the complex χ fields. Dissipation mediated through the on-shell modes of the waterfall field will be exponentially

suppressed by the increased waterfall field masses, albeit with the system evolving for longer in the strong dissipative regime, $Q > 1$, due to the overall increased dissipation.

Ultimately the evolution for the full dissipation coefficient with thermal corrections included yields a total of approximately 52 e-folds of inflation with an observational consistent primordial spectrum for presently observable CMB scales. It is also apparent that the warm inflation consistency conditions, $T > H$, $\Gamma_{\chi_{R,I}} > H$ and $m_{\chi_{I,R}} > T$, are maintained during this period, as are the warm inflation slow-roll conditions $|\eta_\phi, \epsilon_\phi| < (1+Q)$. The condition $m_{\chi_{I,R}} > T$ provides the largest constraint on the number of e-folds, only becoming violated very close to the waterfall transition. This justifies our approximation that contributions to the effective potential and entropy density from relativistic degrees of freedom within the X sector are Boltzmann-suppressed and can be neglected, along with thermal mass corrections to the inflaton. Once again since $\Gamma_{\chi_I} > \Gamma_{\chi_R}$ we only plot the most restrictive condition.

We can better understand the evolution of the system, particularly leading up to the waterfall transition, by studying the evolution of the temperature-dependent critical field value $\phi_c(T) = \sqrt{M^2 - \alpha^2 T^2/2g^2}$, shown in Fig.(7.13-7.14).

The temperature of the radiation bath increases during the inflationary period, as can be seen with T/H increasing for an approximately constant Hubble parameter. The increasing ambient temperature decreases the critical field value, which in the particular example becomes pure imaginary at approximately 10 e-folds. At this point the inflaton field can become arbitrarily small whilst still maintaining the stability of the metastable vacuum state. At the same time the nature of the ϕ dependence of the dissipation coefficient means that smaller values of the inflaton field will lead to a decrease in dissipative processes, causing the dissipative ratio Q to fall which in turn causes the temperature of the radiation

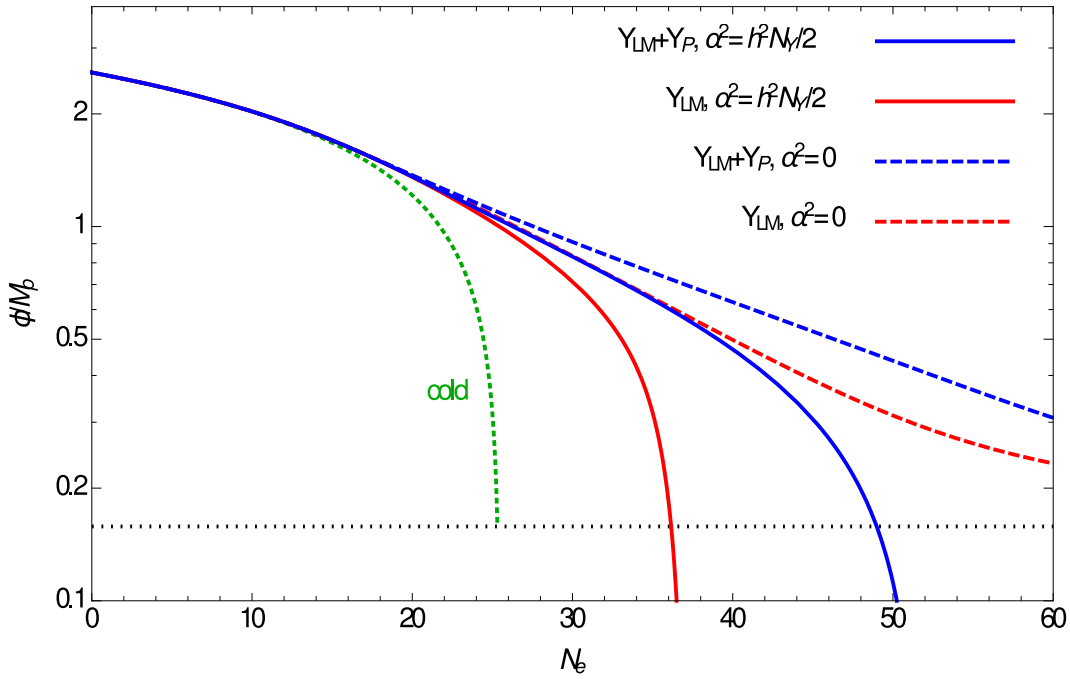

Figure 7.7: Numerical evolution of the inflaton field value ϕ using the full form of the field and radiation equations, considering only the low-momentum contribution to the dissipation coefficient (red curves) and the full dissipation coefficient including on-shell modes (blue curves), both excluding (dashed curves) and including (solid curves) thermal corrections to the waterfall sector masses. The evolution in the supercooled regime (dotted green curve) and the chosen value of M (dashed black line) are also included. These results are obtained for $g = 10^{-3}$, $h = 0.34$, $N_X = 5 \times 10^6$, $N_Y = 50$ and $M = 0.16 M_P$, choosing $Q_* \simeq 10^{-3}$ ($\phi_* = 2.58 M_P$). For this choice of parameters, the spectral index is $n_s \simeq 0.962$ and the tensor-to-scalar ratio is $r = 0.019$, with the amplitude of the power spectrum normalized to the observational value $\Delta^2_{\mathcal{R}} \approx 2.2 \times 10^{-9}$.

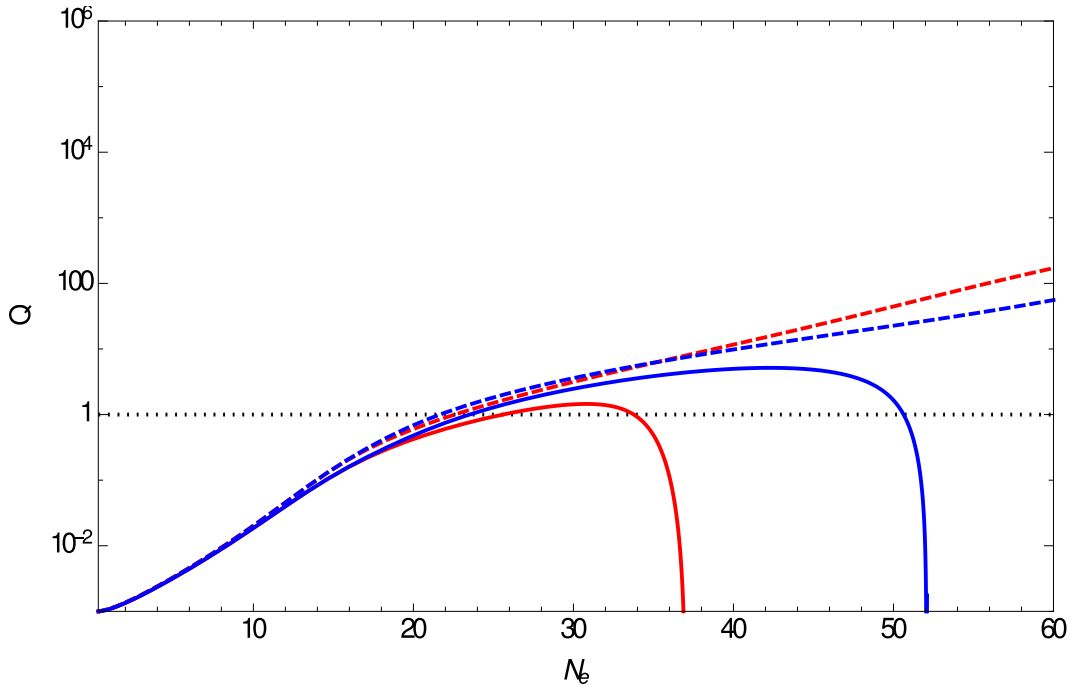

Figure 7.8: Numerical evolution of the dissipative ratio Q using the full form of the field and radiation equations, considering only the low-momentum contribution to the dissipation coefficient (red curves) and the full dissipation coefficient including on-shell modes (blue curves), both excluding (dashed curves) and including (solid curves) thermal corrections to the waterfall sector masses. These results are obtained for $g = 10^{-3}$, $h = 0.34$, $N_X = 5 \times 10^6$, $N_Y = 50$ and $M = 0.16 M_P$, choosing $Q_* \simeq 10^{-3}$ ($\phi_* = 2.58 M_P$). For this choice of parameters, the spectral index is $n_s \simeq 0.962$ and the tensor-to-scalar ratio is $r = 0.019$, with the amplitude of the power spectrum normalized to the observational value $\Delta^2_{\mathcal{R}} \approx 2.2 \times 10^{-9}$.

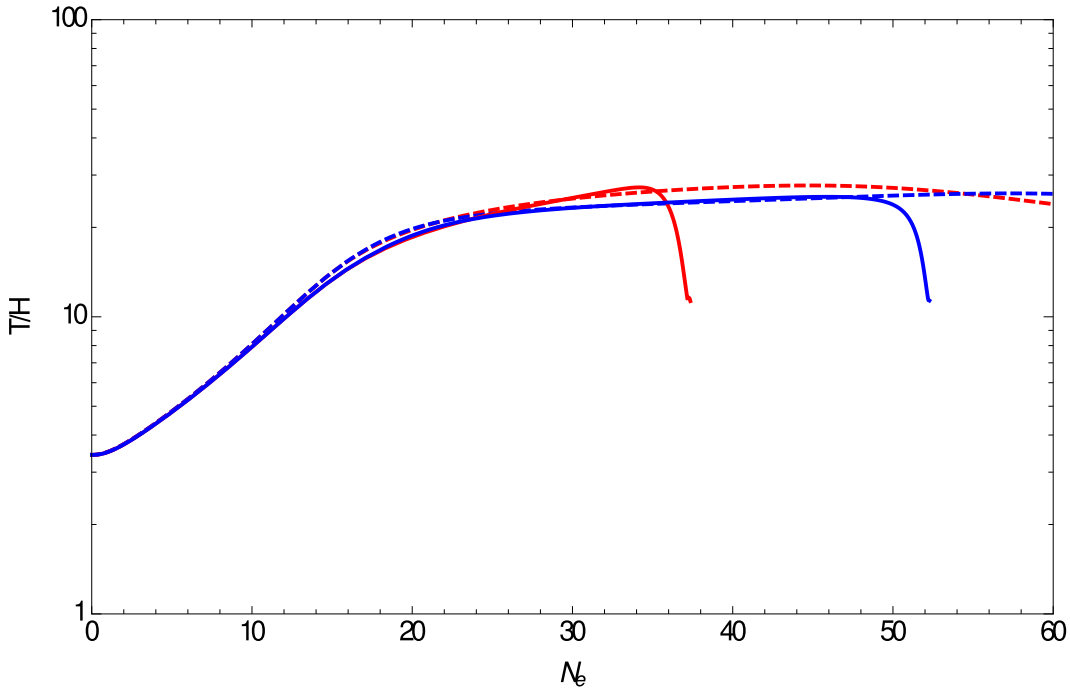

Figure 7.9: Numerical evolution of T/H using the full form of the field and radiation equations, considering only the low-momentum contribution to the dissipation coefficient (red curves) and the full dissipation coefficient including on-shell modes (blue curves), both excluding (dashed curves) and including (solid curves) thermal corrections to the waterfall sector masses. These results are obtained for $g = 10^{-3}$, $h = 0.34$, $N_X = 5 \times 10^6$, $N_Y = 50$ and $M = 0.16 M_P$, choosing $Q_* \simeq 10^{-3}$ ($\phi_* = 2.58 M_P$). For this choice of parameters, the spectral index is $n_s \simeq 0.962$ and the tensor-to-scalar ratio is $r = 0.019$, with the amplitude of the power spectrum normalized to the observational value $\Delta^2_{\mathcal{R}} \approx 2.2 \times 10^{-9}$.

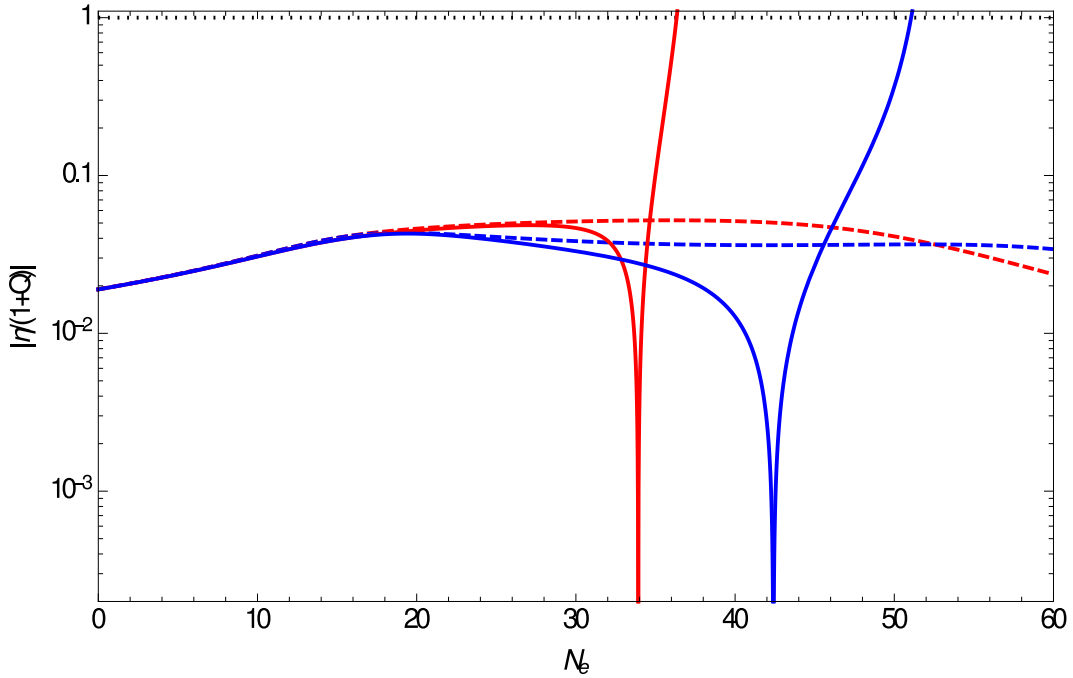

Figure 7.10: Numerical evolution of $|\eta_\phi/(1+Q)|$ using the full form of the field and radiation equations, considering only the low-momentum contribution to the dissipation coefficient (red curves) and the full dissipation coefficient including on-shell modes (blue curves), both excluding (dashed curves) and including (solid curves) thermal corrections to the waterfall sector masses. These results are obtained for $g = 10^{-3}$, $h = 0.34$, $N_X = 5 \times 10^6$, $N_Y = 50$ and $M = 0.16 M_P$, choosing $Q_* \simeq 10^{-3}$ ($\phi_* = 2.58 M_P$). For this choice of parameters, the spectral index is $n_s \simeq 0.962$ and the tensor-to-scalar ratio is $r = 0.019$, with the amplitude of the power spectrum normalized to the observational value $\Delta^2_{\mathcal{R}} \approx 2.2 \times 10^{-9}$.

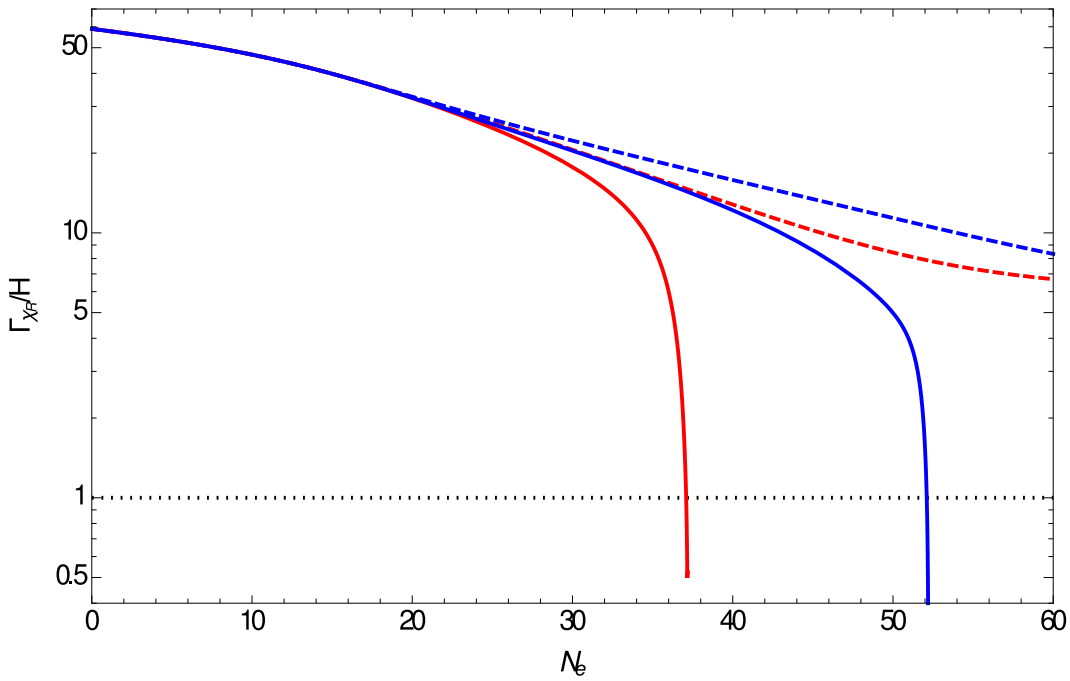

Figure 7.11: Numerical evolution of Γ_{χ_R}/H using the full form of the field and radiation equations, considering only the low-momentum contribution to the dissipation coefficient (red curves) and the full dissipation coefficient including on-shell modes (blue curves), both excluding (dashed curves) and including (solid curves) thermal corrections to the waterfall sector masses. These results are obtained for $g = 10^{-3}$, $h = 0.34$, $N_X = 5 \times 10^6$, $N_Y = 50$ and $M = 0.16 M_P$, choosing $Q_* \simeq 10^{-3}$ ($\phi_* = 2.58 M_P$). For this choice of parameters, the spectral index is $n_s \simeq 0.962$ and the tensor-to-scalar ratio is $r = 0.019$, with the amplitude of the power spectrum normalized to the observational value $\Delta^2_{\mathcal{R}} \approx 2.2 \times 10^{-9}$.

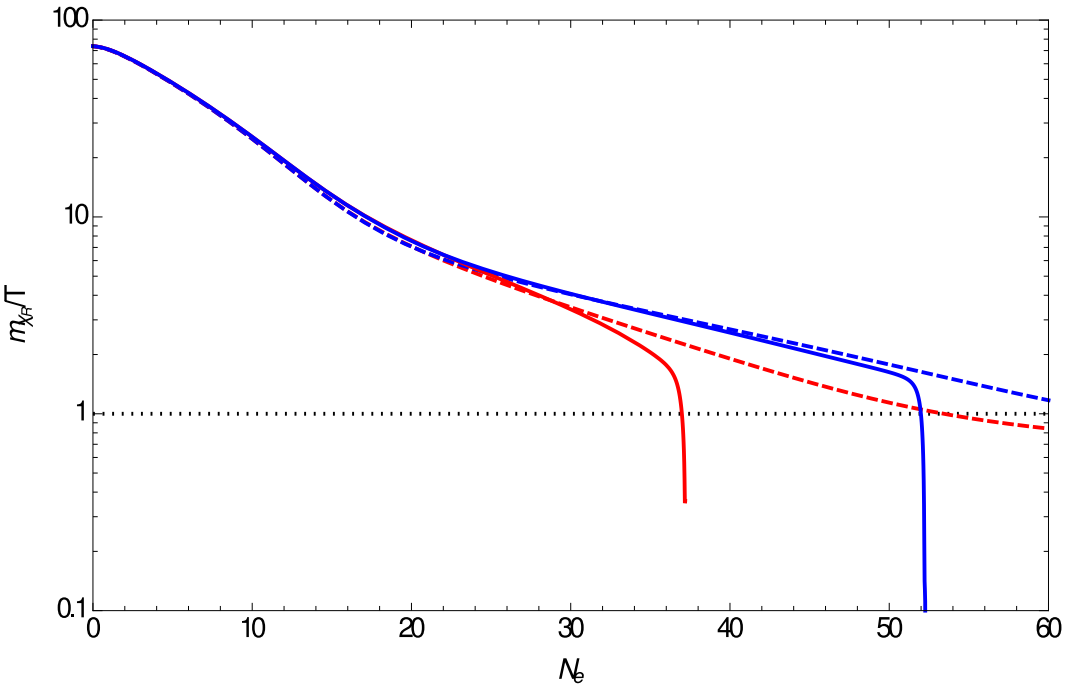

Figure 7.12: Numerical evolution of $m_{\chi R}/T$ using the full form of the field and radiation equations, considering only the low-momentum contribution to the dissipation coefficient (red curves) and the full dissipation coefficient including on-shell modes (blue curves), both excluding (dashed curves) and including (solid curves) thermal corrections to the waterfall sector masses. These results are obtained for $g = 10^{-3}$, $h = 0.34$, $N_X = 5 \times 10^6$, $N_Y = 50$ and $M = 0.16 M_P$, choosing $Q_* \simeq 10^{-3}$ ($\phi_* = 2.58 M_P$). For this choice of parameters, the spectral index is $n_s \simeq 0.962$ and the tensor-to-scalar ratio is $r = 0.019$, with the amplitude of the power spectrum normalized to the observational value $\Delta^2_{\mathcal{R}} \approx 2.2 \times 10^{-9}$.

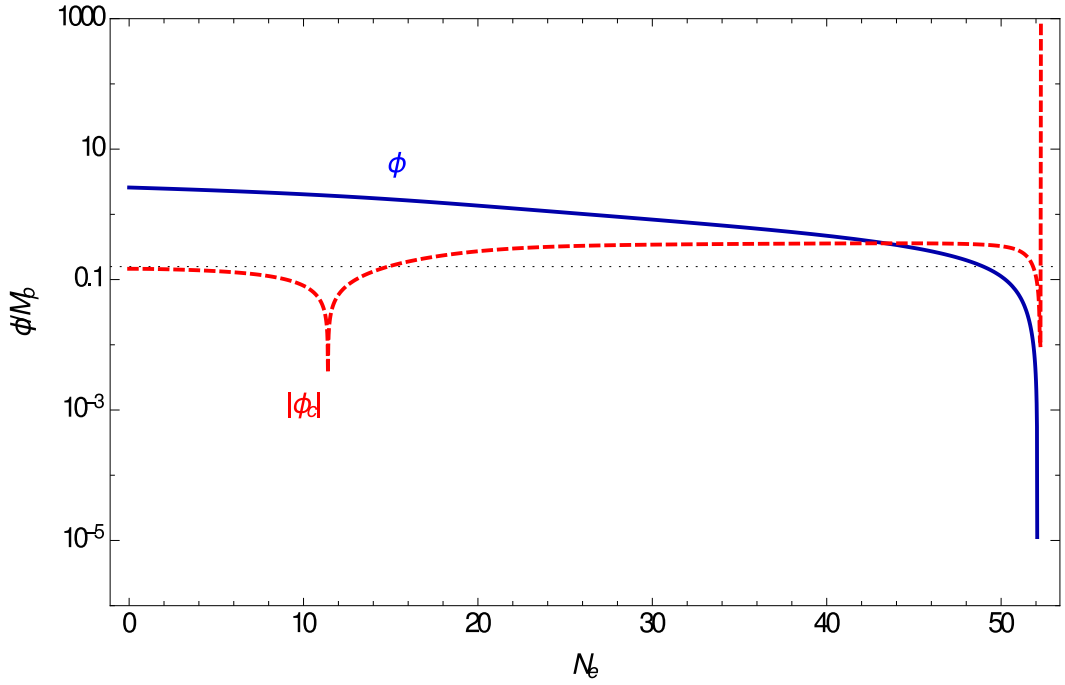

Figure 7.13: Evolution of the inflaton field compared to the finite temperature critical field value $\phi_c = \sqrt{M^2 - \alpha^2 T^2/2g^2}$, which reduces to $\phi_c = M$ at zero temperature (dotted black line). These results correspond to the same parameter choices as in the previous figures, using the full form of the dissipation coefficient and including thermal corrections to the field masses in the waterfall sector.

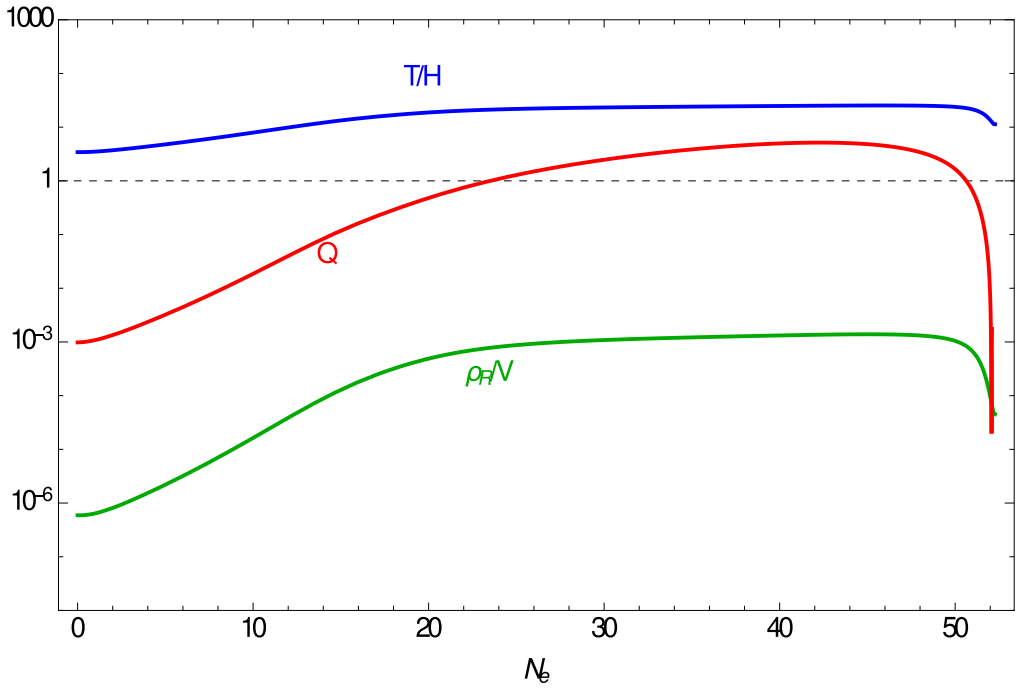

Figure 7.14: The evolution of the radiation abundance and related dynamical quantities. These results correspond to the same parameter choices as in the previous figures, using the full form of the dissipation coefficient and including thermal corrections to the field masses in the waterfall sector.

bath to drop. The result of this is that the critical field value becomes real, triggering the waterfall transition. This is a direct consequence of including thermal mass corrections, as without them the mass of the real scalar component of the waterfall field tends to zero, $m_{\chi_R} \to 0$, at finite inflaton values as $\phi \to M$, causing Q to increase.

We can then conclude that including thermal mass corrections reverses the tendency for radiation to naturally come to dominate the energy density of the universe through particle production, as is the case when thermal corrections are not included. Thus, in order to bring the universe into a radiation dominated era a phase of (p)reheating is required after the waterfall transition, with the decay of fields in the inflaton and waterfall sectors transferring the vacuum energy into relativistic degrees of freedom. This phase of reheating will however take place from an already warm universe, with $T/H > 1$ maintained up to the waterfall transition, as opposed to the standard supercooled scenario in which the temperature has been exponentially suppressed.

Fig. (7.15-7.20) show the effect on the dynamical evolution of varying the effective coupling $h^2 N_Y$. This effective coupling determines the size of the thermal mass corrections and also modifies the strength of the dissipation coefficient, for both the low-momentum and pole contributions. In order to start from the same initial conditions we have modified the basic parameters of model so as to keep $g^2 N_X$, C_ϕ, g_* and V_0 constant.

As is apparent in the figure the lower values of $h^2 N_Y$ result in a larger number of e-folds of inflation. Dissipative effects are less suppressed by thermal masses and the contribution to dissipation mediated by the on-shell modes is resonantly enhanced for smaller decay widths (by keeping C_ϕ constant the low-momentum contribution is not directly affected). In the figure shown the transition between the low-momentum dominated and pole-dominated dissipative regimes is also more pronounced, which is due to the fact that the dissipation coefficient has

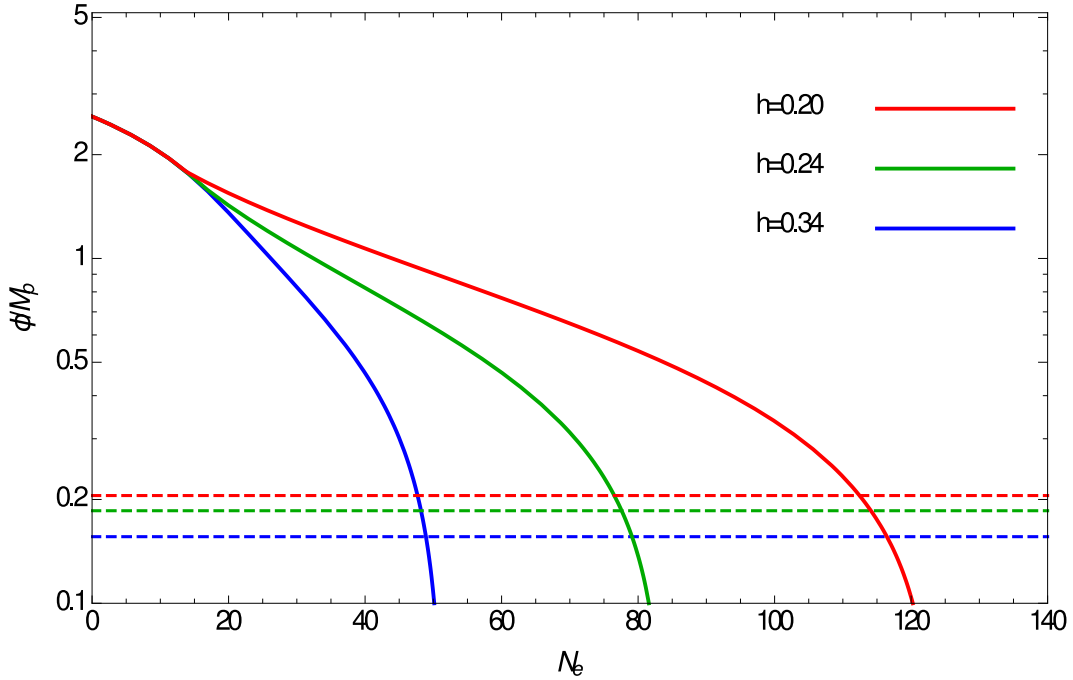

Figure 7.15: Numerical evolution of the inflaton field ϕ using the full dissipation coefficient and including thermal mass corrections for different values of the coupling h, keeping N_Y, $g^2 N_X$, V_0 and C_ϕ constant, as well as the initial inflaton value, so as to fix the same initial conditions as in the previous analysis. Note that this corresponds to changing the value of the effective coupling $h^2 N_Y$ and hence the effects of thermal masses and the magnitude of on-shell dissipation. The dashed horizontal lines in the plot give the $T = 0$ critical value $\phi_c = M$ in each case.

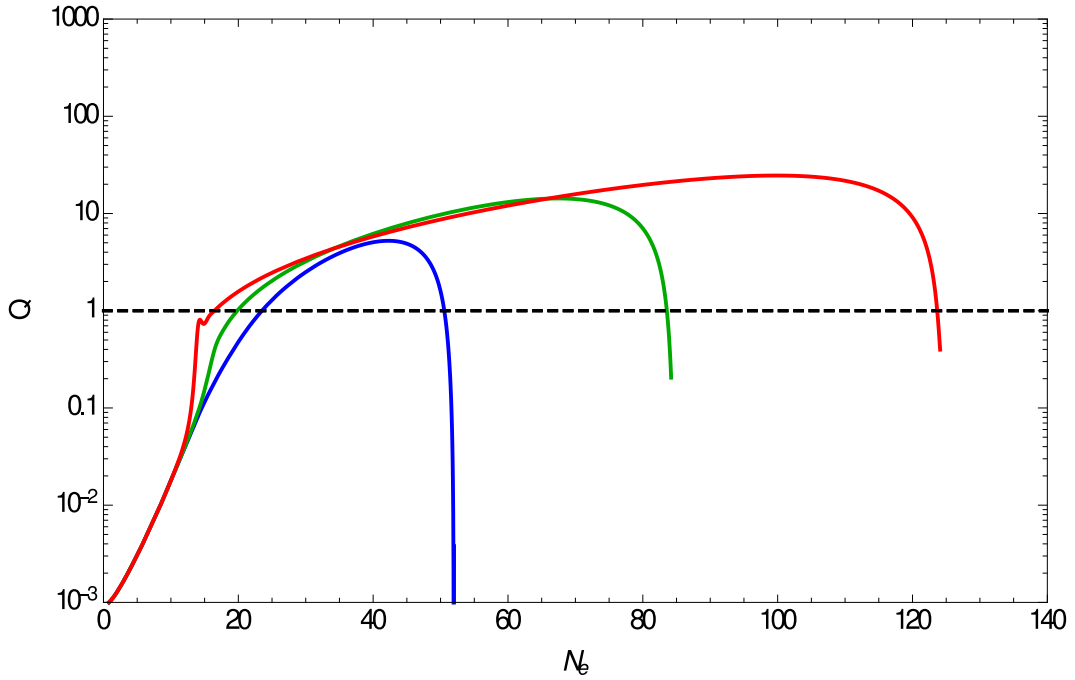

Figure 7.16: Numerical evolution of the dissipative ratio Q using the full dissipation coefficient and including thermal mass corrections for different values of the coupling h, keeping N_Y, g^2N_X, V_0 and C_ϕ constant, as well as the initial inflaton value, so as to fix the same initial conditions as in the previous analysis. Note that this corresponds to changing the value of the effective coupling h^2N_Y and hence the effects of thermal masses and the magnitude of on-shell dissipation.

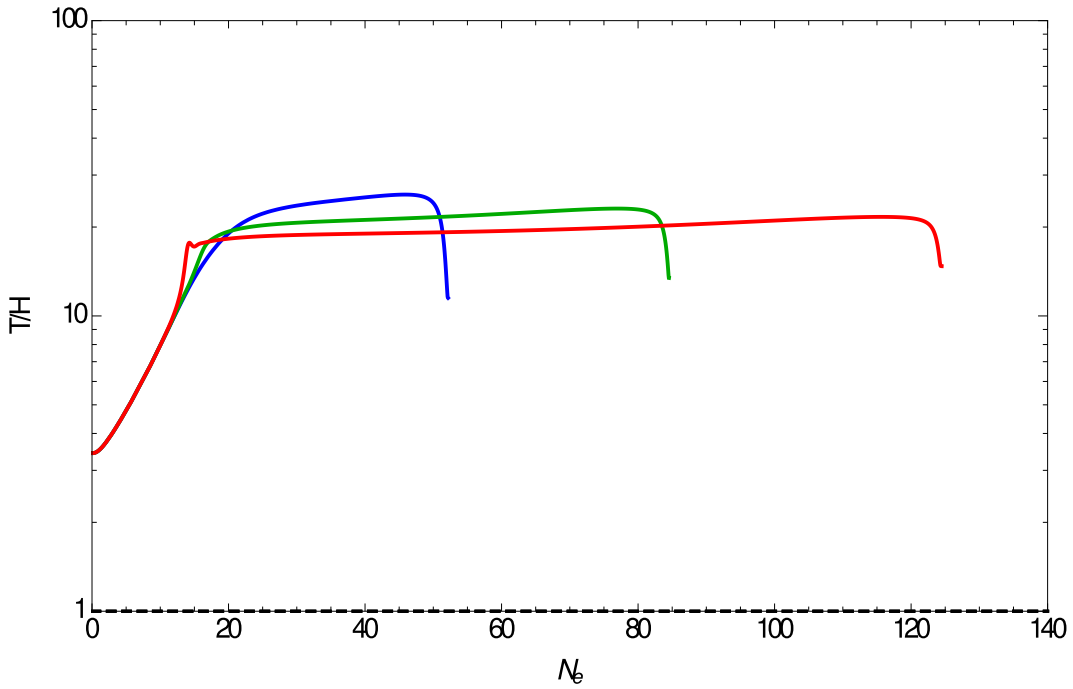

Figure 7.17: Numerical evolution of T/H using the full dissipation coefficient and including thermal mass corrections for different values of the coupling h, keeping N_Y, $g^2 N_X$, V_0 and C_ϕ constant, as well as the initial inflaton value, so as to fix the same initial conditions as in the previous analysis. Note that this corresponds to changing the value of the effective coupling $h^2 N_Y$ and hence the effects of thermal masses and the magnitude of on-shell dissipation.

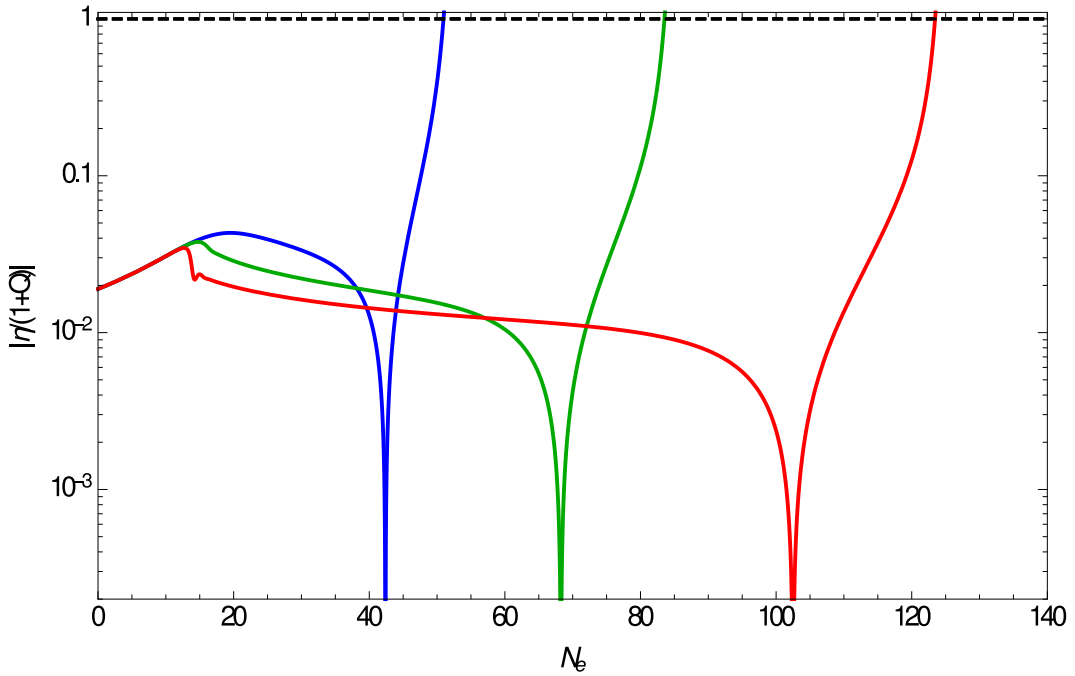

Figure 7.18: Numerical evolution of $|\eta_\phi|/(1+Q)$ using the full dissipation coefficient and including thermal mass corrections for different values of the coupling h, keeping N_Y, $g^2 N_X$, V_0 and C_ϕ constant, as well as the initial inflaton value, so as to fix the same initial conditions as in the previous analysis. Note that this corresponds to changing the value of the effective coupling $h^2 N_Y$ and hence the effects of thermal masses and the magnitude of on-shell dissipation.

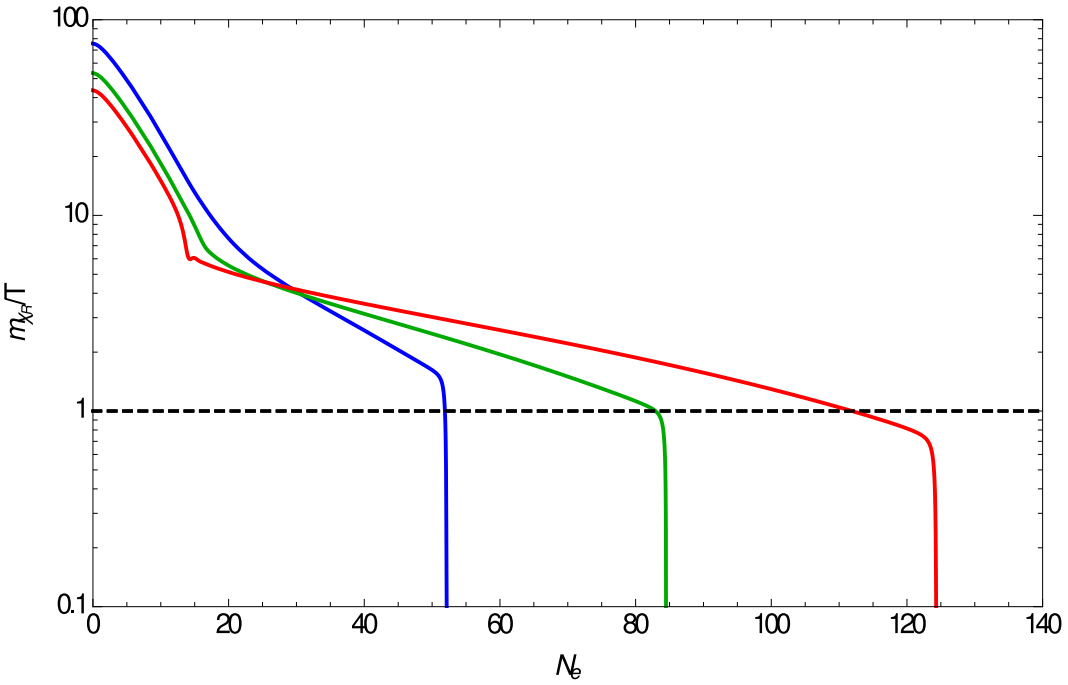

Figure 7.19: Numerical evolution of $m_{\chi T}/T$ using the full dissipation coefficient and including thermal mass corrections for different values of the coupling h, keeping N_Y, $g^2 N_X$, V_0 and C_ϕ constant, as well as the initial inflaton value, so as to fix the same initial conditions as in the previous analysis. Note that this corresponds to changing the value of the effective coupling $h^2 N_Y$ and hence the effects of thermal masses and the magnitude of on-shell dissipation.

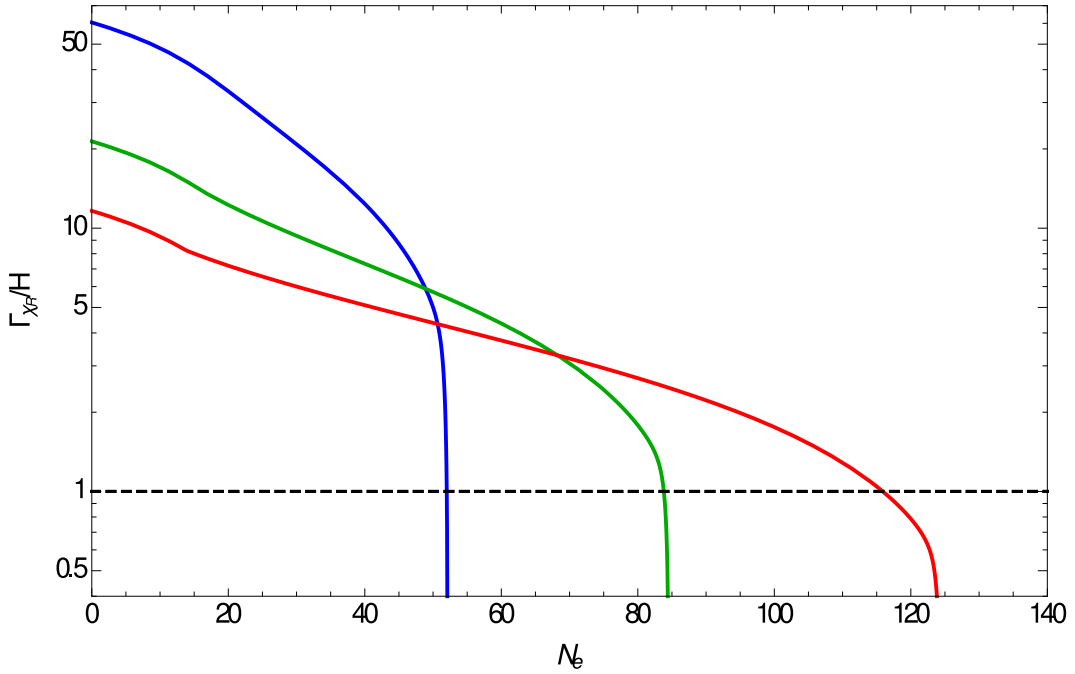

Figure 7.20: Numerical evolution of Γ_{χ_R}/H using the full dissipation coefficient and including thermal mass corrections for different values of the coupling h, keeping N_Y, $g^2 N_X$, V_0 and C_ϕ constant, as well as the initial inflaton value, so as to fix the same initial conditions as in the previous analysis. Note that this corresponds to changing the value of the effective coupling $h^2 N_Y$ and hence the effects of thermal masses and the magnitude of on-shell dissipation.

an exponential dependence on the field masses for on-shell production, and that $\Upsilon_{LM}/\Upsilon_P \propto h^4 N_Y$. The number of e-folds of inflation is however constrained at smaller values of $h^2 N_Y$ since the decay width of the waterfall field must exceed the Hubble parameter, with $\Gamma_{\chi_{R,I}} > H$, otherwise dissipation shuts down.

Thus we conclude that thermal corrections can significantly modify the inflationary dynamics in SUSY hybrid inflation, with the strongest effect being close to the waterfall transition. Dissipative effects damp the inflaton's motion which prolongs inflation whilst sourcing a thermal bath that backreacts onto the properties of the waterfall fields. The thermal mass corrections that are induced lower the critical field value to below the zero-temperature value, but also suppress dissipation, causing the inflaton field to approach the critical value faster. This effect can be seen in the evolution for both the low-momentum dissipation coefficient and the full dissipation coefficient.

7.1.3 Slow-roll Violation

We have seen how dissipative effects can significantly delay the onset of the waterfall transition, with SUSY mass splittings in the waterfall sector particularly enhancing the dissipation coefficient. We have also seen how thermal corrections to the waterfall field masses suppress dissipation for small inflaton values, resulting in the dissipative ratio Q decreasing and a drop in the temperature that ultimately brings about the waterfall transition. Thus the most pronounced effect of including thermal mass corrections is immediately before the waterfall transition. The waterfall transition is not however the only way that inflation can end in the hybrid model, with slow-roll inflation only maintained for:

$$\eta_\phi, \epsilon_\phi < (1 + Q) \ . \tag{7.7}$$

Significantly, we find that if we start the inflaton at larger field values then these slow-roll conditions will fail before the tachyonic instability in the waterfall sector causes the waterfall transition. From initial conditions that give a primordial spectrum consistent with CMB observations by the Planck mission we once again evolve the equations of motion for the inflaton field ϕ and the temperature T with respect to the number of e-folds. In Fig. (7.21-7.26) the green lines represent the evolution of the system during cold inflation, with dissipative effects excluded. The red and blue lines represent the evolution of the system in warm inflation with thermal corrections to the waterfall fields included. The red lines show the evolution when only the low-momentum contribution to the dissipation coefficient, Υ_{LM}, is considered. The blue lines show the evolution for the full dissipation coefficient $\Upsilon = \Upsilon_{LM} + \Upsilon_P$.

Higher values for r have been found in [118,119]. What is apparent is that once again the SUSY hybrid construction can yield $50 - 60$ e-folds of inflation with a primordial spectrum consistent with Planck data. The larger initial inflaton field value ϕ produces a larger tensor-to-scalar ratio with $r = 0.050$, showing that hybrid models are also capable of producing detectable gravity waves. In this example inflation does not end with the onset of the waterfall transition, but with the failure of the slow-roll conditions. In both the case with just the low-momentum contribution to the dissipation coefficient, and the case with the full dissipation coefficient, the inflaton field value is above the critical field value when inflation ends. In this way the SUSY hybrid model starts to behave almost like a chaotic model.

As inflation ends the ratio of the temperature to the Hubble parameter, T/H, dramatically rises, and radiation comes to dominate the energy density of the universe. As we have seen in the previous section the most significant effect of thermal mass corrections to the waterfall sector is that dissipation is suppressed immediately before the hybrid transition. Since in this case inflation ends before

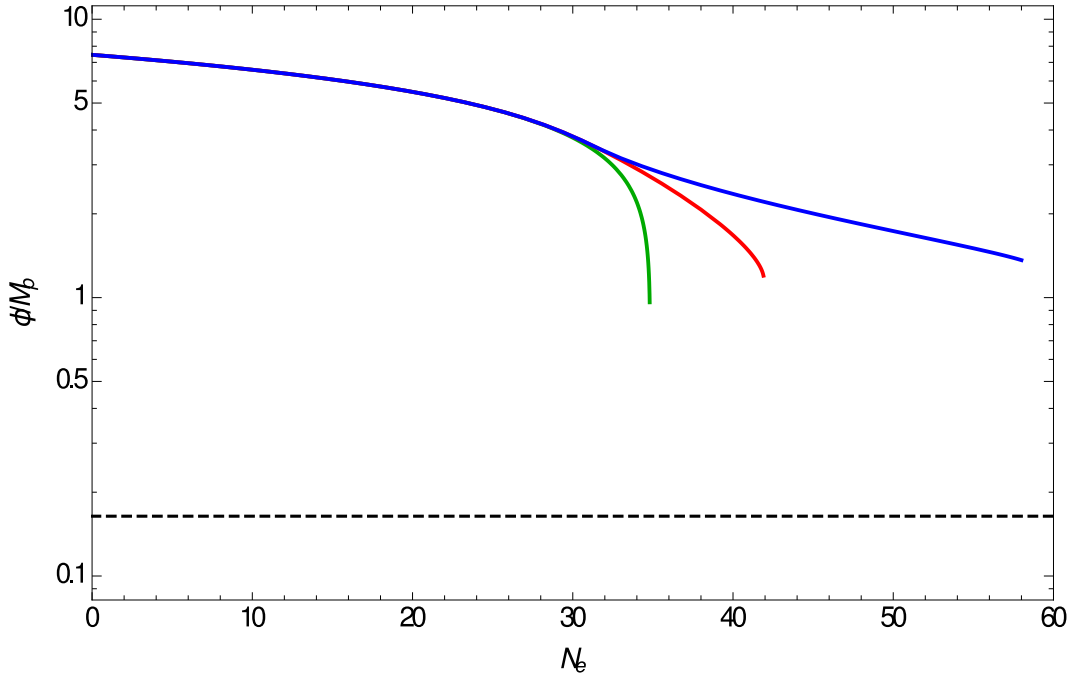

Figure 7.21: The evolution of the inflaton field value ϕ during SUSY warm hybrid inflation for $g = 0.00215$, $h = 0.342$, $N_x = 5 \times 10^6$, $N_y = 10$, and $M = 0.144 m_p$, with an initial value for the inflaton field $\phi_i = \phi_* = 7.45 m_p$ and initial value of Q, $Q_i = Q_* = 2.28 \times 10^{-6}$. The spectral index is $n_s = 0.960$, spectrum $\Delta_R^2 = 2.7 \times 10^{-9}$, and tensor-to-scalar ratio $r = 0.050$. The green lines show the evolution of the system during cold inflation. The red lines show the evolution when only the low-momentum contribution to the dissipation coefficient, Υ_{LM}, is considered. The blue lines show the evolution for the full dissipation coefficient $\Upsilon = \Upsilon_{LM} + \Upsilon_P$. Thermal corrections to the waterfall field masses are included in both the red and blue cases.

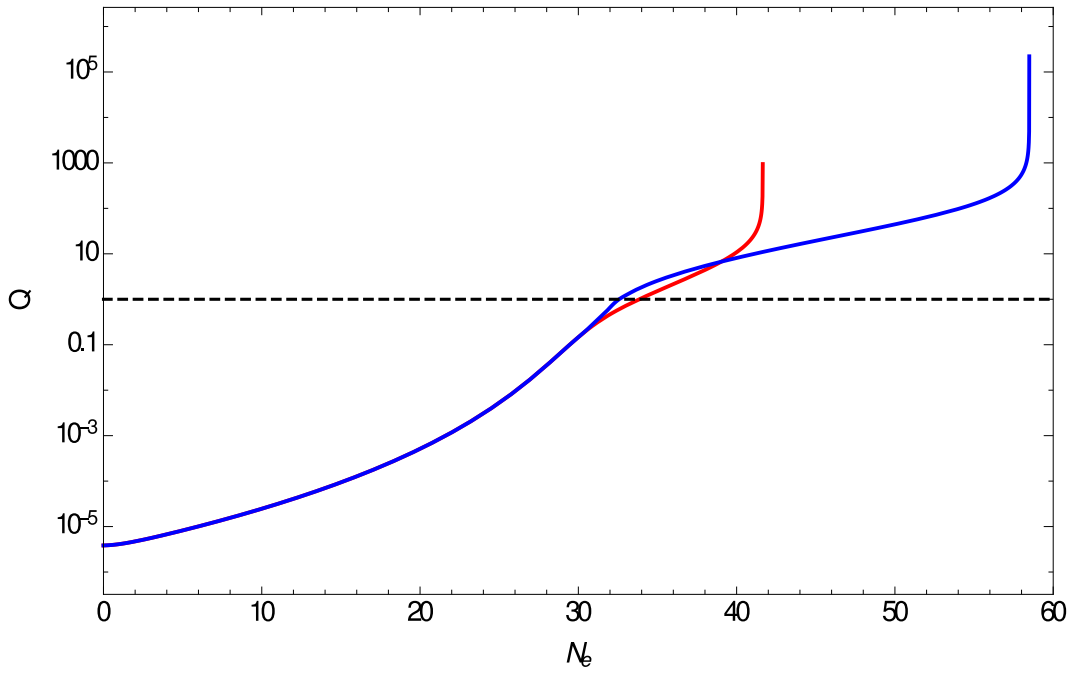

Figure 7.22: The evolution of the dissipative Q during SUSY warm hybrid inflation for $g = 0.00215$, $h = 0.342$, $N_x = 5 \times 10^6$, $N_y = 10$, and $M = 0.144 m_p$, with an initial value for the inflaton field $\phi_i = \phi_* = 7.45 m_p$ and initial value of Q, $Q_i = Q_* = 2.28 \times 10^{-6}$. The spectral index is $n_s = 0.960$, spectrum $\Delta_R^2 = 2.7 \times 10^{-9}$, and tensor-to-scalar ratio $r = 0.050$. The red lines show the evolution when only the low-momentum contribution to the dissipation coefficient, Υ_{LM}, is considered. The blue lines show the evolution for the full dissipation coefficient $\Upsilon = \Upsilon_{LM} + \Upsilon_P$. Thermal corrections to the waterfall field masses are included in both cases.

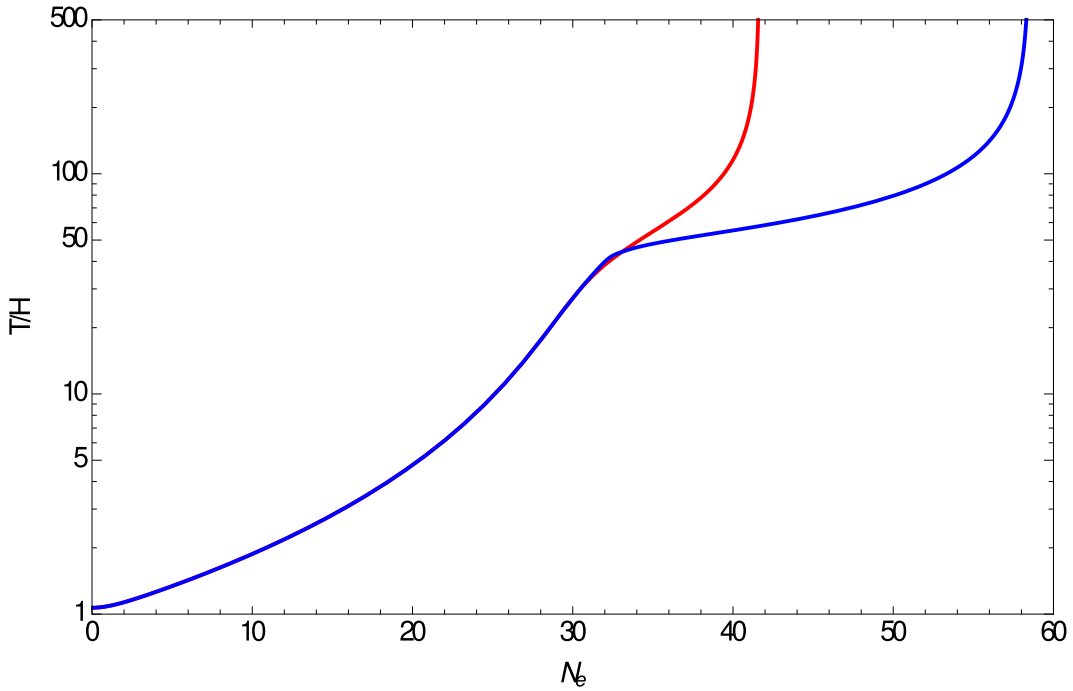

Figure 7.23: The evolution of T/H during SUSY warm hybrid inflation for $g = 0.00215$, $h = 0.342$, $N_x = 5 \times 10^6$, $N_y = 10$, and $M = 0.144 m_p$, with an initial value for the inflaton field $\phi_i = \phi_* = 7.45 m_p$ and initial value of Q, $Q_i = Q_* = 2.28 \times 10^{-6}$. The spectral index is $n_s = 0.960$, spectrum $\Delta_R^2 = 2.7 \times 10^{-9}$, and tensor-to-scalar ratio $r = 0.050$. The red lines show the evolution when only the low-momentum contribution to the dissipation coefficient, Υ_{LM}, is considered. The blue lines show the evolution for the full dissipation coefficient $\Upsilon = \Upsilon_{LM} + \Upsilon_P$. Thermal corrections to the waterfall field masses are included in both cases.

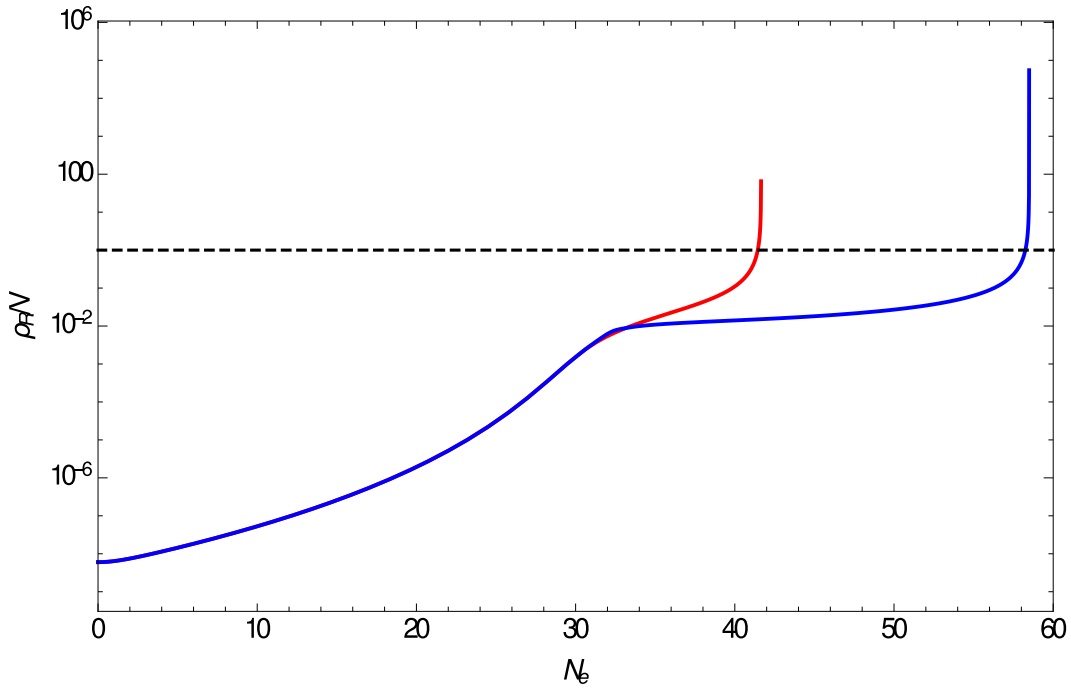

Figure 7.24: The evolution of the radiation energy density relative to the potential ρ_R/V during SUSY warm hybrid inflation for $g = 0.00215$, $h = 0.342$, $N_x = 5 \times 10^6$, $N_y = 10$, and $M = 0.144 m_p$, with an initial value for the inflaton field $\phi_i = \phi_* = 7.45 m_p$ and initial value of Q, $Q_i = Q_* = 2.28 \times 10^{-6}$. The spectral index is $n_s = 0.960$, spectrum $\Delta_R^2 = 2.7 \times 10^{-9}$, and tensor-to-scalar ratio $r = 0.050$. The red lines show the evolution when only the low-momentum contribution to the dissipation coefficient, Υ_{LM}, is considered. The blue lines show the evolution for the full dissipation coefficient $\Upsilon = \Upsilon_{LM} + \Upsilon_P$. Thermal corrections to the waterfall field masses are included in both cases.

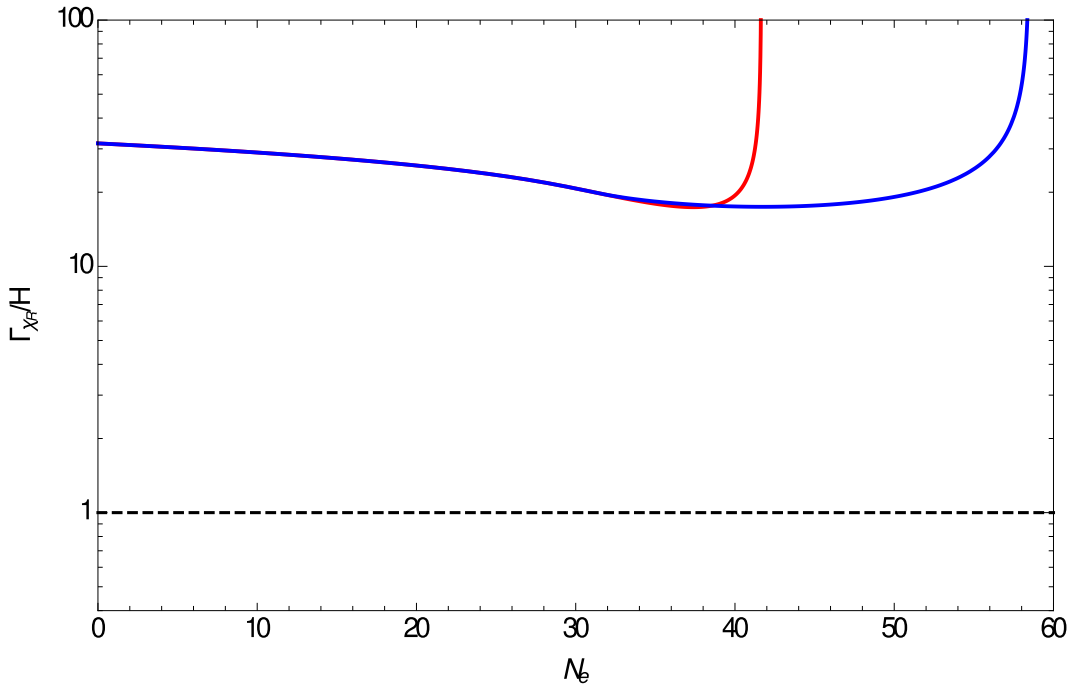

Figure 7.25: The evolution of Γ_{χ_R}/H during SUSY warm hybrid inflation for $g = 0.00215$, $h = 0.342$, $N_x = 5 \times 10^6$, $N_y = 10$, and $M = 0.144 m_p$, with an initial value for the inflaton field $\phi_i = \phi_* = 7.45 m_p$ and initial value of Q, $Q_i = Q_* = 2.28 \times 10^{-6}$. The spectral index is $n_s = 0.960$, spectrum $\Delta_R^2 = 2.7 \times 10^{-9}$, and tensor-to-scalar ratio $r = 0.050$. The red lines show the evolution when only the low-momentum contribution to the dissipation coefficient, Υ_{LM}, is considered. The blue lines show the evolution for the full dissipation coefficient $\Upsilon = \Upsilon_{LM} + \Upsilon_P$. Thermal corrections to the waterfall field masses are included in both cases.

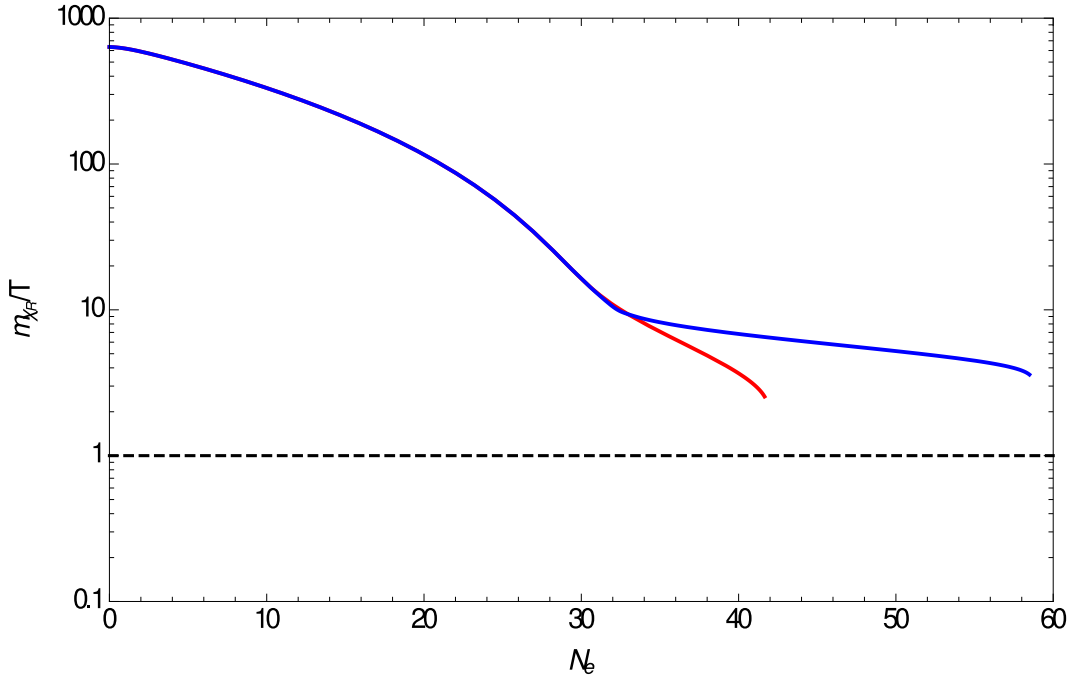

Figure 7.26: The evolution of m_{χ_R}/T during SUSY warm hybrid inflation for $g = 0.00215$, $h = 0.342$, $N_x = 5 \times 10^6$, $N_y = 10$, and $M = 0.144 m_p$, with an initial value for the inflaton field $\phi_i = \phi_* = 7.45 m_p$ and initial value of Q, $Q_i = Q_* = 2.28 \times 10^{-6}$. The spectral index is $n_s = 0.960$, spectrum $\Delta_R^2 = 2.7 \times 10^{-9}$, and tensor-to-scalar ratio $r = 0.050$. The red lines show the evolution when only the low-momentum contribution to the dissipation coefficient, Υ_{LM}, is considered. The blue lines show the evolution for the full dissipation coefficient $\Upsilon = \Upsilon_{LM} + \Upsilon_P$. Thermal corrections to the waterfall field masses are included in both cases.

the inflaton reaches its critical field value the thermal corrections to the waterfall sector do not significantly suppress dissipative effects and the system remains in the strong dissipative regime with $Q < 1$ until the end of inflation. Thus there is no need for a reheating phase to bring the universe into a radiation-dominated era as dissipation naturally allows for radiation to take over as inflation ends.

Chapter 8

Brane-Antibrane Inflation

Inflationary cosmology provides a robust explanation for many of the observed features of our universe, notably the large scale homogeneity, isotropy and spatial flatness, whilst also providing the mechanism for the seeding of large scale structure. Despite this phenomenological success there has yet to emerge a compelling underlying microphysical model within a fundamental UV complete theory of quantum gravity that explains the dynamics of inflation.

The best-known candidate for a theory of quantum gravity is string theory and the need for a microphysical description of the underlying physical mechanism responsible for driving inflation has motivated the study of string theory inflation models. Inflation in string theory has been the subject of many reviews, in particular [120–125].

The realization that spacetime might contain p-branes onto which the standard model particles might be attached has motivated the study of how p-branes might provide a framework within which an inflationary system can be constructed. Significantly, inflation can be realized geometrically and higher-dimensionally through D-branes in the Braneworld, in which D-branes are dynamical objects that can propagate through a higher-dimensional bulk space. Brane-Antibrane inflation has emerged as one of the most attractive scenarios

in realizing inflation in string theory, with the interbane distance providing the geometrical origin of the inflaton field [126–132]. Furthermore, brane-antibrane inflation is a concrete implementation of SUSY hybrid inflation within a UV complete particle physics model. Inflation in these systems does not however seem entirely generic, with, for example, the interbrane distance required to achieve sufficient inflation in flat space exceeding the average size of the compact manifold [126]. This is the η-problem of brane-antibrane inflation.

Warm inflation scenarios are generically free of the η-problem and this has motivated the study of brane-antibrane inflation in the warm regime [25, 63, 67]. In this chapter I will introduce some of the basic features of D-Branes and how a brane-antibrane inflationary system can be realized with the motion of D-Branes through a higher-dimensional space. Then I will discuss how brane-antibrane inflation has been previously implemented in the warm regime in [68].

8.1 D-Branes

A Dp-brane is a hypersurface upon which open strings can end with Dirichlet boundary conditions. When we consider an open string in a higher dimensional spacetime manifold we must impose appropriate boundary conditions for the ends of the string. There are actually two types of condition that can be imposed, Neumann boundary conditions and Dirichlet boundary conditions. Under Neumann boundary conditions the movement of the ends of the open strings is such that there is no momentum flowing through the boundaries, whereas under Dirichlet boundary conditions ends of strings are held in a fixed position. If we imagine an open string in a hyperspace with $\mathcal{D}$ space-time dimensions then the ends of the strings can satisfy the Neumann conditions in $p+1$ space-time dimensions, and Dirichlet conditions in the remaining $\mathcal{D}-p-1$ orthogonal directions. Imposing these boundary conditions results in the ends of

the open strings being localized on two p-dimensional hypersurfaces. Dp-branes are these p-dimensional hypersurfaces.

In Type IIB string theory a Dp-brane has p spatial dimensions and exists within a (9+1) dimensional bulk space (for instance, the worldvolume of a D3-brane spans the 3 non-compact dimensions that expand during inflation, whilst wrapping $d_{||} = p - 3$ of the compact directions). These directions have a size $L_{||}$, while the remaining $d_{\perp} = 9 - p$ compact directions have a size $L_{\perp}$. The compact manifold within which the D-branes exist has a volume:

$$V_6 = V_{||} V_{\perp} = L_{||}^{p-3} L_{\perp}^{9-p} \ . \tag{8.1}$$

In the braneworld framework [133] the particles of the standard model are open string modes with endpoints attached to a stack of Dp-branes, where 3 of the p dimensions are the 3 dimensions of our macroscopic universe and the remaining $p - 3$ span some higher dimensional bulk space in which closed string modes like the graviton can propagate. The mass and charge of a Dp-brane is determined by the Dp-brane tension, which for D3-branes is given by the expression:

$$T_3 = \frac{2\pi}{(2\pi l_s)^4 g_s} \ , \tag{8.2}$$

where l_s is the fundamental string length and g_s is the string coupling. The open strings stuck to a stack of N D-branes are in representations of an SU(N) group with Yang-Mills coupling determined by the size of the compact dimension parallel to the branes worldvolume:

$$g_{YM}^2 = 2\pi g_s \left(\frac{2\pi l_s}{L_{||}} \right)^{p-3} \ . \tag{8.3}$$

8.2 Inflation with D-Branes

One of the most well-motivated inflationary models in string theory is brane-antibrane inflation [126]. In superstring models Dp-Branes act as sources of an interaction which has a strength of gravitational intensity and is mediated by the exchange of what are known as Ramond-Ramond (RR) fields [134]. In the closed string spectrum these RR-fields correspond to bosonic states, similar to gauge fields and so are part of the same supermultiplet as the graviton and gravitino in higher-dimensional superstring theory. For sources of the same sign (for instance two branes) the interaction is repulsive and for sources of opposite sign (for instance a brane and an antibrane) the interaction is attractive. In a system consisting of two identical and static parallel branes the gravitational attraction is exactly balanced by the repulsion due to the exchange of RR fields and the system remains static. This is because Dp-branes are solutions of the supergravity equations of motion that preserve half of the supersymmetries of the 10D space while $\overline{\mathrm{D}p}$-branes (antibranes) preserve the other half. The cancellation of the gravitational and RR interactions for parallel branes with the same sign charge is due to this configuration preserving supersymmetry. A system comprised of D3-branes and $\overline{\mathrm{D3}}$-branes will break supersymmetry completely and leads to a finite energy density that can be responsible for driving inflation. If we replace one of the branes in the system with an antibrane the interaction arising from the exchange of RR fields becomes attractive. There is no cancellation of the gravitational force and the net result is an attraction between the brane and antibrane.

An inflationary system can be obtained by considering the interaction between a brane and an antibrane. When separated at sufficient distance, the attractive forces between the brane and antibrane generate an inflationary potential, with the coordinate parameterizing the interbrane distance acting as the inflaton field.

The simplest example of brane-antibrane inflation in Type IIB string theory

involves a stack of N_c (the number of branes in the stack) D3-branes and $\tilde{N}_c$ $\overline{\text{D3}}$-branes (antibranes) spanning the non-compact directions 0123 and separated by a distance r in a six-dimensional flat torus with volume $V_6 = L^6$, which, since a flat toroidal compactification is the simplest example, will be our focus (although brane-antibrane inflation can be implemented in more complicated Calabi-Yau compactifications). This separation of the brane and antibrane stacks by a distance r on a compactification manifold M is illustrated in Fig. (8.1) and Fig. (8.2). Inflation will occur as the brane and antibrane stacks move towards

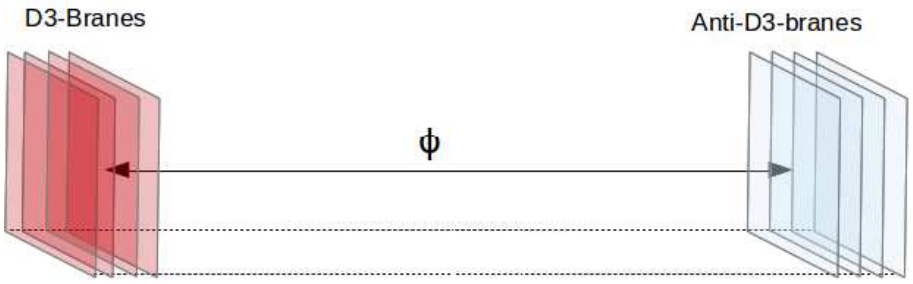

Figure 8.1: Brane-antibrane inflation is implemented with a stack of branes and a stack of antibranes separated within a compact space. Inflation proceeds with the stack of branes moving towards the stack of antibranes, with the interbane distance being interpreted as the inflaton.

each other through the higher-dimensional bulk space, with the relative brane-antibrane position parameterizing the inflaton field ϕ and the inflaton potential $V(\phi)$ arising from their interactions. As has already been mentioned, D-branes are hypersurfaces onto which the endpoints of open strings are attached and in the brane-antibrane system there are therefore strings stretched between the brane and antibrane stacks, spanning the interbrane distance. Inflation will end when the lightest mode of the strings stretched between the brane and antibrane stacks becomes tachyonic. This will happen at an interbrane distance of order the inverse string mass scale $1/M_s$, ending inflation with a tachyonic instability just as in hybrid inflation. For this reason we assume inflation starts with interbrane

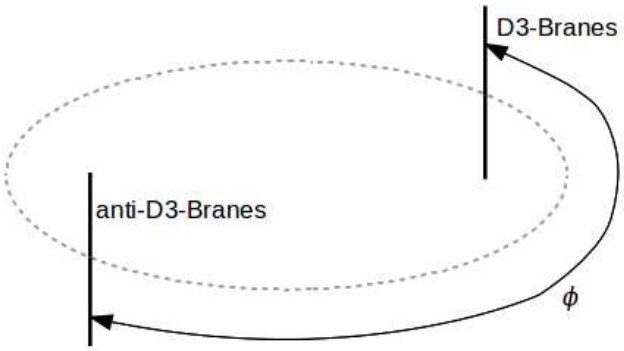

Figure 8.2: The brane and antibrane stacks are separated within a compact space, with the compact space being a circumference and the brane and antibrane stacks are placed at the antipodal points where they are approximately stable. If they are displaced slightly from this position then they start to move towards each other.

distance $r \gg l_s$, where l_s is the fundamental string length.

At large separations the force arising from the interactions relating to gravity and RR fields is well approximated by a Coulomb interaction [134], with the potential taking the form [135]:

$$V(r) = 2T_3 \left(1 - \frac{1}{2\pi^3} \frac{T_3}{m_{10,p}^8 r^4}\right) \ , \tag{8.4}$$

where T_3 is the D3-brane tension and the 10D planck mass is defined $m_{10,p}^{-8} = 8\pi G_{10}$. This can be rewritten in terms of a canonically normalized scalar field ϕ giving a potential which, at large field values can drive inflation [127]:

$$V(\phi) = 2T_3 \left(1 - \frac{1}{2\pi^3} \frac{T_3^3}{m_{10,p}^8 \phi^4}\right) \ . \tag{8.5}$$

We therefore have a potential that can be responsible for driving inflation and contains a constant term in the potential given by the brane tension that is completely analogous to the constant term that arises in the hybrid potential due to supersymmetry breaking.

The η problem

We have seen how an inflationary scalar potential is generated in a brane-antibrane system, with the interbrane distance corresponding to the scalar inflaton field ϕ. As we have seen previously, the slow-roll conditions in standard supercooled slow-roll inflation are given by:

$$\epsilon_\phi = \frac{m_p^2}{2}\left(\frac{V_{,\phi}}{V}\right)^2 < 1 \ , \tag{8.6}$$

$$\eta_\phi = m_p^2 \frac{V_{,\phi\phi}}{V} < 1 \ , \tag{8.7}$$

where once again $V_{,\phi}$ and $V_{,\phi\phi}$ are the first and second derivative of the potential with respect to the field ϕ. These conditions, dependent on the form of the potential, must be satisfied for a slow-roll inflationary phase lasting $50-60$ e-folds. The 4D planck mass m_p is related to the 10D planck mass through the relation:

$$m_p^2 = m_{10,p}^8 L^6 \ , \tag{8.8}$$

where L^6 is the volume of the compact manifold M. From this the η parameter is evaluated to be [135]:

$$\eta_\phi = -\frac{10}{\pi}(L/r)^6 \ - 0.3(L/r)^6 \ . \tag{8.9}$$

Thus we need an interbrane separation r greater than the length of the compactified extra dimension L in order to maintain slow-roll inflation with $\eta < 1$. The problem is that within the compact manifold the brane and antibrane can only be separated by a distance $r \leq L/2$, meaning it is impossible to keep the slow-roll parameter η less than 1. This is the η-problem of brane-antibrane inflation [126].

8.3 Warm Brane-Antibrane Inflation

As we have already seen in this thesis, warm inflation scenarios are less constrained by the η-problem, with dissipative effects retarding the evolution of the inflaton field and allowing for a prolonging of the inflationary phase. This has motivated the study of brane-antibrane inflation in the warm regime. It was shown in [68] that warm inflation scenarios can be easily implemented in brane-antibrane constructions and offer a robust solution to the η-problem of brane-antibrane inflation.

Implementing the two-stage decay mechanism of warm inflation requires both the existence of light degrees of freedom to act as the ultimate destination for inflaton energy and mediator fields to enable the transfer of inflaton energy to this light sector. Characteristically brane-antibrane inflation in fact naturally includes degrees of freedom coupled to the inflaton in the form of massive open strings stretched over the interbrane distance with endpoints fixed on the brane and antibrane stacks. The coupling of these states to the inflaton field determines their mass, with the associated fields becoming heavy at the large interbrane distances involved in initial configurations of brane-antibrane inflation. This crucially enables the dissipation of inflaton energy to be mediated. As has already been noted, below a certain critical interbrane distance of order the string length these states become tachyonic and trigger the end of inflation. Brane-antibrane inflation is therefore completely analogous with SUSY hybrid inflation, with the waterfall fields being equivalent to the ground states of these strings stretched over the interbrane distance.

Implementing warm inflation within a brane-antibrane construction however requires going beyond a model simply involving a stack of D3-branes separated by some distance in a compact manifold from a stack of $\overline{\text{D3}}$-branes. In particular, implementing the two-stage decay chain for the inflaton requires the introduction of light fields to act as the ultimate destination for inflaton energy. Furthermore,

the existence of these light states is in fact required, regardless of whether the two-stage mechanism of warm inflation is implemented, in order to incorporate the Standard Model particles or any of its extensions in the system once inflation has ended. One possible way the incorporation of light degrees of freedom can be done is by including additional branes of different dimensionality [136].

In the previous section we have seen that brane-antibrane inflation can be implemented with a stack of N_c D3-branes and $\tilde{N}_c$ $\overline{\text{D3}}$-branes spanning the non-compact directions 0123 and separated by a distance r in a six-dimensional flat torus with volume $V_6 = L^6$. Light degrees of freedom can be incorporated with the inclusion of N_f D7-Branes that span the 01234567 directions (with the 4567 directions being compact). This will enable the introduction of light matter particles that correspond to open strings attached to either the D7-stack and the D3-stack or the D7-stack and the $\overline{\text{D3}}$-stack.

In this setup the two-stage mechanism of warm inflation can be implemented, with dissipation of inflaton energy mediated by heavy states corresponding to strings stretched between the D3 and $\overline{\text{D3}}$ stacks to light degrees of freedom that correspond to strings stretched between the D7-stack and either the D3-stack or the $\overline{\text{D3}}$-stack.

8.3.1 Dissipation with D-Branes

We have outlined the necessary ingredients to implement the two-stage decay chain in a brane-antibrane construction and can now investigate the details of such a scenario. Consider a setup in type IIB string theory with a stack of N_c D3-branes and $\tilde{N}_c$ $\overline{\text{D3}}$-branes that span the 0123 directions and N_f D7-Branes spanning the 01234567 directions. Each brane will have attached to it strings with endpoints fixed either on the same brane or a different brane and with a stack of n branes there are n^2 different strings filling adjoint supermultiplets of the $U(n)$ gauge group.

An isolated stack of parallel D-branes will preserve $\mathcal{N} = 4$ supersymmetry in the effective 4-dimensional theory, but typically a setup including intersecting branes will break some of these supersymmetries. The D3/$\overline{\text{D3}}$-D7 construction described above has $\mathcal{N} = 2$ supersymmetry, containing an $\mathcal{N} = 4$ vector multiplet from the D3-stack, in the adjoint representation of $U(N_c + \tilde{N}_c)$, a similar $U(N_f)$ multiplet from the D7-stack and an $\mathcal{N} = 2$ hypermultiplet from strings in the D3/$\overline{\text{D3}}$-D7 sector. In $\mathcal{N} = 1$ supersymmetric language this includes adjoint chiral multiplets Φ_i, with i=1,2,3, and N_f (anti)fundamental chiral superfields Q, $\tilde{Q}$ which correspond to strings stretched between the D7-stack and either the D3-stack or the $\overline{\text{D3}}$-stack. The superpotential describing the interactions between the chiral superfields is then written [137]:

$$W = \sqrt{2} g_{YM} \text{Tr} \Phi_1 \left[\Phi_2, \Phi_3\right] + \sqrt{2} g_{YM} \tilde{Q} \Phi_3 Q \ , \tag{8.10}$$

with the closed string coupling g_s related to the gauge coupling $g_{YM} = 2\pi g_s$. When the brane stacks are separated a scalar vacuum expectation value is generated, with the vacuum expectation value of the real and imaginary scalar components of Φ_1 corresponding to separation in the 4 and 5 directions. Separation of the brane stacks in the 6 and 7 directions corresponds to generating a scalar vev of the real and imaginary scalar components of Φ_2 and separation in the 8 and 9 directions corresponds to generating a vev of the real and imaginary scalar components of Φ_3 (456789 being the compactified directions). Notice that since the D7-branes already wrap the 4567 directions, the scalar vacuum expectation value of Φ_3 determines the D3/$\overline{\text{D3}}$-D7 separation and the fields in the Q and $\tilde{Q}$ sectors only gain masses if the D3-branes are separated from the D7-branes. It was shown in [68] that the separation between the D3/$\overline{\text{D3}}$ and the D7 stacks is naturally small with the D7-branes effecting the metric and making it energetically favorable for both the D3 and $\overline{\text{D3}}$ to lie on top of the D7-branes. This ensures the existence of light degrees of freedom in the Q and $\tilde{Q}$ sectors

enabling implementation of the two-stage mechanism.

If, as an example, we consider the case with:

$$N_c = \tilde{N}_c = N_f = 1 \ , \tag{8.11}$$

then we have a $U(2)$ theory on the worldvolume of the D3-branes. This results in an $\mathcal{N} = 2$ supersymmetric worldvolume theory that is described by a $U(2)$ $\mathcal{N} = 4$ vector multiplet and an $\mathcal{N} = 2$ hypermultiplet, where $U(2)$ is a gauge symmetry. Separating the D3 and $\overline{\text{D3}}$-brane, which we denote by A and B, in one of the directions transverse to their worldvolumes turns on a scalar vacuum expectation value and leads to a $U(1)_A \times U(1)_B$ gauge theory with abelian gauge fields on the worldvolume of each brane and the superfields can be written as [68]:

$$\Phi_i = \begin{pmatrix} \Phi_i^A & X_i \\ \tilde{X}_i & \Phi_i^B \end{pmatrix}, \quad Q = \begin{pmatrix} Y^A \\ Y^B \end{pmatrix} \ , \quad \tilde{Q} = \begin{pmatrix} \tilde{Y}^A \\ \tilde{Y}^B \end{pmatrix}.$$

The superfields $\Phi_i^{A,B}$ correspond to the positions of each D3-brane in the compact space, while X_i and $\tilde{X}_i$ correspond to mediator fields stretched between the two branes. The $Y^{A,B}$ and $\tilde{Y}^{A,B}$ correspond to the open strings in the D3^{A,B} - D7 sectors. Using this decomposition this superpotential can be written:

$$\begin{aligned} W \ = \ & \sqrt{2} g_{YM} \Big[\Phi_1^{AB} X_2 \tilde{X}_3 - \Phi_1^{AB} X_3 \tilde{X}_2 + \Phi_2^{AB} X_3 \tilde{X}_1 - \Phi_2^{AB} X_1 \tilde{X}_3 + \Phi_3^{AB} X_1 \tilde{X}_2 \\ & - \Phi_3^{AB} X_2 \tilde{X}_1 + \tilde{Y}^A X_3 Y^B + \tilde{Y}^B \tilde{X}_3 Y^A + \tilde{Y}^A \Phi_3^A Y^A + \tilde{Y}^B \Phi_3^B Y^B \Big] \ , \end{aligned} \tag{8.12}$$

where we have defined the positions of the branes relative to each other as $\Phi_i^{AB} = \Phi_i^A - \Phi_i^B$. As has previously been noted, the branes and antibranes preserve different halves of the supersymmetry, resulting in a non-vanishing potential for inflation. With supersymmetry broken the open strings stretched between the D3 and $\overline{\text{D3}}$ stacks become non-supersymmetric with the scalar masses of the X

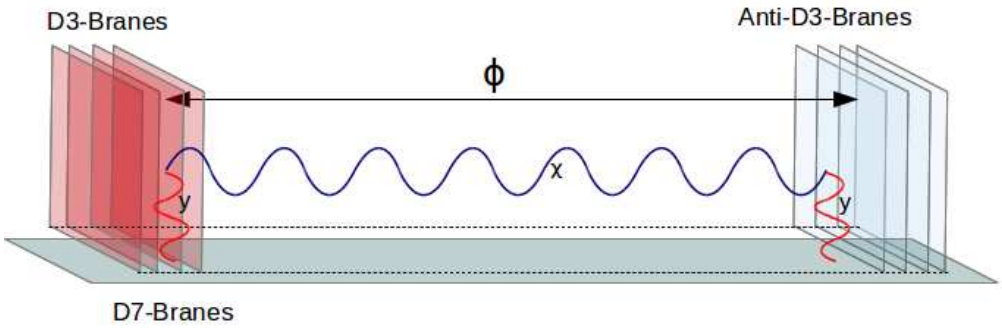

Figure 8.3: Warm inflation can be implemented in the brane-antibrane set up with the inclusion of a $D7$-brane. Fields that correspond to strings stretched between the brane and antibrane stacks mediate dissipation of inflaton energy to light fields that correspond to strings stretched between the brane and antibrane stacks and the $D7$-branes.

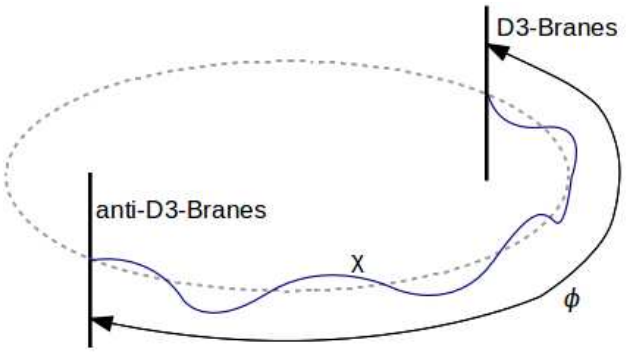

Figure 8.4: Warm inflation can be implemented in a brane-antibrane system with dissipation mediated by fields corresponding to strings stretched between the brane and antibrane stacks.

and $\tilde{X}$ fields being shifted by a factor inversely proportional to the fundamental string tension. The fermion masses are however unchanged and the supertrace $\mathrm{STr}M^2 = 0$ is preserved with supersymmetry being softly broken [138], as was the case in the hybrid model presented in the first part of this thesis.

The interactions in the superpotential enable the implementation of the two stage mechanism for warm inflation. The inflaton is coupled to heavy fields in the X and $\tilde{X}$ sectors, corresponding to strings stretched between the D3 and $\overline{\mathrm{D3}}$, which are in turn coupled to light fields in the Y and $\tilde{Y}$ sectors. These fields couple to the Φ_3^A and Φ_3^B separately, but not to the inflaton field driving inflation $\Phi_3^{AB} = \Phi_3^A - \Phi_3^B$, and will remain light given the separation between the D3/$\overline{\mathrm{D3}}$ and the D7 stacks is negligible. Furthermore, the number of mediator fields are related to the number of N_c D3-branes and $\tilde{N}_c$ $\overline{\mathrm{D3}}$-branes through the expression:

$$N_X = 2N_c\tilde{N}_c \ , \tag{8.13}$$

with the number of decay channels related to the number of D7-branes:

$$N_Y = N_f. \tag{8.14}$$

As has been stated, in order achieve $50-60$ e-folds of inflation in the warm regime with $T/H > 1$ we typically require $N_X \simeq 10^4 - 10^6$. In the brane-antibrane construction this field multiplicity can be achieved with $N_c \simeq \tilde{N}_c \simeq 10^2 - 10^3$ branes.

8.4 Summary

In this chapter we have outlined how inflation can be realized geometrically and higher-dimensionally through D-branes in the Braneworld. Brane-antibrane inflation proceeds with a stack of D3-branes moving in a compact space towards

a stack of $\overline{\text{D3}}$-branes. The inflationary potential is generated by the interactions between the brane stacks with the inflaton field being parameterized by the interbrane distance. Simple constructions of brane-antibrane inflation do however suffer from the η-problem, with a sufficiently long period of inflation requiring that the brane stacks are initially separated by a distance greater than is possible in the compact manifold. This has motivated the study of brane-antibrane inflation in the warm regime, which is typically free of the η-problem. We have outlined how the two-stage mechanism can be implemented, with fields associated with the strings stretched between the D3 and $\overline{\text{D3}}$ mediating dissipation of inflaton energy to light degrees of freedom that are associated with strings stretched between the D3/$\overline{\text{D3}}$ stacks and a stack of D7-branes.

Chapter 9

Dissipation from Compactification

In the previous chapter we discussed how the two-stage mechanism of warm inflation can be realized in a brane-antibrane construction, with dissipation of inflaton energy being mediated by fields that are associated with strings stretched between the brane and antibrane stacks. The higher-dimensional space within which the brane-antibrane system exists is compact, meaning that the extra spatial dimensions are not infinite but are effectively curled up in themselves. This allows for strings that are stretched between the brane and antibrane stacks to be wound around the extra dimensions an arbitrary number of times. In particular, for every string stretched over the shortest distance between the brane and antibrane stacks there will additionally exist an infinite number of strings of increasing winding number, corresponding to the number of times the string is wrapped around the extra dimension. These strings of increasing winding number correspond in effect to heavier and heavier flavors of the mediator fields of the two stage mechanism. Dissipative effects associated with strings stretched directly between the brane and antibrane stacks have been studied in [68]. The research presented in this chapter builds on this implementation of brane-

antibrane systems in warm inflation by investigating the additional dissipative effects arising from strings of increasing winding number. In the following sections I will review the idea of how string winding modes can be modeled as brane images. I will then show how we have calculated an enhancement to dissipation arising from string winding modes and I will present the results for the enhancement to the dissipation coefficient. Following this I will present the numerical results for the evolution of a brane-antibrane system in the warm regime with dissipation from string winding modes included.

9.1 Brane Images

In order to study the dissipative effects arising from string winding modes it is useful to start with a framework in which the evolution of the brane-antibrane system and the presence of string winding modes can be understood. The compact geometry within which the system exists can be modeled with a probe antibrane moving towards a stack of branes located at the origin within a lattice of images of the brane stack [139–141]. The lattice can be thought of as a space containing an infinite number of copies, or "images", of the brane stack, separated by the size of the compact extra dimension. The distance from the probe brane to any individual image is analogous to the winding number of the string stretched between the probe and that particular image, with strings stretched between the probe and images increasing in length the further away the image is in the lattice. The distribution of images in the lattice is dependent on the specific type of compactification studied. The most basic case is that of a flat 6-torus, with flat toroidal compactifications generating a covering space given by a hypercubic lattice of images. Whilst there are more complicated compactifications which will have a different distribution of images the hypercubic lattice generated by the flat torus is the simplest and so is an appropriate starting point for an investigation

into the effect of string winding modes. In the following section we outline the

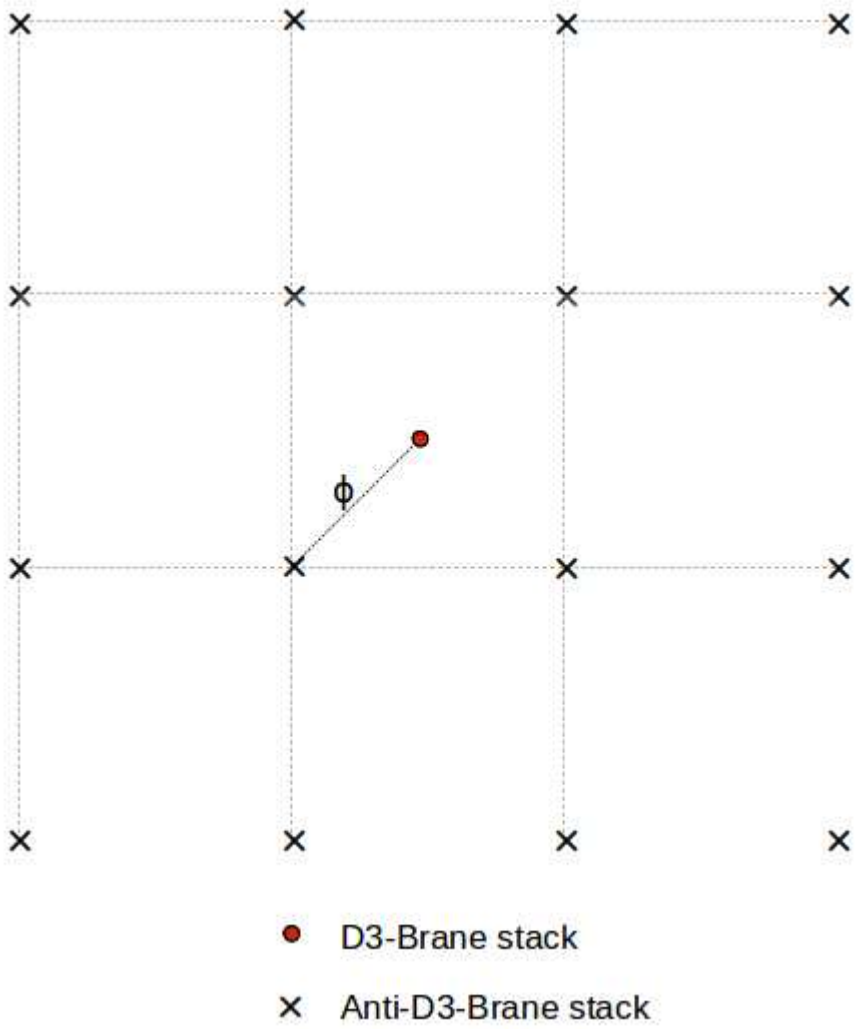

Figure 9.1: The compactified geometry of the brane-antibrane setup can be modeled as a probe brane moving through a hypercubic lattice of images of the antibrane stack.

effect that these images can have in a dissipative brane-antibrane inflation system. As was described in the previous Chapter, the warm brane-antibrane construction involves 3 components:

- The inflaton field, responsible for slow-roll inflation and corresponding to the D3-$\overline{\text{D3}}$ interbrane distance.

- Heavy mediator X and $\tilde{X}$ fields that correspond to strings stretched between the D3 and $\overline{\text{D3}}$ stacks. The mass of these heavy fields is determined by the D3-$\overline{\text{D3}}$ interbrane distance and hence the coupling to the inflaton. In the warm regime these fields mediate dissipation of inflaton energy to light degrees of freedom, damping the inflaton's motion.

- Light Y and $\tilde{Y}$ fields that correspond to strings with end points attached to either the D3 or $\overline{\text{D3}}$ stack and an additional stack of D7 branes. These fields are coupled to the heavy mediator fields and act as the ultimate destination for the inflaton energy.

As the probe brane moves towards the D3 stack located at the origin the strings stretched between the probe and the D3 stack mediate dissipation of inflaton energy to the light sector. In a brane-antibrane construction with a probe brane moving through a hypercubic lattice of brane images there are, in addition to strings stretched between the probe and D3 stack, strings stretched between the probe and each image of the D3 stack within the infinite hypercubic lattice. These strings correspond to heavier flavors of the original X and $\tilde{X}$ mediator fields, becoming heavier the further away the brane image is.

9.2 String Winding Modes Dissipation Coefficient

Understanding dissipative effects arising from string winding modes requires a formulation of the contribution towards dissipation from a string of arbitrary winding number and then a summation over all the winding modes appearing in the hypercubic lattice. We have seen in the previous Chapter that the two-stage decay mechanism of warm inflation is implemented within the brane-antibrane

construction with a superpotential of the form [68]:

$$W = \sqrt{2} g_{YM} \mathrm{Tr} \Phi_1 \left[\Phi_2, \Phi_3\right] + \sqrt{2} g_{YM} \tilde{Q} \Phi_3 Q \ , \tag{9.1}$$

where the vacuum expectation value of the real and imaginary components of $\Phi_{1,2,3}$ correspond to the separation of the brane stacks in the 45, 67 and 89 directions respectively and light degrees of freedom are contained within the Q and $\tilde{Q}$ sectors. We have also shown that this superpotential can be decomposed to:

$$\begin{aligned} W &= \sqrt{2} g_{YM} \Big[\Phi_1^{AB} X_2 \tilde{X}_3 - \Phi_1^{AB} X_3 \tilde{X}_2 + \Phi_2^{AB} X_3 \tilde{X}_1 - \Phi_2^{AB} X_1 \tilde{X}_3 + \Phi_3^{AB} X_1 \tilde{X}_2 \\ &\quad - \Phi_3^{AB} X_2 \tilde{X}_1 + \tilde{Y}^A X_3 Y^B + \tilde{Y}^B \tilde{X}_3 Y^A + \tilde{Y}^A \Phi_3^A Y^A + \tilde{Y}^B \Phi_3^B Y^B \Big] \ , \end{aligned} \tag{9.2}$$

where the superfields $\Phi_i^{A,B}$ correspond to the positions of each D3-brane in the compact space, while X_i and $\tilde{X}_i$ correspond to mediator fields stretched between the two branes. Φ_i^{AB} corresponds to the relative distance between the D3 and $\overline{\mathrm{D3}}$ stacks and the $Y^{A,B}$ and $\tilde{Y}^{A,B}$ correspond to the open strings in the D3^{A,B} - D7 sectors. The lagrangian derived from this superpotential has mass mixing terms of the form:

$$\begin{aligned} \mathcal{L}_{mass} &= 2 g_{YM}^2 \Big(|\phi_1|^2 |\chi_2|^2 - \phi_1 \chi_2 \phi_2^\dagger \chi_1^\dagger - \phi_2 \chi_1 \phi_1^\dagger \chi_2^\dagger + |\phi_2|^2 |\chi_1|^2 \\ &+ |\phi_1|^2 |\chi_3|^2 - \phi_1 \chi_3 \phi_3^\dagger \chi_1^\dagger - \phi_3 \chi_1 \phi_1^\dagger \chi_3^\dagger + |\phi_3|^2 |\chi_1|^2 \\ &+ |\phi_2|^2 |\chi_3|^2 - \phi_2 \chi_3 \phi_3^\dagger \chi_2^\dagger - \phi_3 \chi_2 \phi_2^\dagger \chi_3^\dagger + |\phi_3|^2 |\chi_2|^2 \Big) \ , \end{aligned} \tag{9.3}$$

where $\phi_{1,2,3}$ are the scalar components of the superfields $\Phi_{1,2,3}$ and $\chi_{1,2,3}$ are the scalar components of the $X_{1,2,3}$ superfields. This lagrangian can be rewritten in mass matrix form with eigenvalues:

$$\begin{aligned}\lambda_1 &= |\phi_1|^2 + |\phi_2|^2 + |\phi_3|^2 \\ \lambda_2 &= 0 \\ \lambda_3 &= |\phi_1|^2 + |\phi_2|^2 + |\phi_3|^2\end{aligned}$$

and eigenvectors:

$$\begin{bmatrix} -\phi_3 \\ 0 \\ \phi_1 \end{bmatrix}, \quad \begin{bmatrix} \phi_1 \\ \phi_2 \\ \phi_3 \end{bmatrix}, \quad \begin{bmatrix} -\phi_2 \\ \phi_1 \\ 0 \end{bmatrix}.$$

As has been stated the vacuum expectation value of the real and imaginary scalar components of Φ_3 is determined by the separation between the D3/$\overline{\text{D3}}$ and the D7 stacks in the 8 and 9 directions. It has also been stated that the presence of the D7-Branes modifies the geometry to make it energetically favorable for the D3 and $\overline{\text{D3}}$ stacks to sit on top of the D7 stack [68], allowing us to greatly simplify the potential by taking the vev of the real and imaginary scalar components of Φ_3 to be negligible.

It is worth noting that the scalar vev is not negligible when we consider images of the D3 brane stack along the 8 and 9 directions. For each image of the central D3 stack interacting with the probe $\overline{\text{D3}}$ there is an analogous copy of the superpotential in Eq. (9.1). For these images the vev of the real and imaginary scalar components of Φ_3 is non-zero and so the corresponding fields in the Q and $\tilde{Q}$ sector become heavy, preventing dissipation into light degrees of freedom. Therefore we will not be considering dissipation mediated by fields corresponding to string winding modes in the 8 and 9 directions.

Our focus will be on dissipative effects arising from string winding modes in the 4567 directions which will be dependent on the scalar vacuum expectation values in the Φ_1 and Φ_2 sectors. To investigate dissipative effects associated with these winding modes we are therefore interested in the particle physics interactions that enable the transfer of inflaton energy, specifically the interactions coming from

the F-terms $|F_{\chi_3}|^2 = |\partial W/\partial\chi_3|^2$ and $|F_{\tilde{\chi}_3}|^2 = |\partial W/\partial\tilde{\chi}_3|^2$, given by:

$$\begin{aligned} |F_{\chi_3}|^2 &= |\phi_1\tilde{\chi}_2 - \phi_2\tilde{\chi}_1 + \tilde{y}^A y^B|^2 \\ &= |\phi_1\tilde{\chi}_2 - \phi_2\tilde{\chi}_1|^2 + (\phi_1\tilde{\chi}_2 - \phi_2\tilde{\chi}_1)\tilde{y}^A y^B + \text{h.c.} \end{aligned} \tag{9.4}$$

$$\begin{aligned} |F_{\tilde{\chi}_3}|^2 &= |\phi_1\chi_2 - \phi_2\chi_1 + \tilde{y}^B y^A|^2 \\ &= |\phi_1\chi_2 - \phi_2\chi_1|^2 + (\phi_1\chi_2 - \phi_2\chi_1)\tilde{y}^A y^B + \text{h.c.}\ , \end{aligned} \tag{9.5}$$

where y^A, y^B, $\tilde{y}^A$ and $\tilde{y}^B$ are the scalar components of Y^A, Y^B, $\tilde{Y}^A$ and $\tilde{Y}^B$ respectively. Writing the lagrangian in mass matrix form, normalizing the eigenvectors and performing the rotation we can redefine the fields:

$$\chi = \frac{\phi_1\chi_2 - \phi_2\chi_1}{(|\phi_1|^2 + |\phi_2|^2)^{\frac{1}{2}}}\ , \tag{9.6}$$

$$\tilde{\chi} = \frac{-\phi_1\tilde{\chi}_2 + \phi_2\tilde{\chi}_1}{(|\phi_1|^2 + |\phi_2|^2)^{\frac{1}{2}}}\ , \tag{9.7}$$

and rewrite the F-terms in the form:

$$\begin{aligned} |F_{\chi_3}|^2 &= 2g_{YM}^2(|\phi_1|^2 + |\phi_2|^2)|\tilde{\chi}|^2 \\ &\quad +2g_{YM}^2(|\phi_1|^2 + |\phi_2|^2)^{\frac{1}{2}}\tilde{\chi}\tilde{y}^A y^B + \text{h.c.} \end{aligned} \tag{9.8}$$

$$\begin{aligned} |F_{\tilde{\chi}_3}|^2 &= 2g_{YM}^2(|\phi_1|^2 + |\phi_2|^2)|\chi|^2 \\ &\quad +2g_{YM}^2(|\phi_1|^2 + |\phi_2|^2)^{\frac{1}{2}}\chi\tilde{y}^A y^B + \text{h.c.}\ . \end{aligned} \tag{9.9}$$

From these expressions we deduce that we have a mass for the χ and $\tilde{\chi}$ mediator fields:

$$m_{\chi,\tilde{\chi}} = \sqrt{2} g_{YM} (|\phi_1|^2 + |\phi_2|^2)^{\frac{1}{2}} \ , \tag{9.10}$$

and a decay width:

$$\Gamma_{\chi,\tilde{\chi}} = \sqrt{2} g_{YM} (|\phi_1|^2 + |\phi_2|^2)^{\frac{1}{2}} \ . \tag{9.11}$$

The brane images of the D3 stack are separated throughout the hypercubic lattice by the size of the compact extra dimension v. The distance between the probe $\overline{\text{D3}}$ and a given brane image is therefore determined by the distance between the probe and the brane stack at the origin plus the distance between the probe and the brane image. Since the value of the inflaton field is parameterized by the interbrane distance we therefore define the inflaton field associated with the n_ith brane image away in the ith direction from the origin as:

$$\varphi_i \to \phi_i + n_i v \ , \tag{9.12}$$

where ϕ_i is the distance between the probe and the brane stack located at the origin in the ith direction. The total inflaton vev is given by summing over all brane images in the hypercubic lattice, $\phi^2 = \sum_i (\phi_i + n_i v)^2$. Including the brane images, we can approximate the masses of the χ and $\tilde{\chi}$ mediator fields to be:

$$m_{\chi,\tilde{\chi}} = \sqrt{2} g_{YM} (|\phi_1 + n_1 v|^2 + |\phi_2 + n_2 v|^2)^{\frac{1}{2}} \ . \tag{9.13}$$

As previously noted, separating the D3 and $\overline{\text{D3}}$ stacks in the 4567 directions generates a vacuum expectation value of the real and imaginary scalar components of the Φ_1 and Φ_2 superfields, which we will denote as ϕ_{1R}, ϕ_{1I}, ϕ_{2R} and ϕ_{2I}. Decomposing to the real and imaginary components the lagrangian describing interactions involving an arbitrary string winding mode contributing

to dissipation becomes:

$$\begin{aligned}\mathcal{L} &= 2g_{YM}^2 \sum_{i=1,2} \left(|\phi_{iR} + n_i v|^2 + |\phi_{iI} + m_i v|^2\right) |\chi|^2 \\ &+ 2g_{YM}^2 \sum_{i=1,2} (|\phi_{iR} + n_i v|^2 + |\phi_{iI} + m_i v|^2)^{\frac{1}{2}} \chi y^\dagger \tilde{y} + h.c. \end{aligned} \tag{9.14}$$

where, since we have now introduced the real and imaginary components of ϕ_1 and ϕ_2, the letter m is used to denote the number of brane images in the imaginary direction and n will become the number of images in the real direction. If we set our initial conditions with the probe brane at the centre of the hypercubic lattice the vacuum expectation values generated in each direction will be equal:

$$\phi = \phi_{1R} = \phi_{1I} = \phi_{2R} = \phi_{2I} \ , \tag{9.15}$$

with $\phi_{3R} = \phi_{3I} = 0$ due to the separation between the D3/$\overline{\text{D3}}$ branes and the D7-branes being negligible. Studying this case in comparison to the standard two-stage decay chain of warm inflation the resulting coupling is given by the expression:

$$2g_{YM}^2 \sum_{n,m=0}^{\infty} \left(2\left[4\phi + (n_i + m_i)v\right]\right) \ . \tag{9.16}$$

We have now derived expressions for the mass, decay width and coupling of fields associated with strings of arbitrary winding number that have interactions that implement the two-stage decay chain of warm inflation. By comparing these results with the standard two-stage decay mechanism we are able to derive an expression for the resulting dissipation coefficient for dissipative effects arising from a string of arbitrary winding number:

$$\Upsilon = C_\phi \frac{T^3}{64\phi^2} \sum_{i=1,2} \frac{4\phi^2(4\phi + (n_i + m_i)v)^2 \left[(\phi + n_i v)^2 + (\phi + m_i v)^2\right]^2}{(|\phi + n_i v|^2 + |\phi + m_i v|^2)^4} \ . \tag{9.17}$$

Neglecting the number of brane images by setting $n_i = m_i = 0$ we recover the standard leading order low-momentum contribution to the dissipation coefficient $\Upsilon_{lm} = C_\phi T^3/\phi^2$. Normalizing the ϕ field with the size of the compactified extra dimension $\phi = xv$ and with the condition $0 \leq x \leq 1/2$, we can write the expression for the dissipation coefficient:

$$\Upsilon = C_\phi \frac{T^3}{\phi^2} \sum_{i=1,2} \frac{4x^2(4x + n_i + m_i)^2 \left[(x + n_i)^2 + (x + m_i)^2\right]^2}{64(|x + n_i|^2 + |x + m_i|^2)^4} \ . \tag{9.18}$$

From this expression it is apparent that the dissipation coefficient associated with a string of arbitrary winding number is the standard dissipation coefficient multiplied by a factor that depends on the distance between the probe and the origin, here represented by x, and the winding number, which is determined by n and m. We can find the total enhancement to the dissipation coefficient by summing over all the winding modes:

$$f(\Lambda, x) = \sum_{n,m=0}^{\Lambda} \frac{4x^2(4x + n_i + m_i)^2 \left[(x + n_i)^2 + (x + m_i)^2\right]^2}{64\left(|x + n_i|^2 + |x + m_i|^2\right)^4} \ . \tag{9.19}$$

where the summation over i is assumed and a cut off Λ in the summation has been imposed. The expression for full dissipation coefficient, including dissipative effects arising from string winding modes, is therefore given by:

$$\Upsilon = C_\phi \frac{T^3}{\phi^2} f(\Lambda, x) \ . \tag{9.20}$$

9.2.1 Cutting Off the Brane Images

The function $f(\Lambda, x)$ is quadratically divergent with respect to the number of brane images that are summed over and so a cut off Λ has been imposed on the summation. We can understand this cut off by asking whether increasingly massive mediator fields will contribute towards dissipative effects that are enabled

by the two-stage decay mechanism. In particular fields with masses above the planck scale will collapse to form classical black holes. As classical objects we do not expect these fields to contribute towards dissipation through the two-stage mechanism and so we will only consider dissipation mediated by fields with sub-planckian masses. If we set the upper bound on the mass of the mediator field to be the planck mass then:

$$m_X = g_{YM}(\phi_0 + nv) \leq m_p \ . \tag{9.21}$$

Assuming the cut off is for a large winding number we can approximate $\phi_0 \ll nv$ and $m_X \cong g_{YM} nv \ll m_p$. This leads us to the maximum number of brane images:

$$\Lambda = \frac{1}{g_{YM}} \frac{m_p}{v} \ , \tag{9.22}$$

and since $m_p^2 = (4\pi L^6)/(g_s^2(2\pi l_s)^8)$, $\phi = \sqrt{T_3} r$ and $T_3 = 1/(g_s(2\pi)^3 l_s^4)$:

$$\phi = \frac{1}{g_s^{1/2}(2\pi)^{3/2} l_s^2} r \ , \tag{9.23}$$

and $g_{YM}^2 = 2\pi g_s$ with $v = \sqrt{T_3} L = L/(\sqrt{g_s}(2\pi)^{3/2} l_s^2)$ gives:

$$\Lambda = \frac{\pi^{-1/2}}{g_s} \left(\frac{L}{2\pi l_s} \right)^2 \ . \tag{9.24}$$

Noting that since $l_s = m_s^{-1}$, we arrive at the result:

$$m_p^2 = \frac{4\pi}{g_s^2} \left(\frac{L}{2\pi l_s} \right)^6 \frac{1}{(2\pi l_s)^2} \ . \tag{9.25}$$

Substituting this into the expression for the cut off gives:

$$\Lambda = \left(\frac{1}{\pi g_s^2} \frac{m_p^4}{m_s^4} \right)^{1/6} \ . \tag{9.26}$$

From Eq. (9.24) it can be seen that the cut-off can be large for large volume compactifications $L \gg l_s$ (i.e. when there is a large hierarchy between the Planck scale and the fundamental string scale). If we take, as an example, $m_s \sim$ 1 TeV then $m_p/m_s \approx 10^{15}$, which, from Eq. (9.26), gives $\Lambda \approx 10^{10}\pi^{-1/6}g_s^{-1/3}$.

9.2.2 Numerical Results for Enhancing the Dissipation Coefficient

The behavior of the enhancement to the dissipation coefficient can be understood in two situations. Firstly, by varying the interbrane distance x for a fixed cut off Λ, and conversely, by fixing the interbrane distance and varying the cut off Λ. This results in two expressions for which the enhancement $f(\Lambda, x)$ can be fitted to:

$$f(\Lambda, \frac{1}{2}) = 1 + 4.2\Lambda^2 \ , \tag{9.27}$$

$$f(\Lambda, x) = 1 + A(\Lambda)x^2 \ . \tag{9.28}$$

From these relations we get $A(\Lambda) = 17.5\Lambda^2$. The dependence of the enhancement to the dissipation coefficient on the interbrane distance x and the cut off Λ can now be described in the general case with the function:

$$f(\Lambda, x) = 1 + 17.5\Lambda^2 x^2 \ , \tag{9.29}$$

and so the dissipation coefficient becomes:

$$\Upsilon = C_\phi \frac{T^3}{\phi^2} f(\Lambda, x) \ . \tag{9.30}$$

The plot in Fig. (9.2) shows the enhancement to the dissipation coefficient for an increasing cut off for the brane images, with dots showing the summed values for a specific number of brane images and the line showing the fitted function. As the cut off increases the enhancement diverges quadratically. The plot in

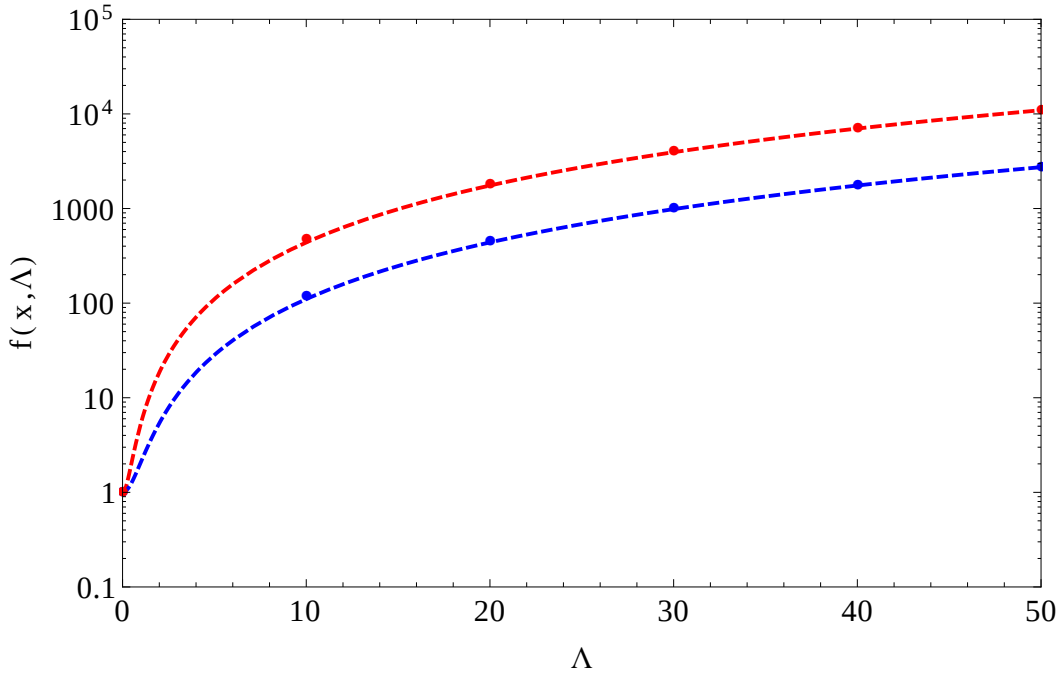

Figure 9.2: Enhancement to the dissipation coefficient Υ as a function of the cut off Λ in the number of brane images the summation is performed over. The interbrane distance is $x = 0.25$ for the blue results and $x = 0.5$ for the red results.

Fig. (9.3) shows the dependence of the enhancement to the dissipation coefficient on the interbrane distance for several different cut offs for the brane images, with dependence being quadratic in this case. The dots show the summed values for the specific number of brane images and the line shows the fitted function.

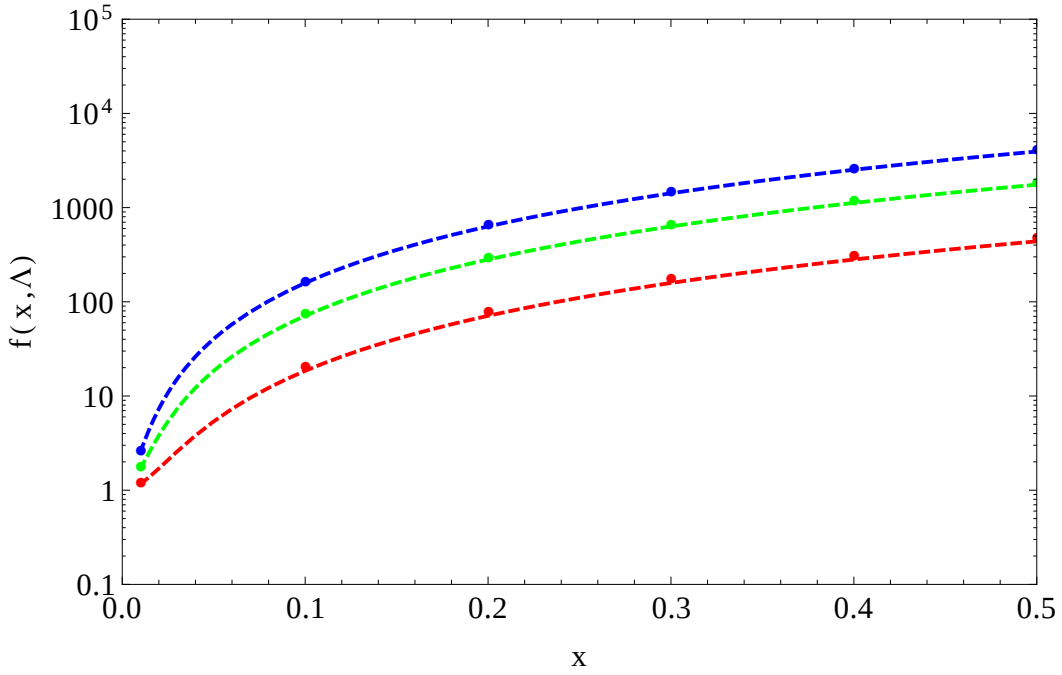

Figure 9.3: Enhancement to the dissipation coefficient Υ as a function of the interbrane distance x. The cut off is $\Lambda = 10$ for the red results, $\Lambda = 20$ for the green results and $\Lambda = 30$ for the blue results.

9.3 Slow-Rolling Down the Hill in a Hypercubic Lattice

Now that we understand the effect of string winding modes on the dissipation coefficient we can study the effect of string winding modes on the dynamics of the brane-antibrane system. In a typical brane-antibrane set up the inflationary dynamics are determined by five fundamental parameters:

- The fundamental string coupling $g_s = g_{YM}^2/2\pi$
- The fundamental string mass m_s
- The number of D3-branes N_c
- The number of $\overline{\text{D3}}$-branes $\tilde{N}_c$
- The number of D7-branes N_f

In the brane-antibrane system the inflationary potential results from the interactions between the probe antibrane in the background created by the hypercubic lattice of brane images. In particular, when placed at the antipodal point in the centre of the hypercubic cell the probe antibrane is in fact pulled equally in all directions, resulting in an unstable maximum, which can be best approximated with a Hilltop potential [140]. The simplest example of a Hilltop potential is similar to a quadratic potential, but with negative mass squared:

$$V = V_0 \left(1 - \frac{\gamma^2}{2}\psi^2\right), \qquad V_0 = \frac{m_s^4}{4\pi^3 g_s}\tilde{N}_c \ , \tag{9.31}$$

The inflaton field ψ is given by the separation between the probe brane and the antipodal point at the the centre of the hypercubic lattice and the inflaton mass is $\gamma = 0.33 m_p$ [140]. In this model the inflaton field has an initial value close to 0 which increases during inflation as the inflaton rolls off the top of the potential. As the field rolls down the potential inflation can end with slow-roll being violated or with the inflaton reaching a value $v/2$, meaning that the probe has reached the D3-brane stack located at the origin.

9.3.1 Warm Inflation Dynamics in a Hypercubic Lattice

Taking the limit that the cut off $\Lambda \gg 1$, the ϕ dependence of the dissipation coefficient is replaced by a dependence on the size of the compactified extra dimension v. This allows us to investigate the effect of brane images on the inflationary dynamics by comparing the evolution of the system with the standard low-momentum contribution to the dissipation coefficient:

$$\Upsilon = C_\phi \frac{T^3}{\phi^2}, \quad \text{with} \quad C_\phi = 0.08 g_{YM}^2 N_c \tilde{N}_c N_f \ , \tag{9.32}$$

and the dissipation coefficient with the effect of string winding modes included:

$$\Upsilon = \tilde{C}_\phi \frac{T^3}{v^2}, \quad \text{with} \quad \tilde{C}_\phi = 17.5\Lambda^2 C_\phi \ . \tag{9.33}$$

Eliminating the ϕ dependence of the dissipation coefficient modifies the warm inflation equations of motion. The equation of motion for the dissipative ratio Q becomes:

$$dQ/dN_e = \frac{Q}{1+7Q}\left(10\epsilon_\psi - 6\eta_\psi\right) \ . \tag{9.34}$$

Likewise the equation of motion for the temperature relative to the Hubble parameter becomes:

$$d\ln(T/H)/dN_e = \frac{2(T/H)}{1+7Q}\left(\frac{2+4Q}{1+Q}\epsilon_\psi - \eta_\psi\right) \ , \tag{9.35}$$

and the relation between the dissipative ratio Q and the inflaton field ϕ:

$$Q^{1/3}(1+Q)^2 = 2\epsilon_\psi \left(\frac{m_p}{H}\right)^2 \left(\frac{\tilde{C}_\phi}{3}\right)^{1/3} \left(\frac{\tilde{C}_\phi}{4C_R}\right) \left(\frac{H}{v}\right)^{8/3} \ . \tag{9.36}$$

In warm inflation if inflaton particles were not produced sufficiently fast when the largest currently observable scales left the horizon then any non-trivial occupation numbers will be quickly redshifted away by the expansion and, in the weak dissipative limit $Q_* \ll 1$, the spectral index n_s is given by Eq. (4.25) shown earlier in this thesis. This result was based on the standard form of the dissipation coefficient. When the effect of string winding modes are included in the dissipation coefficient the slow-roll solution for T/H when the largest observable scales left the horizon becomes:

$$\frac{T_*}{H_*} = \left(3\frac{Q_*}{\tilde{C}_\phi}\left(\frac{v}{H}\right)^2\right)^{1/3} \ , \tag{9.37}$$

and the expression for the spectral index becomes:

$$n_s - 1 = 2\eta_{\psi_*} - 6\epsilon_{\psi_*} + \frac{2\kappa_*}{1+\kappa_*}\left(7\epsilon_{\psi_*} - 4\eta_{\psi_*}\right) \ . \tag{9.38}$$

9.3.2 Numerical Results

We now have all the ingredients necessary to study the effect of string winding modes on the inflationary dynamics. Taking into account string winding modes when setting initial conditions we can use the equations of motion derived in the previous section to numerically evolve the system with respect to the number of e-folds. Setting the five fundamental parameters defining the system:

- The fundamental string coupling $g_s = 1/\sqrt{2\pi}$
- The fundamental string mass $m_s = 0.00003225 m_p$
- The number of D3-branes $N_c = 10$
- The number of $\overline{\text{D3}}$-branes $\tilde{N}_c = 5$
- The number of D7-branes $N_f = 1$

and choosing the initial inflaton field value ψ_* near the centre of the hypercubic cell to give the correct spectrum (in this case $\psi_* = 3.94198 \times 10^{-6} m_p$) we get initial conditions:

$$Q_* = 0.00554651 \tag{9.39}$$

$$T_*/H_* = 8.83632 \tag{9.40}$$

$$\Delta^2_{\mathcal{R}} = 2.20 \times 10^{-9} \tag{9.41}$$

$$n_s = 0.961176 \tag{9.42}$$

$$r = 1.05606 \times 10^{-11} \tag{9.43}$$

Significantly the inclusion of string winding modes allows the number of branes N_c and the number of antibranes $\tilde{N}_c$ to be reduced from $N_c \approx \tilde{N}_c \approx \mathcal{O}(10^3)$ to $N_c \approx \tilde{N}_c \approx \mathcal{O}(10)$ whilst keeping $T_*/H_* > 1$. Fig. (9.4-9.9) show the evolution of the brane-antibrane system once the effects of brane images have been taken into account. The solid blue line in Fig. (9.4) shows the evolution of the system in the cold regime, in which dissipative effects are neglected and the radiation energy density is quickly redshifted. The solid red line shows the evolution from the same set of initial conditions in the warm regime with the dissipative effects of string winding modes included. As inflation proceeds the field value increases with dissipative effects in the warm regime slowing the evolution of the inflaton field. With dissipative effects from string winding modes included T/H, ρ_R/V and Q all slowly increase during the inflationary period, with the condition $m_\chi > T$ being maintained for over 60 e-folds.

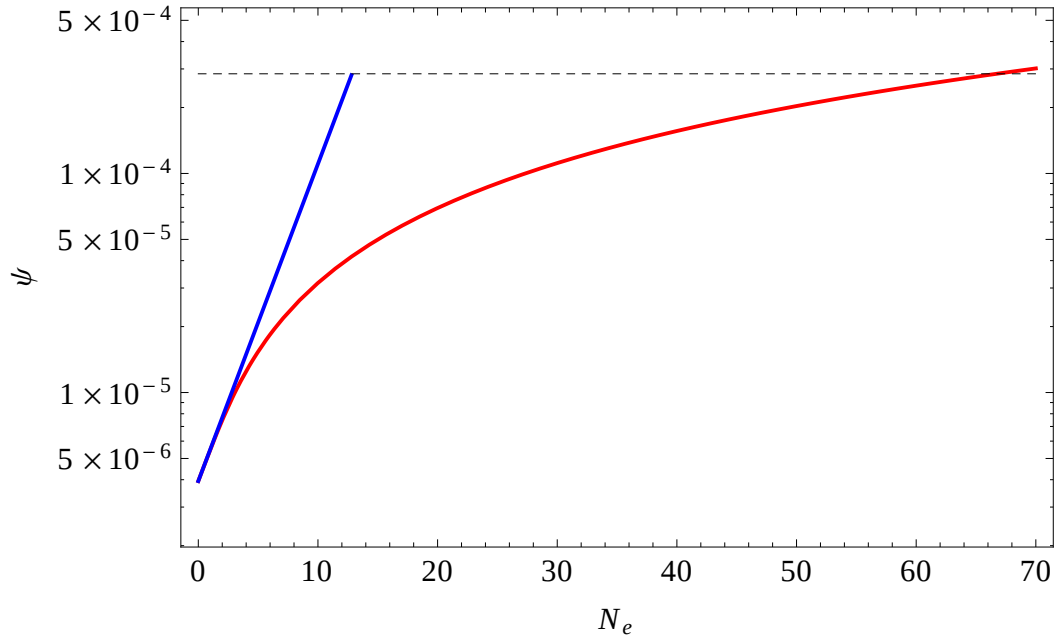

Figure 9.4: The evolution of the inflaton field ϕ in the brane-antibrane construction. The solid blue line shows the evolution of the system in the cold regime, in which dissipative effects are neglected. The solid red line shows the evolution from the same set of initial conditions in the warm regime with the dissipative effects of string winding modes included. The input parameters are $g_s = 1/\sqrt{2\pi}$, $m_s = 0.00003225 m_p$, $N_c = 10$, $\tilde{N}_c = 5$, $N_f = 1$, whilst the initial conditions are $Q_* = 0.00554651$, $T_*/H_* = 8.83632$, $\Delta^2_{\mathcal{R}} = 2.20 \times 10^{-9}$, $n_s = 0.961176$ and $r = 1.05606 \times 10^{-11}$.

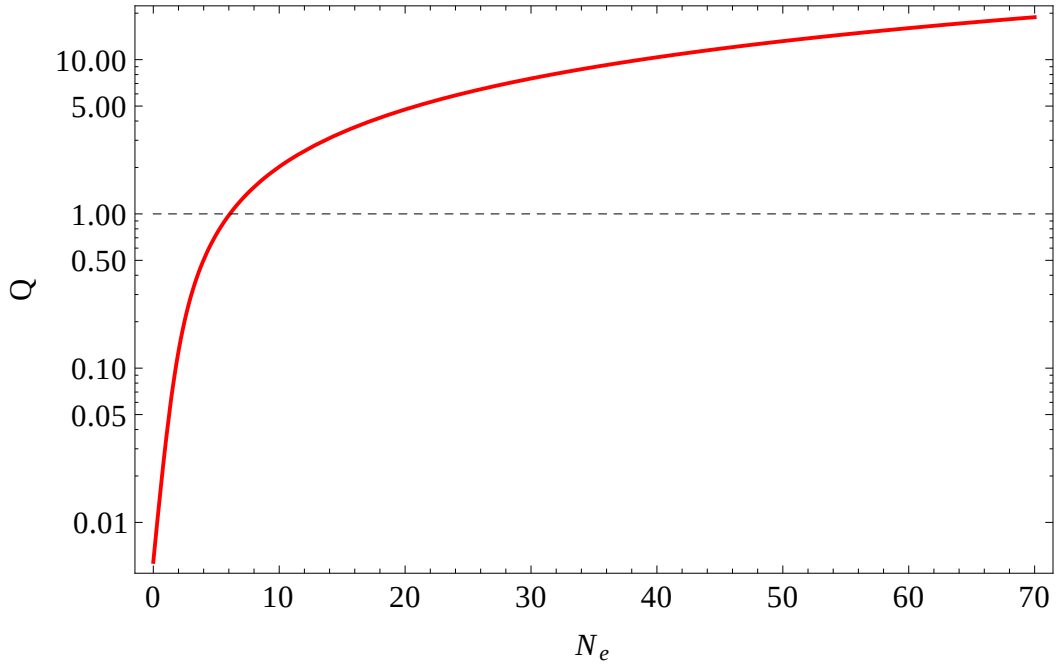

Figure 9.5: The evolution of the dissipative ratio Q in the warm regime with dissipative effects from string winding modes included. The input parameters are $g_s = 1/\sqrt{2\pi}$, $m_s = 0.00003225 m_p$, $N_c = 10$, $\tilde{N}_c = 5$ and $N_f = 1$, whilst the initial conditions are $Q_* = 0.00554651$, $T_*/H_* = 8.83632$, $\Delta^2_{\mathcal{R}} = 2.20 \times 10^{-9}$, $n_s = 0.961176$ and $r = 1.05606 \times 10^{-11}$.

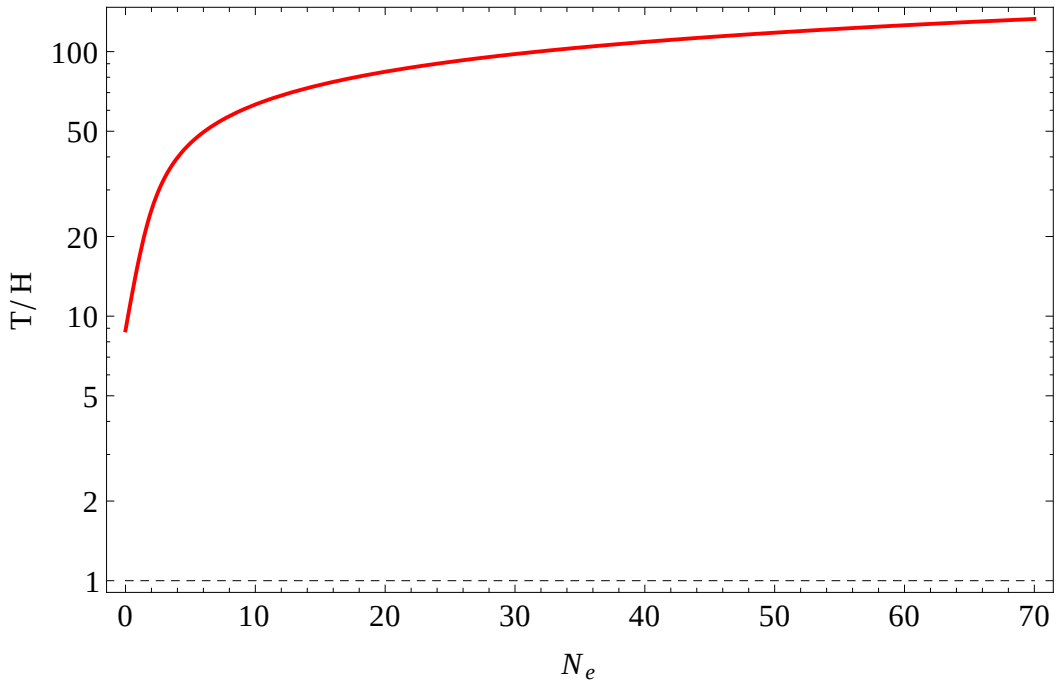

Figure 9.6: The evolution of T/H in the warm regime with dissipative effects from string winding modes included. The input parameters are $g_s = 1/\sqrt{2\pi}$, $m_s = 0.00003225 m_p$, $N_c = 10$, $\tilde{N}_c = 5$ and $N_f = 1$, whilst the initial conditions are $Q_* = 0.00554651$, $T_*/H_* = 8.83632$, $\Delta^2_{\mathcal{R}} = 2.20 \times 10^{-9}$, $n_s = 0.961176$ and $r = 1.05606 \times 10^{-11}$.

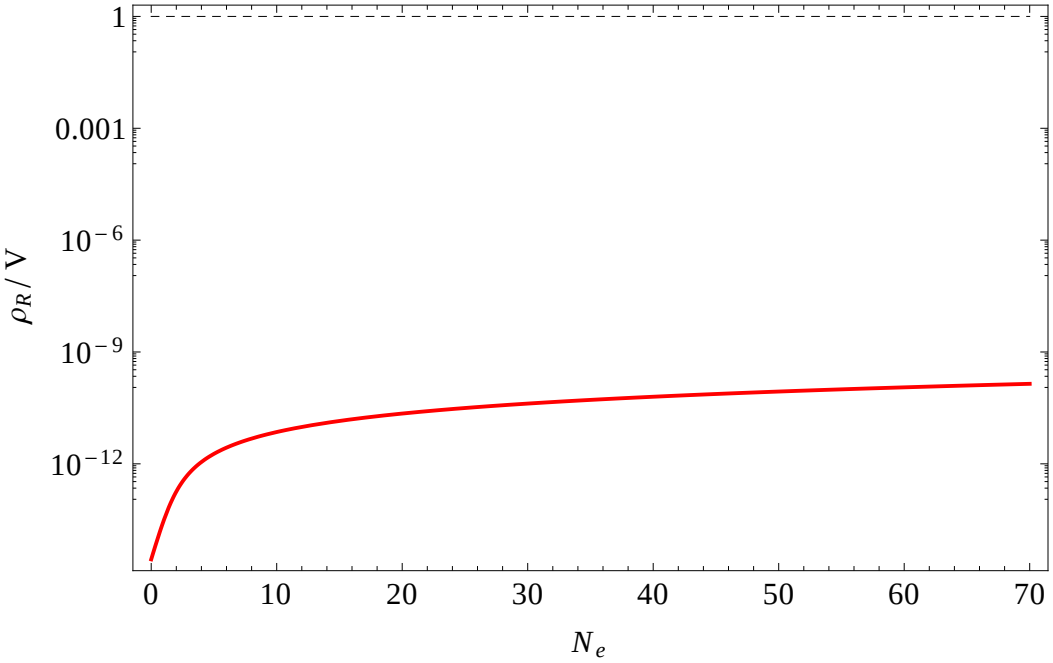

Figure 9.7: The evolution of the ratio of the radiation energy density to the potential, ρ_R/V, in the warm regime with dissipative effects from string winding modes included. The input parameters are $g_s = 1/\sqrt{2\pi}$, $m_s = 0.00003225 m_p$, $N_c = 10$, $\tilde{N}_c = 5$ and $N_f = 1$, whilst the initial conditions are $Q_* = 0.00554651$, $T_*/H_* = 8.83632$, $\Delta^2_{\mathcal{R}} = 2.20 \times 10^{-9}$, $n_s = 0.961176$ and $r = 1.05606 \times 10^{-11}$.

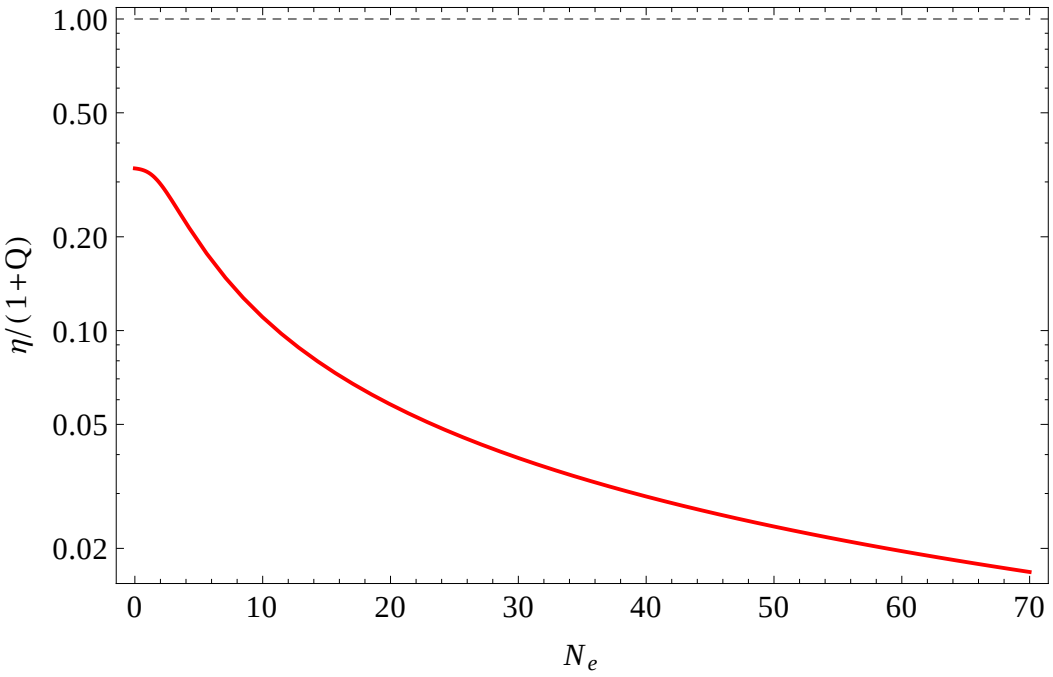

Figure 9.8: The evolution of the slow-roll condition $|\eta|/(1+Q)$ in the warm regime with dissipative effects from string winding modes included. The input parameters are $g_s = 1/\sqrt{2\pi}$, $m_s = 0.00003225 m_p$, $N_c = 10$, $\tilde{N}_c = 5$ and $N_f = 1$, whilst the initial conditions are $Q_* = 0.00554651$, $T_*/H_* = 8.83632$, $\Delta^2_{\mathcal{R}} = 2.20 \times 10^{-9}$, $n_s = 0.961176$ and $r = 1.05606 \times 10^{-11}$.

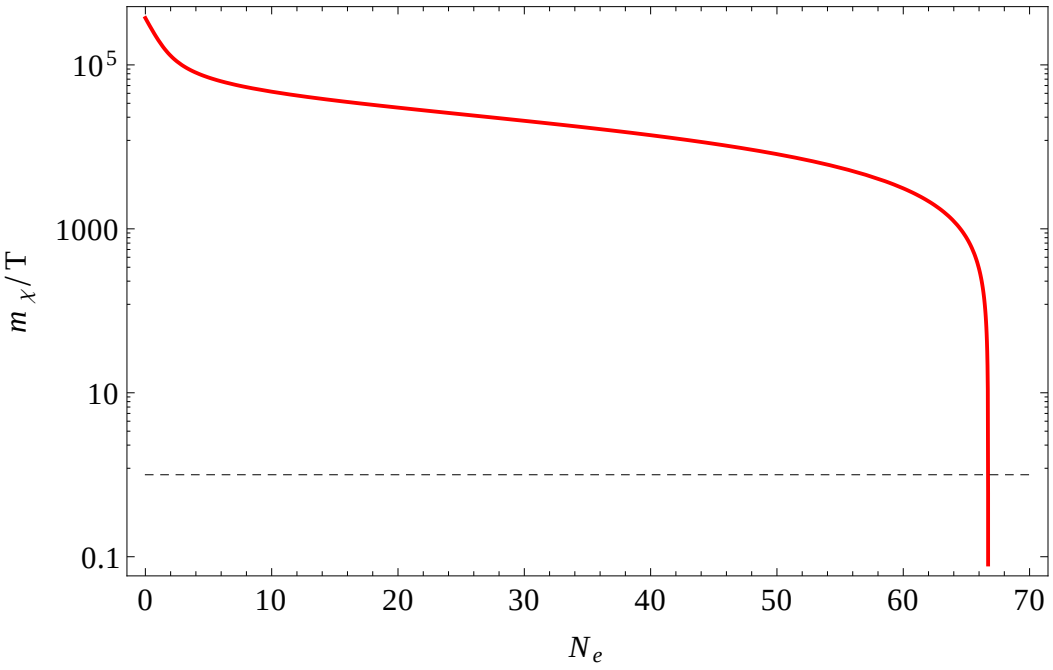

Figure 9.9: The evolution of the mass of the mediator field relative to the temperature, m_{χ_R}/T, in the warm regime with dissipative effects from string winding modes included. The input parameters are $g_s = 1/\sqrt{2\pi}$, $m_s = 0.00003225 m_p$, $N_c = 10$ and $\tilde{N}_c = 5$, $N_f = 1$, whilst the initial conditions are $Q_* = 0.00554651$, $T_*/H_* = 8.83632$, $\Delta^2_{\mathcal{R}} = 2.20 \times 10^{-9}$, $n_s = 0.961176$ and $r = 1.05606 \times 10^{-11}$.

9.4 Summary

We have studied dissipative effects related to string winding modes in brane-antibrane inflation. We have shown that the presence of string winding modes significantly enhances dissipation, even for a brane-antibrane system containing $\mathcal{O}(10)$ branes, and provides a very natural way in which the large field multiplicities involved in warm inflation can be justified. The effect of including dissipative effects from string winding modes changes the form of the dissipation coefficient which in turn modifies the inflationary dynamics causing the system to evolve more slowly. This combination of the enhancement to the dissipation coefficient and slowing of the rate at which the system evolves will go some way towards alleviating the η-problem associated with brane-antibrane inflation constructions. We are still investigating the details of this scenario in different regimes, but so far the results show that this may be a very natural way in which warm inflation can be implemented.

Chapter 10

Conclusion

The work presented in this thesis has focused on studying dissipative effects in two projects. The first was a study of dissipative and thermal effects on the dynamics and observational predictions for supersymmetric hybrid inflation driven by radiative corrections. Warm inflation can naturally be implemented in hybrid models of inflation since the coupling between the inflaton and the waterfall field not only modifies the effective potential but also the full effective action of the inflaton field. The result of this is that the effective potential has a logarithmic slope and the inclusion of a dissipation coefficient acting as a friction term in the inflaton's equation of motion. This causes the inflaton field evolve more slowly during the inflationary phase, allowing for $50-60$ e-folds of inflation with a primordial spectrum consistent with the results of the Planck mission at the 95% CL [3].

In the SUSY hybrid model we studied the consequences of several effects that have not been previously studied in models of warm inflation. Firstly we have investigated the effect of including the SUSY mass splitting for the chiral multiplets directly coupled to the inflaton field, showing that their inclusion parametrically enhances the dissipation coefficient, especially close to the waterfall transition. We have also, for the first time, included dissipative

effects associated with both the on-shell "pole" and off-shell "low-momentum" modes of the waterfall fields mediating dissipation of inflaton energy to light degrees of freedom in the quasi-thermal bath. The "low-momentum" contribution to the dissipation coefficient is the dominant contribution at large inflaton field values due to the Boltzmann-suppression of the "pole" contribution, with $\Delta m_\phi^2 \sim g^2 N_X T^2 \gtrsim H^2$. Towards the end of inflation the smaller values for the inflaton field result in the pole contribution becoming the dominant contribution, further enhancing the amount of dissipation and resulting in a prolonged period of inflation before the waterfall transition.

We have also considered the backreaction of the radiation bath, produced by the dissipation of inflaton energy mediated by the waterfall fields, on the masses of the fields in the waterfall sector, with the effect being a modification to the effective potential and dissipation coefficient. In particular thermal corrections were shown to increase the waterfall field masses, causing the fields in the waterfall sector to remain in a metastable minimum with non-vanishing vacuum energy delaying the hybrid transition. Thermal corrections also had the effect of suppressing dissipation close to the waterfall transition so, despite the system evolving in the warm regime, radiation does not become the dominant component of energy density in the universe during the waterfall transition. Therefore a separate phase of reheating is required to bring the universe into a radiation-dominated era once inflation has ended, albeit from a temperature already above the Hubble parameter $T/H > 1$.

We have also seen how the initial value for the inflaton field can effect the inflationary dynamics, with larger initial values for the inflaton field resulting in an inflationary phase that ends with a violation of slow-roll before the onset of the waterfall transition. In this scenario radiation naturally comes to dominate the energy density of the universe through particle production and a separate reheating phase is not required. This scenario also results in a larger tensor-

to-scalar ratio, $r = 0.05$, than the simulations with a lower initial inflaton field value.

An important aspect of our analysis was the use of the CJT formalism [110] to improve the form of the effective potential. The corrections involved in this formalism are of a higher order in the couplings and field multiplicities and so do not have a significant on the dynamical evolution. They do however provide leading corrections to the entropy density associated with the waterfall sector, making the effective potential independent of their physical masses corresponding to the solutions of the gap equations. This results in the elimination of any negative contributions to the entropy density associated with the 1-loop correction from the Coleman-Weinberg approximation to the effective potential. Thus the only contribution to entropy density comes from relativistic degrees of freedom, which are suitably suppressed in the waterfall sector due to their large masses. The CJT formalism has been used here to define the effective potential during the inflationary phase but we expect it will have applications in other cosmological scenarios that involve scalar fields at finite temperature, such as in the standard reheating scenario.

The second project presented in this thesis involved studying dissipative effects in brane-antibrane inflation. Brane-Antibrane inflation remains one of the most attractive scenarios for realizing inflation within a fundamental theory of quantum gravity, and is a concrete implementation of SUSY hybrid inflation in a UV complete particle physics model. We have shown the role that compactified extra dimensions can play in brane-antibrane systems in the warm inflation scenario, where interactions between the inflaton and other fields leads to dissipation of inflaton energy to other degrees of freedom. Brane-Antibrane inflation has previously been implemented in the warm regime in [68], with dissipation of inflaton energy mediated through degrees of freedom corresponding to strings stretched between the brane and antibrane stacks. Whilst these strings have end

points fixed to both the D3 and $\overline{\text{D3}}$ stacks, the compact nature of the geometry within which the system is constructed allows these strings to have different winding modes.

We have investigated dissipative effects in brane-antibrane inflation arising from these winding string modes. Compactification effects may offer the best way so far to naturally motivate large field multiplicities and warm inflation models. Even though the winding modes become progressively heavier their numbers increase faster and the resulting enhancement to the dissipation coefficient is significant, even for a system involving only a few branes and antibranes. The enhancement due to winding string modes also modifies the form of the dissipation coefficient, having the effect of modifying the inflationary dynamics by reducing the speed at which the system evolves. This combination of enhanced dissipation and also a slowing of the evolution of the system may go some towards alleviating the η-problem associated with generic brane-antibrane inflation models. We are still investigating the details of this scenario in different regimes, but so far the results show that this may be a very natural way in which warm inflation can be implemented.

Appendix A

Inflation Dynamics

The evolution of the inflaton field in standard supercooled inflation is given by:

$$\ddot{\phi}(t) + 3H\dot{\phi}(t) + V_{,\phi} = 0 \ , \tag{A.1}$$

where $V_{,\phi}$ is the derivative of the scalar potential $V(\phi)$ with respect to the inflation field value ϕ. The expansion rate is given by:

$$H^2 = \left(\frac{\dot{\phi}^2}{2} + V(\phi) \right) / 3m_p^2 \ . \tag{A.2}$$

Inflation happens with $\dot{\phi}^2 \ll V(\phi)$, so making the approximations $3H^2 m_p^2 \simeq V(\phi)$ and $\ddot{\phi}(t) \ll H\dot{\phi}(t)$ the equation of motion reduces to the slow-roll version:

$$3H\dot{\phi} + V_{,\phi} = 0 \ . \tag{A.3}$$

The slow-roll parameter ϵ_ϕ is derived from the condition $\dot{\phi}^2/2 < V(\phi)$ using the relations $3H^2 m_p^2 \simeq V(\phi)$ and $\ddot{\phi}(t) \ll H\dot{\phi}(t)$:

$$\epsilon_\phi = \frac{m_p^2}{2} \left(\frac{V_{,\phi}}{V} \right)^2 < 1 \ . \tag{A.4}$$

Differentiating the expression for ϵ_ϕ gives the η_ϕ parameter:

$$\eta_\phi = m_p^2 \frac{V_{,\phi\phi}}{V} < 1 \ , \tag{A.5}$$

where $V_{,\phi\phi}$ is the second derivative of the potential $V(\phi)$ with respect to the field ϕ. In warm inflation the equation of motion for the inflaton field is modified by the inclusion of a dissipation coefficient acting as a friction term:

$$\ddot{\phi}(t) + (3H + \Upsilon)\dot{\phi}(t) + V_{,\phi} = 0 \ . \tag{A.6}$$

Any energy lost by the inflaton field will be gained by some other fluid component ρ_α, with the evolution equation:

$$\dot{\rho}_\alpha + 3H(\rho_\alpha + p_\alpha) = \Upsilon(\rho_\phi + p_\phi) \ . \tag{A.7}$$

If inflaton energy is dissipated into light degrees of freedom which quickly thermalize and become radiation then $\rho_\alpha = \rho_R$ and $p_\alpha = p_R$. The evolution of the radiation energy density ρ_R becomes:

$$\dot{\rho}_R + 4H\rho_R = \Upsilon\dot{\phi}^2 \ . \tag{A.8}$$

Using the expression for the dissipative ratio $Q = \Upsilon/3H$ the equations of motion for the inflaton field ϕ and the radiation energy density ρ_R in the slow-roll regime become:

$$3H(1+Q)\dot{\phi} \simeq -V_{,\phi} \ , \tag{A.9}$$

$$4\rho_R \simeq 3Q\dot{\phi}^2 \ , \tag{A.10}$$

respectively. Since the slow-roll equation of motion for the inflaton field includes the dissipative ratio Q the slow-roll conditions become modified in the warm

regime:

$$\epsilon_\phi, |\eta_\phi| < (1+Q) \ . \tag{A.11}$$

In the large field limit the leading contribution to the dissipation coefficient comes from the low-momentum off-shell modes of the mediator fields, given as:

$$\Upsilon = C_\phi \frac{T^3}{\phi^2} \ . \tag{A.12}$$

Relating this to the dissipative ratio one obtains the expression:

$$Q = \frac{C_\phi}{3} \left(\frac{T}{H}\right)^3 \left(\frac{H}{\phi}\right)^2 \ . \tag{A.13}$$

Using the expression $\rho_R = C_R T^4$, with $C_R = \pi^2 g_*/30$, we obtain an expression:

$$\dot{\phi}^2 = 4C_R \left(\frac{T}{H}\right) H^4 \left(\frac{1}{C_\phi}\right) \left(\frac{\phi}{H}\right)^2 \ . \tag{A.14}$$

Substituting this into Eq. (A.9) we arrive at the result:

$$Q^{1/3}(1+Q)^2 = \frac{1}{(3H)^2} \left(\frac{C_\phi}{3}\right)^{1/3} \frac{C_\phi}{4C_R} \left(\frac{H}{\phi}\right)^{8/3} \frac{V_{,\phi}^2}{H^4} \ , \tag{A.15}$$

which can be written:

$$Q^{1/3}(1+Q)^2 = 2\epsilon_\phi \left(\frac{C_\phi}{3}\right)^{1/3} \left(\frac{C_\phi}{4C_R}\right) \left(\frac{H}{\phi}\right)^{8/3} \left(\frac{m_p}{H}\right)^2 \ . \tag{A.16}$$

Appendix B

Warm Inflation Equations of Motion

The equation of motion for the inflaton in terms of the number of e-folds can be found using:

$$\frac{d}{dN_e}\frac{\phi}{m_p} = \frac{1}{H}\frac{d}{dt}\frac{\phi}{m_p} \ . \tag{B.1}$$

Using $\dot{\phi} = -V_{,\phi}/(3H(1+Q))$ this expression becomes:

$$\frac{d}{dN_e}\frac{\phi}{m_p} = -\frac{\phi}{m_p}\frac{\sigma_\phi}{1+Q} \ , \tag{B.2}$$

where we have introduced the slow-roll parameter $\sigma_\phi = m_p^2(V_{,\phi}/\phi V)$. The equation of motion for the dissipative ratio is found by using the expression for the dissipation coefficient to eliminate T from the Eq. (A.16). Given the derivatives:

$$\frac{d}{dN_e}\epsilon_\phi = \frac{\epsilon_\phi}{1+Q}\left(4\epsilon_\phi - 2\eta_\phi\right) \ , \tag{B.3}$$

$$\frac{d}{dN_e}\left(\frac{m_p}{H}\right)^2 = \frac{2\epsilon_\phi}{1+Q}\left(\frac{m_p}{H}\right)^2 \ , \tag{B.4}$$

$$\frac{d}{dN_e}\left(\frac{H}{\phi}\right)^{8/3} = \left(\frac{8}{3}\sigma_\phi - \frac{8}{3}\epsilon_\phi\right)\frac{1}{1+Q}\left(\frac{H}{\phi}\right)^{8/3} \ , \tag{B.5}$$

the derivative of Q with respect to N_e can be taken, giving:

$$\frac{dQ}{dN_e} = \frac{Q}{1+7Q}\left(10\epsilon_\phi - 6\eta_\phi + 8\sigma_\phi\right) \ . \tag{B.6}$$

The equation of motion for the temperature with respect to the Hubble parameter is then found by differentiating the expression:

$$\left(\frac{T}{H}\right)^4 = \frac{3}{2C_R}\frac{Q}{(1+Q)^2}\epsilon_\phi\left(\frac{m_p}{H}\right)^2 \ , \tag{B.7}$$

with respect to the number of e-folds. Making use of the expressions for $d(\phi/m_p)/dN_e$ and dQ/dN_e the equation of motion for T/H can now be derived:

$$\frac{d}{dN_e}\ln(T/H) = \frac{2}{1+7Q}\left(\frac{2+4Q}{1+Q}\epsilon_\phi - \eta_\phi + \frac{1-Q}{1+Q}\right) \ . \tag{B.8}$$

Bibliography

[1] Alan H. Guth. The Inflationary Universe: A Possible Solution to the Horizon and Flatness Problems. *Phys.Rev.*, D23:347–356, 1981.

[2] Andrei D. Linde. A New Inflationary Universe Scenario: A Possible Solution of the Horizon, Flatness, Homogeneity, Isotropy and Primordial Monopole Problems. *Phys.Lett.*, B108:389–393, 1982.

[3] P.A.R. Ade et al. Planck 2013 results. XXII. Constraints on inflation. 2013.

[4] Arjun Berera and Li-Zhi Fang. Thermally induced density perturbations in the inflation era. *Phys.Rev.Lett.*, 74:1912–1915, 1995.

[5] Arjun Berera. Warm inflation. *Phys.Rev.Lett.*, 75:3218–3221, 1995.

[6] Andrei D. Linde. Hybrid inflation. *Phys.Rev.*, D49:748–754, 1994.

[7] S. Perlmutter et al. Measurements of Omega and Lambda from 42 high redshift supernovae. *Astrophys.J.*, 517:565–586, 1999.

[8] Edwin Hubble. A relation between distance and radial velocity among extra-galactic nebulae. *Proc.Nat.Acad.Sci.*, 15:168–173, 1929.

[9] Daniel Baumann. TASI Lectures on Inflation. 2009.

[10] William H. Kinney. TASI Lectures on Inflation. 2009.

[11] Edward W. Kolb and Michael S. Turner. The Early Universe. *Front.Phys.*, 69:1–547, 1990.

[12] Scott Dodelson. Modern cosmology. 2003.

[13] Joao G. Rosa. Introduction to Cosmology. 2013.

[14] George F. Smoot, C.L. Bennett, A. Kogut, E.L. Wright, J. Aymon, et al. Structure in the COBE differential microwave radiometer first year maps. *Astrophys.J.*, 396:L1–L5, 1992.

[15] D.N. Spergel et al. First year Wilkinson Microwave Anisotropy Probe (WMAP) observations: Determination of cosmological parameters. *Astrophys.J.Suppl.*, 148:175–194, 2003.

[16] David H. Lyth and Antonio Riotto. Particle physics models of inflation and the cosmological density perturbation. *Phys.Rept.*, 314:1–146, 1999.

[17] Andrew R. Liddle and D.H. Lyth. Cosmological inflation and large scale structure. 2000.

[18] Daniel Baumann and Hiranya V. Peiris. Cosmological Inflation: Theory and Observations. *Adv.Sci.Lett.*, 2:105–120, 2009.

[19] David H. Lyth. Particle physics models of inflation. *Lect.Notes Phys.*, 738:81–118, 2008.

[20] Andrei D. Linde. Particle physics and inflationary cosmology. *Contemp.Concepts Phys.*, 5:1–362, 1990.

[21] Arjun Berera. Interpolating the stage of exponential expansion in the early universe: A Possible alternative with no reheating. *Phys.Rev.*, D55:3346–3357, 1997.

[22] H.P. de Oliveira and Rudnei O. Ramos. Dynamical system analysis for inflation with dissipation. *Phys.Rev.*, D57:741–749, 1998.

[23] Wo-lung Lee and Li-Zhi Fang. Density perturbations of thermal origin during inflation. *Int.J.Mod.Phys.*, D6:305–322, 1997.

[24] Mauricio Bellini. Towards a theory of warm inflation of the universe. *Class.Quant.Grav.*, 16:2393–2402, 1999.

[25] Arjun Berera and Thomas W. Kephart. The Ubiquitous Inflaton in String-Inspired Models. *Phys.Rev.Lett.*, 83:1084–1087, 1999.

[26] Arjun Berera. Warm inflation at arbitrary adiabaticity: A Model, an existence proof for inflationary dynamics in quantum field theory. *Nucl.Phys.*, B585:666–714, 2000.

[27] Arjun Berera. A Quantum field theory warm inflation model. *AIP Conf.Proc.*, 478:50–53, 1999.

[28] Wolung Lee and Li-Zhi Fang. Mass density perturbations from inflation with thermal dissipation. *Phys.Rev.*, D59:083503, 1999.

[29] Arjun Berera, Marcelo Gleiser, and Rudnei O. Ramos. A First principles warm inflation model that solves the cosmological horizon / flatness problems. *Phys.Rev.Lett.*, 83:264–267, 1999.

[30] Arjun Berera, Thomas W. Kephart, and Stuart D. Wick. GUT cosmic magnetic fields in a warm inflationary universe. *Phys.Rev.*, D59:043510, 1999.

[31] M. Bellini. Warm inflation and classicality conditions. *Phys.Lett.*, B428:31–36, 1998.

[32] J.M.F. Maia and J.A.S. Lima. Extended warm inflation. *Phys.Rev.*, D60:101301, 1999.

[33] Mauricio Bellini. Warm inflation with back reaction: A Stochastic approach. *Class.Quant.Grav.*, 17:145–151, 2000.

[34] Mauricio Bellini. Warm inflation with coupled thermal quantum fluctuations: A New semiclassical approach. *Nuovo Cim.*, B115:1241–1247, 2000.

[35] A.N. Taylor and Andrew R. Liddle. Gravitino production in the warm inflationary scenario. *Phys.Rev.*, D64:023513, 2001.

[36] Ian G Moss. Derivative expansions of the nonequilibrium effective action. *Nucl.Phys.*, B631:500–516, 2002.

[37] Arjun Berera and Rudnei O. Ramos. The Affinity for scalar fields to dissipate. *Phys.Rev.*, D63:103509, 2001.

[38] Mauricio Bellini. Fresh inflation: A Warm inflationary model from a zero temperature initial state. *Phys.Rev.*, D63:123510, 2001.

[39] Rudnei O. Ramos. Fine tuning solution for hybrid inflation in dissipative chaotic dynamics. *Phys.Rev.*, D64:123510, 2001.

[40] Arjun Berera. Warm inflation dissipative dynamics. 2001.

[41] Luis P. Chimento, Alejandro S. Jakubi, Norberto A. Zuccala, and Diego Pavon. Synergistic warm inflation. *Phys.Rev.*, D65:083510, 2002.

[42] Ian D. Lawrie. Dissipation in equations of motion of scalar fields. *Phys.Rev.*, D67:045006, 2003.

[43] Arjun Berera and Rudnei O. Ramos. Construction of a robust warm inflation mechanism. *Phys.Lett.*, B567:294–304, 2003.

[44] Robert H. Brandenberger and Masahide Yamaguchi. Spontaneous baryogenesis in warm inflation. *Phys.Rev.*, D68:023505, 2003.

[45] Arjun Berera and Rudnei O. Ramos. Absence of isentropic expansion in various inflation models. *Phys.Lett.*, B607:1–7, 2005.

[46] Wolung Lee and Li-Zhi Fang. Correlated hybrid fluctuations from inflation with thermal dissipation. *Phys.Rev.*, D69:023514, 2004.

[47] Arjun Berera and Rudnei O. Ramos. Dynamics of interacting scalar fields in expanding space-time. *Phys.Rev.*, D71:023513, 2005.

[48] Lisa M H Hall and Ian G Moss. Thermal effects on pure and hybrid inflation. *Phys.Rev.*, D71:023514, 2005.

[49] Mar Bastero-Gil and Arjun Berera. Determining the regimes of cold and warm inflation in the SUSY hybrid model. *Phys.Rev.*, D71:063515, 2005.

[50] Mar Bastero-Gil and Arjun Berera. Sneutrino warm inflation in the minimal supersymmetric model. *Phys.Rev.*, D72:103526, 2005.

[51] Jose P. Mimoso, Ana Nunes, and Diego Pavon. Asymptotic behavior of the warm inflation scenario with viscous pressure. *Phys.Rev.*, D73:023502, 2006.

[52] Ian G Moss and Chun Xiong. Dissipation coefficients for supersymmetric inflatonary models. 2006.

[53] Ramon Herrera, Sergio del Campo, and C. Campuzano. Tachyon warm inflationary universe models. *JCAP*, 0610:009, 2006.

[54] Mar Bastero-Gil and Arjun Berera. Warm inflation dynamics in the low temperature regime. *Phys.Rev.*, D76:043515, 2007.

[55] Ian G Moss and Chun Xiong. Non-Gaussianity in fluctuations from warm inflation. *JCAP*, 0704:007, 2007.

[56] Ian G Moss and Chris M Graham. Testing models of inflation with CMB non-gaussianity. *JCAP*, 0711:004, 2007.

[57] Lisa M.H. Hall and Hiranya V. Peiris. Cosmological Constraints on Dissipative Models of Inflation. *JCAP*, 0801:027, 2008.

[58] Juan Carlos Bueno Sanchez, Mar Bastero-Gil, Arjun Berera, and Konstantinos Dimopoulos. Warm hilltop inflation. *Phys.Rev.*, D77:123527, 2008.

[59] Arjun Berera, Ian G. Moss, and Rudnei O. Ramos. Warm Inflation and its Microphysical Basis. *Rept.Prog.Phys.*, 72:026901, 2009.

[60] Ian G. Moss and Chris M. Graham. Particle production and reheating in the inflationary universe. *Phys.Rev.*, D78:123526, 2008.

[61] Mar Bastero-Gil and Arjun Berera. Warm inflation model building. *Int.J.Mod.Phys.*, A24:2207–2240, 2009.

[62] Sergio del Campo and Ramon Herrera. Warm-Intermediate inflationary universe model. *JCAP*, 0904:005, 2009.

[63] Mar Bastero-Gil, Arjun Berera, James B. Dent, and Thomas W. Kephart. Towards Realizing Warm Inflation in String Theory. 2009.

[64] Chris Graham and Ian G. Moss. Density fluctuations from warm inflation. *JCAP*, 0907:013, 2009.

[65] Ramon Herrera. Warm inflationary model in loop quantum cosmology. *Phys.Rev.*, D81:123511, 2010.

[66] Mar Bastero-Gil, Arjun Berera, and Rudnei O. Ramos. Dissipation coefficients from scalar and fermion quantum field interactions. *JCAP*, 1109:033, 2011.

[67] Yi-Fu Cai, James B. Dent, and Damien A. Easson. Warm DBI Inflation. *Phys.Rev.*, D83:101301, 2011.

[68] Mar Bastero-Gil, Arjun Berera, and Joao G. Rosa. Warming up brane-antibrane inflation. *Phys.Rev.*, D84:103503, 2011.

[69] Mar Bastero-Gil, Arjun Berera, Rudnei O. Ramos, and Joao G. Rosa. Warm baryogenesis. *Phys.Lett.*, B712:425–429, 2012.

[70] Mar Bastero-Gil, Arjun Berera, Rudnei O. Ramos, and Joao G. Rosa. General dissipation coefficient in low-temperature warm inflation. *JCAP*, 1301:016, 2013.

[71] Rafael Cerezo and Joao G. Rosa. Warm Inflection. *JHEP*, 1301:024, 2013.

[72] Xiao-Min Zhang and Jian-Yang Zhu. Warm inflation in loop quantum cosmology: a model with a general dissipative coefficient. *Phys.Rev.*, D87(4):043522, 2013.

[73] Mar Bastero-Gil, Arjun Berera, Thomas P. Metcalf, and Joao G. Rosa. Delaying the waterfall transition in warm hybrid inflation. *JCAP*, 1403:023, 2014.

[74] Gabriella Piccinelli, Angel Sanchez, Alejandro Ayala, and Ana Julia Mizher. Warm inflation in the presence of magnetic fields. *Phys.Rev.*, D90(8):083504, 2014.

[75] Andreas Albrecht, Paul J. Steinhardt, Michael S. Turner, and Frank Wilczek. Reheating an Inflationary Universe. *Phys.Rev.Lett.*, 48:1437, 1982.

[76] Arjun Berera. Thermal properties of an inflationary universe. *Phys.Rev.*, D54:2519–2534, 1996.

[77] D.H. Lyth. Large Scale Energy Density Perturbations and Inflation. *Phys.Rev.*, D31:1792–1798, 1985.

[78] Yi Wang. Inflation, Cosmic Perturbations and Non-Gaussianities. *Commun.Theor.Phys.*, 62:109–166, 2014.

[79] Mar Bastero-Gil, Arjun Berera, Ian G. Moss, and Rudnei O. Ramos. Cosmological fluctuations of a random field and radiation fluid. *JCAP*, 1405:004, 2014.

[80] A. Berera. The warm inflationary universe. *Contemp.Phys.*, 47:33–49, 2006.

[81] Stephen P. Martin. A Supersymmetry primer. *Adv.Ser.Direct.High Energy Phys.*, 21:1–153, 2010.

[82] Ian J.R. Aitchison. Supersymmetry and the MSSM: An Elementary introduction. 2005.

[83] Arjun Berera, Marcelo Gleiser, and Rudnei O. Ramos. Strong dissipative behavior in quantum field theory. *Phys.Rev.*, D58:123508, 1998.

[84] Mar Bastero-Gil, Arjun Berera, Rudnei O. Ramos, and Joao G. Rosa. Observational implications of mattergenesis during inflation. 2014.

[85] Lisa M H Hall, Ian G Moss, and Arjun Berera. Scalar perturbation spectra from warm inflation. *Phys.Rev.*, D69:083525, 2004.

[86] A.N. Taylor and A. Berera. Perturbation spectra in the warm inflationary scenario. *Phys.Rev.*, D62:083517, 2000.

[87] Mar Bastero-Gil, Arjun Berera, Ian G. Moss, and Rudnei O. Ramos. Theory of non-Gaussianity in warm inflation. 2014.

[88] M. Bastero-Gil, A. Berera, and R.O. Ramos. Shear viscous effects on the primordial power spectrum from warm inflation. *JCAP*, 1107:030, 2011.

[89] Sam Bartrum, Mar Bastero-Gil, Arjun Berera, Rafael Cerezo, Rudnei O. Ramos, and Joao G. Rosa. The importance of being warm (during inflation). 2013.

[90] Rudnei O. Ramos and L.A. da Silva. Power spectrum for inflation models with quantum and thermal noises. *JCAP*, 1303:032, 2013.

[91] I.G. Moss. Primordial Inflation With Spontaneous Symmetry Breaking. *Phys.Lett.*, B154:120, 1985.

[92] G.R. Dvali, Q. Shafi, and Robert K. Schaefer. Large scale structure and supersymmetric inflation without fine tuning. *Phys.Rev.Lett.*, 73:1886–1889, 1994.

[93] Edmund J. Copeland, Andrew R. Liddle, David H. Lyth, Ewan D. Stewart, and David Wands. False vacuum inflation with Einstein gravity. *Phys.Rev.*, D49:6410–6433, 1994.

[94] Andrei D. Linde and Antonio Riotto. Hybrid inflation in supergravity. *Phys.Rev.*, D56:1841–1844, 1997.

[95] Vedat Nefer Senoguz and Q. Shafi. Testing supersymmetric grand unified models of inflation. *Phys.Lett.*, B567:79, 2003.

[96] Vedat Nefer Senoguz and Q. Shafi. Reheat temperature in supersymmetric hybrid inflation models. *Phys.Rev.*, D71:043514, 2005.

[97] M. Bastero-Gil, S.F. King, and Q. Shafi. Supersymmetric Hybrid Inflation with Non-Minimal Kahler potential. *Phys.Lett.*, B651:345–351, 2007.

[98] Bjorn Garbrecht, Constantinos Pallis, and Apostolos Pilaftsis. Anatomy of F(D)-Term Hybrid Inflation. *JHEP*, 0612:038, 2006.

[99] Mansoor ur Rehman, Vedat Nefer Senoguz, and Qaisar Shafi. Supersymmetric And Smooth Hybrid Inflation In The Light Of WMAP3. *Phys.Rev.*, D75:043522, 2007.

[100] C. Pallis. Kaehler Potentials for Hilltop F-Term Hybrid Inflation. *JCAP*, 0904:024, 2009.

[101] Mansoor Ur Rehman, Qaisar Shafi, and Joshua R. Wickman. Supersymmetric Hybrid Inflation Redux. *Phys.Lett.*, B683:191–195, 2010.

[102] Mansoor Ur Rehman, Qaisar Shafi, and Joshua R. Wickman. Minimal Supersymmetric Hybrid Inflation, Flipped SU(5) and Proton Decay. *Phys.Lett.*, B688:75–81, 2010.

[103] Matthew Civiletti, Mansoor Ur Rehman, Eric Sabo, Qaisar Shafi, and Joshua Wickman. *R*-Symmetry Breaking in Supersymmetric Hybrid Inflation. 2013.

[104] Constantinos Pallis and Qaisar Shafi. Update on Minimal Supersymmetric Hybrid Inflation in Light of PLANCK. *Phys.Lett.*, B725:327–333, 2013.

[105] Sidney R. Coleman and Erick J. Weinberg. Radiative Corrections as the Origin of Spontaneous Symmetry Breaking. *Phys.Rev.*, D7:1888–1910, 1973.

[106] L. Dolan and R. Jackiw. Symmetry Behavior at Finite Temperature. *Phys.Rev.*, D9:3320–3341, 1974.

[107] James M. Cline and Pierre-Anthony Lemieux. Electroweak phase transition in two Higgs doublet models. *Phys.Rev.*, D55:3873–3881, 1997.

[108] Michael Dine, Robert G. Leigh, Patrick Y. Huet, Andrei D. Linde, and Dmitri A. Linde. Towards the theory of the electroweak phase transition. *Phys.Rev.*, D46:550–571, 1992.

[109] J.R. Espinosa, M. Quiros, and F. Zwirner. On the phase transition in the scalar theory. *Phys.Lett.*, B291:115–124, 1992.

[110] John M. Cornwall, R. Jackiw, and E. Tomboulis. Effective Action for Composite Operators. *Phys.Rev.*, D10:2428–2445, 1974.

[111] G. Amelino-Camelia and So-Young Pi. Selfconsistent improvement of the finite temperature effective potential. *Phys.Rev.*, D47:2356–2362, 1993.

[112] Giovanni Amelino-Camelia. On the CJT formalism in multifield theories. *Nucl.Phys.*, B476:255–274, 1996.

[113] J.P. Blaizot, Edmond Iancu, and A. Rebhan. Approximately selfconsistent resummations for the thermodynamics of the quark gluon plasma. 1. Entropy and density. *Phys.Rev.*, D63:065003, 2001.

[114] J.-P. Blaizot, E. Iancu, U. Kraemmer, and A. Rebhan. Hard thermal loops and the entropy of supersymmetric Yang-Mills theories. *JHEP*, 0706:035, 2007.

[115] Herbert Nachbagauer. On the consistent solution of the gap equation for spontaneously broken lambda ϕ^4 theory. *Z.Phys.*, C67:641–646, 1995.

[116] Y. Nemoto, K. Naito, and M. Oka. Effective potential of O(N) linear sigma model at finite temperature. *Eur.Phys.J.*, A9:245–259, 2000.

[117] Song Shu and Jia-Rong Li. The CJT calculation in studying nuclear matter beyond mean field approximation. *Mod.Phys.Lett.*, A23:1769–1780, 2008.

[118] Qaisar Shafi and Joshua R. Wickman. Observable Gravity Waves From Supersymmetric Hybrid Inflation. *Phys.Lett.*, B696:438–446, 2011.

[119] Matthew Civiletti, Constantinos Pallis, and Qaisar Shafi. Upper Bound on the Tensor-to-Scalar Ratio in GUT-Scale Supersymmetric Hybrid Inflation. *Phys.Lett.*, B733:276–282, 2014.

[120] Daniel Baumann and Liam McAllister. Advances in Inflation in String Theory. *Ann.Rev.Nucl.Part.Sci.*, 59:67–94, 2009.

[121] Daniel Baumann and Liam McAllister. Inflation and String Theory. 2014.

[122] David Langlois. Brane cosmology: An Introduction. *Prog.Theor.Phys.Suppl.*, 148:181–212, 2003.

[123] Liam McAllister and Eva Silverstein. String Cosmology: A Review. *Gen.Rel.Grav.*, 40:565–605, 2008.

[124] Andrei D. Linde. Inflation and string cosmology. *Prog.Theor.Phys.Suppl.*, 163:295–322, 2006.

[125] Maurizio Gasperini. The universe before the big bang: Cosmology and string theory. 2008.

[126] C.P. Burgess, M. Majumdar, D. Nolte, F. Quevedo, G. Rajesh, et al. The Inflationary brane anti-brane universe. *JHEP*, 0107:047, 2001.

[127] G.R. Dvali and S.H. Henry Tye. Brane inflation. *Phys.Lett.*, B450:72–82, 1999.

[128] Gary Shiu and S.H. Henry Tye. Some aspects of brane inflation. *Phys.Lett.*, B516:421–430, 2001.

[129] G.R. Dvali, Q. Shafi, and S. Solganik. D-brane inflation. 2001.

[130] Carlos Herdeiro, Shinji Hirano, and Renata Kallosh. String theory and hybrid inflation / acceleration. *JHEP*, 0112:027, 2001.

[131] Juan Garcia-Bellido, Raul Rabadan, and Frederic Zamora. Inflationary scenarios from branes at angles. *JHEP*, 0201:036, 2002.

[132] C.P. Burgess, P. Martineau, F. Quevedo, G. Rajesh, and R.J. Zhang. Brane - anti-brane inflation in orbifold and orientifold models. *JHEP*, 0203:052, 2002.

[133] Zurab Kakushadze and S.H. Henry Tye. Brane world. *Nucl.Phys.*, B548:180–204, 1999.

[134] Joseph Polchinski. Dirichlet Branes and Ramond-Ramond charges. *Phys.Rev.Lett.*, 75:4724–4727, 1995.

[135] Shamit Kachru, Renata Kallosh, Andrei D. Linde, Juan Martin Maldacena, Liam P. McAllister, et al. Towards inflation in string theory. *JCAP*, 0310:013, 2003.

[136] C.P. Burgess, James M. Cline, H. Stoica, and F. Quevedo. Inflation in realistic D-brane models. *JHEP*, 0409:033, 2004.

[137] Johanna Erdmenger, Nick Evans, Ingo Kirsch, and Ed Threlfall. Mesons in Gauge/Gravity Duals - A Review. *Eur.Phys.J.*, A35:81–133, 2008.

[138] John H. Brodie. On Mediating supersymmetry breaking in D-brane models. 2001.

[139] Fernando Quevedo. Lectures on string/brane cosmology. *Class.Quant.Grav.*, 19:5721–5779, 2002.

[140] Sarah Shandera, Benjamin Shlaer, Horace Stoica, and S.H. Henry Tye. Interbrane interactions in compact spaces and brane inflation. *JCAP*, 0402:013, 2004.

[141] Washington Taylor. D-brane field theory on compact spaces. *Phys.Lett.*, B394:283–287, 1997.

Publications

[1] Mar Bastero-Gil, Arjun Berera, Thomas P. Metcalf, Joao G. Rosa,

"Delaying the waterfall transition in warm hybrid inflation" Journal of Cosmology and Astroparticle Physics, arXiv:1312.2961[hep-ph], 2014